Effect of calcium nitrate on buildability and structural build-up in a set-on-demand 3D concrete printing setup

Hossein Rahmani

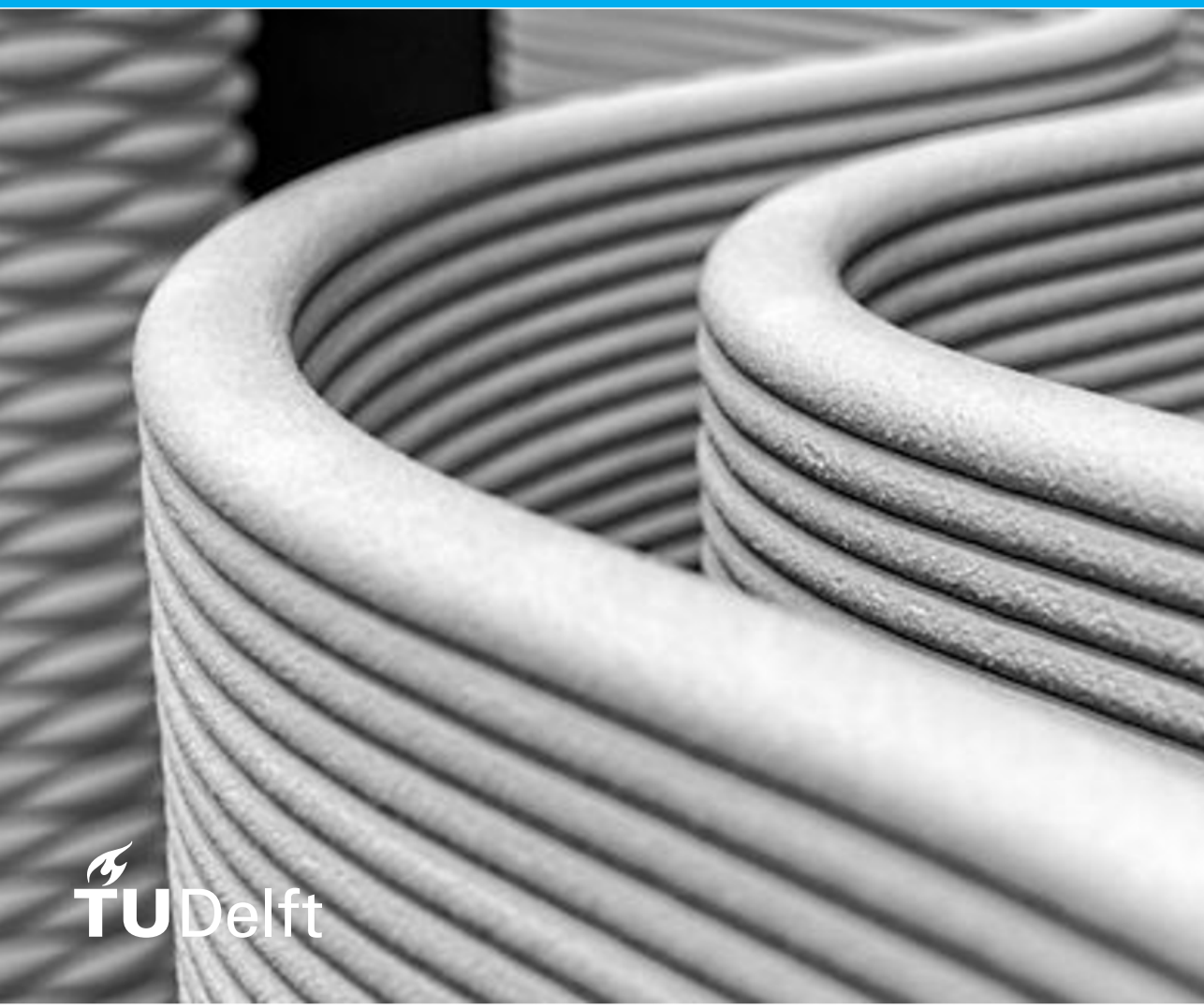

TU Delft

EFFECT OF CALCIUM NITRATE ON BUILDABILITY AND STRUCTURAL BUILD-UP IN A SET-ON-DEMAND 3D CONCRETE PRINTING SETUP

Thesis

This thesis was submitted to the Faculty of Civil Engineering and Geosciences at the Delft University of Technology in order to acquire the Master of Science degree.
To be defended on: Friday, June 16, 2023, at 15:00 PM.
by

HOSSEIN RAHMANI

Student number:	4941292	
Project duration:	May 2022 – June 2023	
Thesis committee:	Dr. O. Copuroglu,	TU Delft, chairman
	Dr. Y. Chen,	TU Delft
	Dr. M. Lukovic	TU Delft

An electronic version of this thesis is available at http://repository.tudelft.nl.

ACKNOWLEDGMENTS

I started in 2020 as a student in the field of Structural Engineering. With unwavering determination, I enthusiastically embraced this path to develop into a proficient structural engineer with a focus on concrete structures.

I am incredibly appreciative to Dr. Copuroglu, my thesis advisor, for giving me the chance to contribute to an innovative project involving the 3D printing of concrete. Therefore, I extend my sincere gratitude to Dr. Copuroglu for his invaluable advice, constant support, and motivational encouragement throughout the entire research process. His extensive knowledge and insightful feedback have played a pivotal role in shaping the direction and scope of my work. I would also like to express my appreciation to Dr. Yu Chen, my daily supervisor, for his tireless assistance, patience, and guidance, which proved crucial in completing my thesis. I sincerely appreciate his priceless assistance and advice, which has enriched my knowledge in this field, and without his assistance, I would not have been able to complete my thesis. I would also like to extend my gratitude to Dr. Lukovic, another esteemed member of my thesis committee, for her valuable feedback and suggestions that greatly enhanced the overall quality of this thesis.

I would like to express my sincere appreciation to Maiko van Leeuwen, Ton Blom, Masi Nuri, and Firas Al-Share for their invaluable technical support and assistance throughout the experimental procedures I conducted. Their expertise and guidance have been instrumental in the success of my research.

Hossein Rahmani
Zaandam, May 2023

ABSTRACT

The economic and environmental advantages of extrusion-based 3D concrete printing have made it a frontrunner in large-scale buildings. Nonetheless, this approach suffers from a contradictory rheological requirement and a high percentage of Portland cement (PC) in its mixture, which challenges its sustainability. It is claimed that the addition of supplementary cementitious materials (SCMs) to the mixture might solve this issue. Fly ash (FA), silica fume (SF), Ground Granulated Blast furnace Slag (GGBS), limestone, and calcined clay are examples of such materials. However, the production of certain of these SCMs, such as FA, SF, and GGBS, is restricted, while others, such as limestone and calcined clay, are plentiful.

To address these challenges, the purpose of this research was to investigate two developed mixtures: limestone calcined clay cement (LC^3-based) and limestone slag cement (slag-based) activated with limestone-based accelerator slurry (with calcium nitrate as an accelerator).

The first phase of this work was the formulation of flowable and pumpable mixtures. The flowability of two cementitious materials (LC^3 and slag-based) and limestone-based accelerator slurry was evaluated. For each mixture, the optimum superplasticizer/ accelerator dose was determined to ensure optimum flowability and pumpability. The optimal dose of superplasticizer for the LC^3- and slag-based mixtures, as determined by flowability, pumping, and flow curve tests, was 0.6% and 0.3% of the binder's mass, respectively. The recommended $Ca(NO_3)_2$ dose for limestone-based accelerator slurry was 7% of the cement weight.

Part two of this research looked at how combining limestone-based accelerator slurry with cementitious materials affected the mixture's fresh qualities. Here, the initial setting time and buildability of the formulated mixes were investigated. At last, a printable mixture of LC^3 was developed containing just 275 kg/m^3 of PC with compressive strength of more than 30 MPa at 28 days of curing.

The third section of this research was devoted to material properties. Here, the development of the mixture's compressive strength, heat evolution, and hydration product was investigated. The compressive strength development of all mixtures was assessed at 7 and 28 days of curing. In general, the compressive strength of LC^3-based mixtures with various accelerator dosages was greater than that of slag-based mixtures with the same accelerator content.

Isothermal calorimetry was employed to investigate the hydration of the mixtures. The findings for LC^3- and slag-based mixtures demonstrated that a larger calcium nitrate dose significantly accelerated the hydration of the fresh mixtures. This acceleration was shown by a quicker induction time, a shifted primary hydration peak to an earlier age of hydration, increased intensity of the primary hydration peak, and greater cumulative heat. Within the first 7 days, LC^3-based mixes had a greater cumulative heat evolution

than slag-based mixtures. Thermogravimetric analysis (TGA) was used to analyze the amount of calcium hydroxide and hydration water in the investigated mixes at various curing periods, including 1h, 4h, and 168h. In general, the results of the TGA test and isothermal calorimetry were comparable.

The final objective of this study was to examine the adaptability of the developed mixture to an actual printing structure. So, the design of a cycle arch bridge in Zaanstad was explored. The results indicate that the developed mixture will be helpful for utilizing in the 3DCP method since the mixture showed encouraging buildability and sustainability behavior.

CONTENTS

List of Figures

1

INTRODUCTION

1.1. GENERAL INTRODUCTION

The origins of 3D printing extend back to the 1980s, despite the impression that it is a new technology [1]. According to some, 3D printing represents the "third industrial revolution" and has the capacity to alter all manufacturing processes [2–4]. 3D printing is sometimes referred to as "digital manufacturing" to underline that the geometries are generated using digital 3D model data from an electronic data source. Some may refer to it as "automated construction" to emphasize that the vast majority of these methods combine some degree of automation with a decrease in manpower to create an element [5]. Till now, several 3D printing techniques for diverse materials such as ceramics [6], metals [7] (see Figure 1.1), and plastic polymers [8] have been created [9]. Regular applications of 3D printing may be found in engineering, aerospace, automobile industries, and even the healthcare industry. However, the construction industry is not among those that have fully adopted this technology [1]. This approach employed in civil construction is regarded to be in its adolescent stage and must grow in a number of technical and economic aspects before achieving full maturity [10].

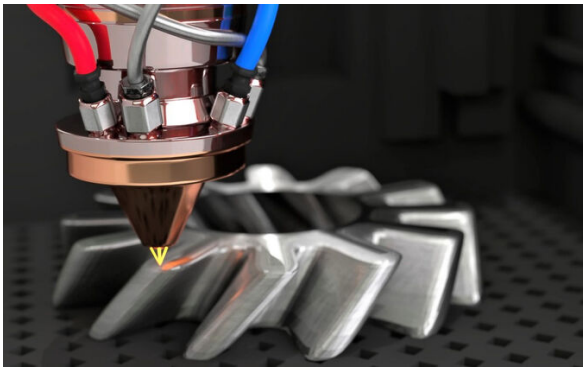

Figure 1.1: A 3D-printed metal gear, adapted from www.metaltechnews.com

3D concrete printing (3DCP) has the ability to increase design flexibility, minimize la-

bor usage [1], and shorten construction time. In addition to reducing building costs by 35–60% [11], the removal of formwork may make 3DCP a low-CO_2 trend in the future of construction. Furthermore, from an environmental point of view, less ordinary Portland cement (OPC) may be utilized by employing 3DCP and decreasing material waste, because the printers construct three-dimensional structures layer by layer without the need for formwork [10, 12]. Four key processes make up the 3DCP procedure: (1) mixing the mixture; (2) transferring the mixture to the print head (Pumping); (3) extruding the mixture from the nozzle (Printing); and (4) sequential application of the mixture to form the structure [13].

As with any technology, 3DCP has a number of limitations and drawbacks, especially when reinforcement is included in the printed structure. The high cost of purchasing 3DCP equipment is a further disadvantage. Rising market competition, however, is widely expected to drive down these prices in the not-too-distant future [1]. Furthermore, 3D concrete printing technology necessitates a significant amount of energy. Consequently, environmental sustainability varies widely from location to location and depends on power-generating sources. Those countries whose power plants use fossil fuels to provide electricity will suffer the worst environmental consequences. As a result, efforts have been undertaken to cut power use and employ renewable energy sources. There was also some thought given to linking printers with solar panels. Solar panels, for example, are embedded into MIT's massive mobile 3D printer, which is being designed to create residences on Mars [14]. Moreover, digital operations have the potential to dramatically cut employment, but they are also generating new positions, particularly in the maintenance, production, and operation of printers. The biggest worry is whether or not the number of lost employment will be balanced by the number of new ones created. The answer seems to be "no," however replies to inquiries of this kind vary [10].

Furthermore, by restricting the diameter of pump systems and extruders, the maximum aggregate size of printed structures may be kept to a minimum. As a result, concrete mixtures have a greater proportion of binders and smaller aggregates, which has a negative impact on the environment [5, 15]. The mechanical strength of 3D-printed structures is another factor to think about. Due of the restricted volume and size of aggregates, concrete's load-bearing capability is very constrained. The existing technical methods are able to print low-rise structures but are incapable of building skyscrapers, see Figure 1.2). So far, the finest accomplishment has been a five-story structure [10]. Although 3DCP is used in a number of countries, there are very few academic studies that provide standard testing for material efficiency and specifications [16].

Finally, in 3DCP, the printed mixture requires particular rheological characteristics to guarantee extrudability and buildability, but in traditional concrete, there is less need to consider the rheological properties of the mixture during the casting [17–19]. This study primarily aimed to address the last issue.

Figure 1.2: A 3DC printed two-story single-family house in Beckum, adapted from (https://sievert.de)

1.2. THE PROBLEM

There are certain requirements for 3DCP fresh state characterization that contradict one another. In other words, pumpability, extrudability, and buildability are the fresh state qualities that are needed from the mixer to the placement of concrete layer by layer for printing. In order to print a structure, the mixture must be delivered through hoses to the nozzle for extrusion before being placed layer by layer. The material's plastic viscosity and yield stress, specifically its dynamic yield stress, must be optimized for smooth passage through the hoses. On the other hand, buildability demands that the material have a high static yield stress in order to limit flow and hence support the deposition of upper concrete layers. To create a balance between these contradictory requirements, the rheology of the mixture must be modified [20]. In particular, a crucial need for 3DCP techniques is a controlled structural build-up. This calls for a high rate of strength development immediately after material placement, but a more gradual speed prior to placement. Set-on-demand, also known as controlled hydration activation, may be employed to address these contradictory criteria. These strategies rely on hydration control to ensure structural stability during 3DCP [17].

The yield stress should grow at least linearly with time during the construction period, with a consistent development for each layer relative to the time of placement [21]. As a result, the hydration kinetics, which might be linear, power law, or exponential, should be changed to match the relevant kinetic needs of the building procedure. Therefore, a constant hydration rate is sufficient if linear strength development is needed [17]. In other words, the printing mix must be thixotropic (high yield stress at rest and a low viscosity while flowing), and setting properly [20–22], all these disagreeing necessities are shown in Figure 1.3).

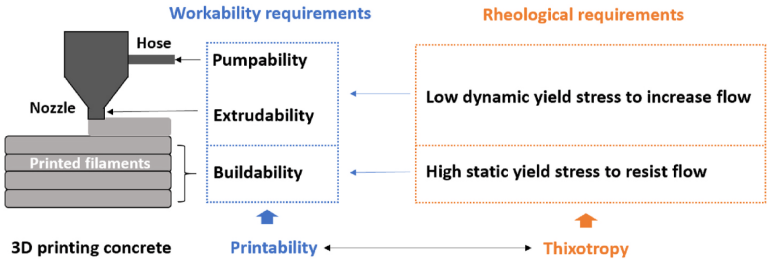

Figure 1.3: Contradictory rheological requirements of 3DCP techniques, adapted from [20]

When analyzing these conflicts, printing speed is still a crucial factor to take into account. In order to ensure that the bond strength between the printed layers is well, it is necessary that the printing speed be sufficiently high. However, the print speed needs to be slow enough to allow the layers to connect adequately with the subsequent layer while still being fresh [20, 22].

Cement content in 3DCP mixture vs the conventional cast mix is another important consideration. Cement content in 3DCP mixes should be doubled or tripled compared to traditional cast mixtures. As a result of its relatively high binder content, 3DCP has been criticized as an unsustainable building technique [13, 23]. This has led to significant concern regarding the long-term sustainability of the 3D printing technique using cement-based materials. Due to the high energy expenditure and carbon dioxide emission associated with OPC production [22].

The carbon footprint of 3DCP must be decreased before digital concrete can compete with traditional building methods [24]. In other words, further research and practical application will need 3DCP greening. This may be accomplished in a number of ways, but one of the most effective methods to reduce the carbon footprint of 3DPC is to investigate alternatives to Portland cement and cement-based cementitious material. To substitute OPC, supplementary cementitious materials (SCMs) such as, fly ash (FA), limestone, granulated blast furnace slag (GGBS), rice husk [13], and calcined clay may be utilized [12, 20, 25]. Contrary to 3D printed concrete, replacing a considerable amount (more than 45%) of OPC with supplementary cementitious materials is not a revolutionary CO_2 reduction technique [12]. Another successful technique to make 3DPC mixtures environmentally friendly is to introduce coarse aggregates to minimize the total amount of binder. Next to cost-effectiveness and concrete technical characteristics, such as lower shrinkage, lower brittleness, higher modulus of elasticity and lower creep, and so on. Some teams have conducted introductory research on this topic [25]. However, because most contemporary 3D printing technologies use small-size hoses and nozzles, coarse aggregates are rarely used in 3DCP [20, 25].

The use of supplementary cementitious materials (SCMs) in place of Portland cement is subject to specific restrictions. Current standards and norms for traditional concrete construction, for example, are inapplicable for guiding 3DCP mix design [20]. Because of the differences in manufacturing methods, the experiences with SCMs in traditional

concrete cannot be immediately applied to 3D printable concrete [12].

Developing a thixotropic material that is simply extrudable and can resist the stresses of following layers without severe deformation is the core issue of 3DCP [26]. This conflicting need demanded the use of advanced additives including accelerators, superplasticizers, retarders, and viscosity modifiers to redesign traditional concrete for 3D printing [26].

Therefore, the parameters in the mix design are so changed to provide optimal pumpability, extrudability, and buildability in order to generate printable concrete with suitable rheological behavior. The point here is that these features go considerably beyond the standard requirements for concrete as stated in codes and guidelines [20]. Currently, the most popular method for determining the ideal mix proportion for printable concrete is still trial and error. However, because it relies on endless experiments to find the ideal combination balance, the procedure lacks solid scientific principles [20].

The goal of this research was to use trial-and-error methods to determine the optimal mix design of 3DCP in terms of pumpability and buildability by using an accelerator (Calcium Nitrate ($Ca(NO_3)_2$)) and a superplasticizer. The mix design method of trial and error is straightforward and practical for determining the best mix proportion of 3DPC. However, as the number of independent factors rises, the work required to determine the optimal mixture will increase exponentially. Thus, the proportions of the key components in the 3DCP mix, such as cement, SCMs, aggregate, and water are held constant. To determine the optimal 3DPC combination, just a few elements, such as the admixtures dose (the accelerator and the superplasticizer), are regarded as independent variables, which greatly simplifies the mix design approach [20].

1.3. RESEARCH QUESTIONS

The main question of this project was to understand, "the synergistic influence of calcium nitrate and MasterGlenium51 superplasticizer on the rheology and buildability of a developed sustainable cementitious material". Therefore, the following sub-questions must be addressed in relation to the main study question.

1. What is the influence of different dosages of MasterGlenium51 superplasticizer on fresh properties of 3DCP mixtures, such as flowability, pumpability, and flow curve?

2. What is the effect of the accelerator on the fresh properties of the pumpable mixtures, such as initial setting time, green strength and buildability?

3. What is the effect of the accelerator on the hardened properties (mechanical properties) of the pumpable mixtures, such as compressive strength?

4. How can the accelerator affect the hydration of the developed sustainable cementitious material?

1

1.4. RESEARCH SCOPE

The primary scope of this study was to examine how calcium nitrate influenced both the fresh and hardened qualities of the developed cementitious material. This study did not cover the 3DCP hardware and configurations. In addition, it was outside the purview of this study to investigate the impact of the accelerator on all of the characteristics of the concrete, since this would have been an extremely time-consuming operation. Consequently, only a couple of the variables associated with the buildability of the concrete mixture's behavior were explored in this investigation. Hence, the fresh state characteristics of the 3DCP mixes, including flowability, stiffness development, and buildability, besides the mechanical and chemical properties of the mixtures were studied.

One of the crucial characteristics of the fresh mixture was flowability, it should be flowable during the pumping process. For stiffness developing at an early age, two aspects of the fresh mixture were evaluated, including initial setting time and green strength. Because these two measurements have the potential to reveal the development of strength in the 3DCP mixes at an early age. The 3DCP mixtures buildability was investigated in order to monitor the ability of shape keeping of the printed samples because of the self-weight of the top printed filament. For mechanical properties, the mixtures' compressive strength development was assessed within 7 and 28 days. In the end, for the chemical properties, the influence of the accelerator on the hydration process and the hydration product of the mixtures were addressed throughout the first seven days.

Table1.1 illustrates a summary of all studied parameters within this project.

Fresh properties	Mechanical properties	Chemical properties
Consistency (Flowability)	Compressive strength	Heat evolution
Pumpability		(Isothermal calorimetry)
Flow curve test		Hydration product
Initial setting time		(Thermogravimetric analysis (TGA))
Green strength development		
Buildability		

Table 1.1: Studied properties in this work

1.5. RESEARCH OUTLINE

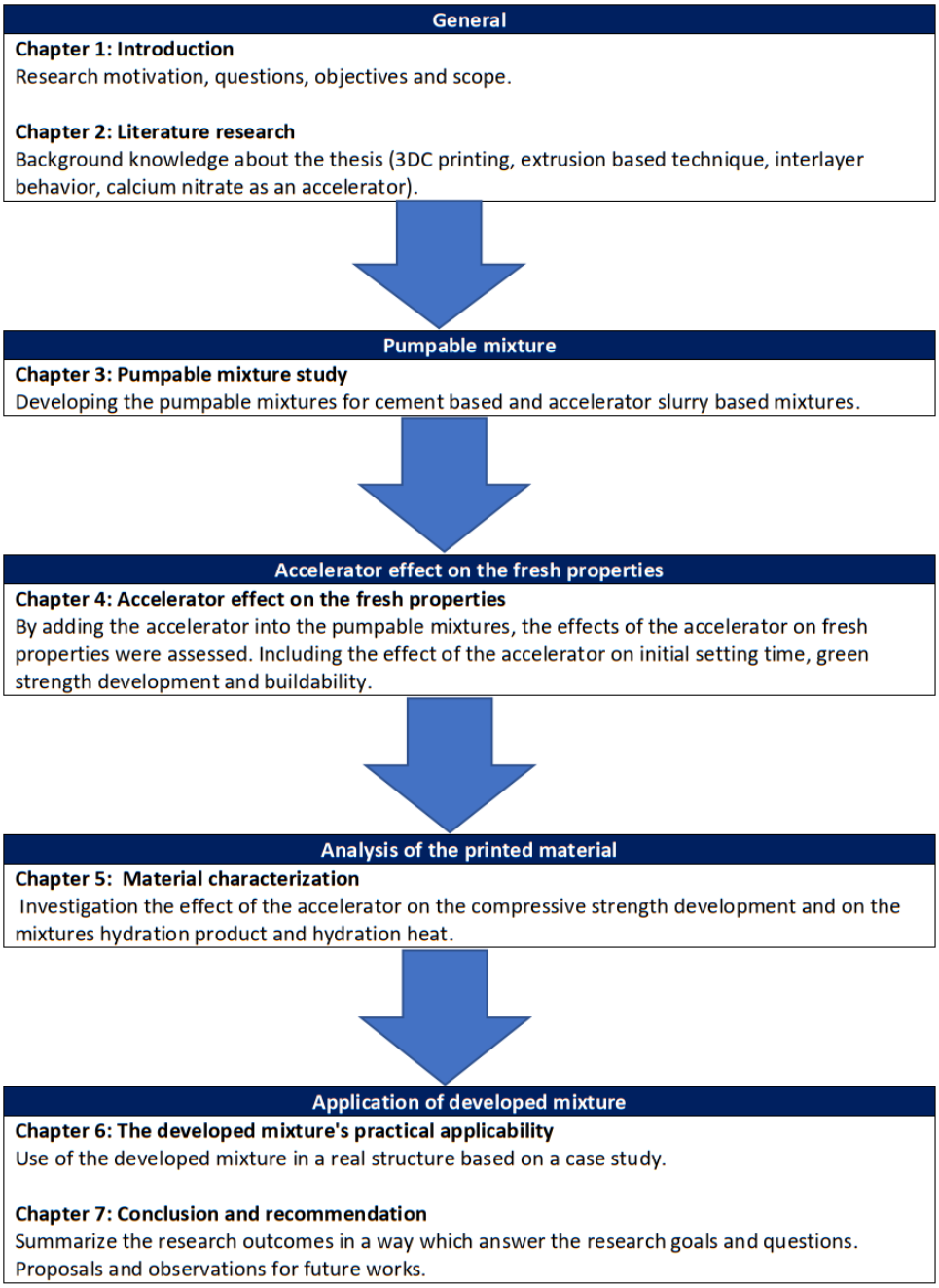

2

LITERATURE RESEARCH

2.1. AVAILABLE METHODS FOR 3DCP

Multiple 3DCP technologies have developed in recent years, opening the road for wider adoption of this innovation in the concrete structure sector. Extrusion-based and powder-based methods provide the backbone of these technologies [27, 28].

2.1.1. POWDER-BASED TECHNIQUE

One of the common 3DCP methods for making complex structures with fine details and complicated geometries is the powder-based technique (also named binder jetting or D-shape). This method is ideally suited for the production of precast elements in an off-site setting. Panels, permanent formworks, and movable interior structures are only a few examples of small-scale architectural components that benefit from the powder-based approach [27]. The working method of this system is as follows: a roller and print head distributes a 3 mm layer of powder on the build platform. The roller then spreads and smoothes a thin coating of powder about 0.1 mm over the powder bed surface. The binder solution is then fed from the binder feeder to the print head and precisely sprayed on the powder bed, then bind the powder particles, and the process is repeated until the part is finished. After a certain period of curing, the created part is detached and any residual powder is eliminated using an air blower. Figure 2.1 depicts the powder-based method[27].

For the benefits of this method, we can think about the elimination of the need for employing a supporting structure when constructing an overhanging construction. This method is ideally suited for the production of unique structural elements away from the construction site. There are several obstacles that need to be cleared before the construction sector can completely benefit from the powder-based 3DCP approach. Problems arise, for example, because the powder-based 3D printers now on the market use proprietary printing materials that are too weak to be used in construction applications. As mentioned by B. Nematollahi et al.[11], attempts to utilize Portland cement in this method have been difficult due to PC setting properties, but this is an area of active investigation [11]. D-shape and Emerging Objects are examples of technologies established with the powder-based 3DCP approach for fabricating large objects, see Figure

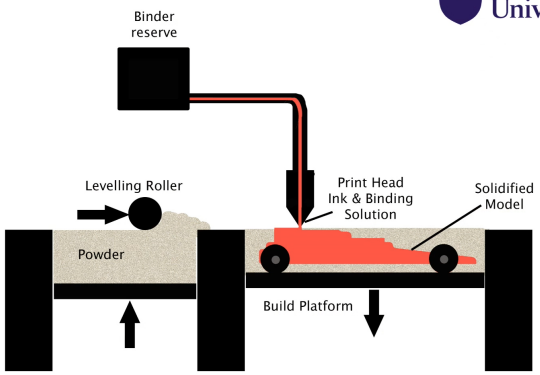

Figure 2.1: Schematic of powder-based technique, adapted from www.lboro.ac.uk

2.2. For example, the 3x3x3-meter Radiolaria Pavilion was a collaborative effort by Shiro Studio and D-shape in 2008[27].

(a)

(b)

Figure 2.2: The structures which produced based on powder-based techniques (a) Radiolaria Pavilion- A complex geometrical example printed by D-shape technology, adapted from www.4dsindia.com (b) a cabin structed by Emerging Object method, adapted from http://emergingobjects.com

As mentioned by C. Barnatt [29], future 3D printers may build on the Moon or Mars. Material extrusion or binder jetting would harden lunar regolith or Martian dust to create human settlements. Figure 2.3 is a visualization of this idea from one of Barnarr 's future visions.

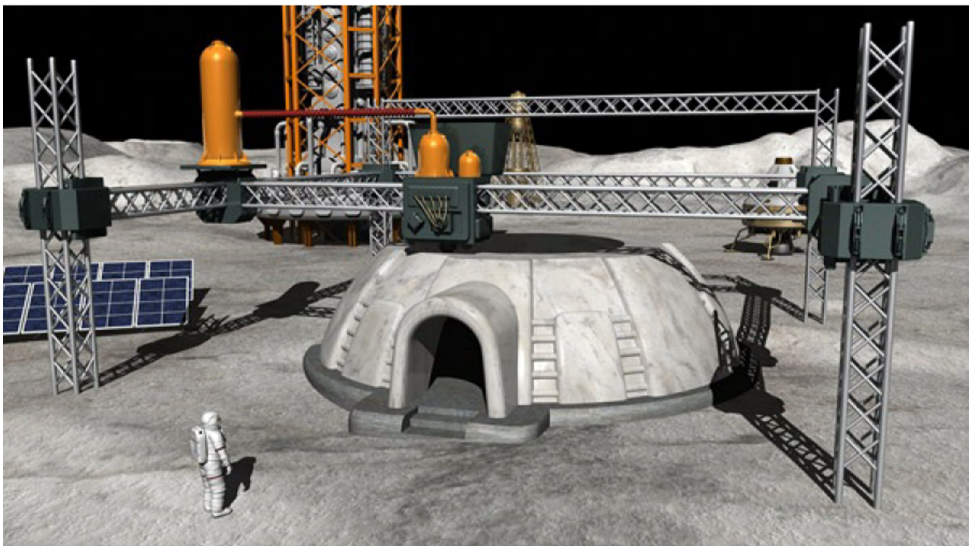

Figure 2.3: Moon-based 3D printer concept art by Christopher Barnarr, adapted from [29]

2.1.2. EXTRUSION BASED TECHNIQUE

Material extrusion is the most widely used 3D printing method. This is any process that builds up objects layer by layer by extruding a semi-liquid material out of a nozzle under computer control. Material extrusion can 3D print concrete, ceramics, chocolate, and even metals [29].

The extrusion-based method for printing concrete structures is used at least by two printing methods, including Contour Crafting (CC) and 3D concrete printing. Moreover, these two methods share a lot in common in terms of printing equipment and printable material varieties [30, 31]. In general the extrusion-based method prints a structure layer by layer by extruding cementitious material from a nozzle placed on a gantry, six-axes robotic arm, or crane. This method has been developed with the intention of being used in an on-site structural applications, such as the fabrication of huge building components with complicated geometry [32]. Figure 2.4 depicts the extrusion-based technique.

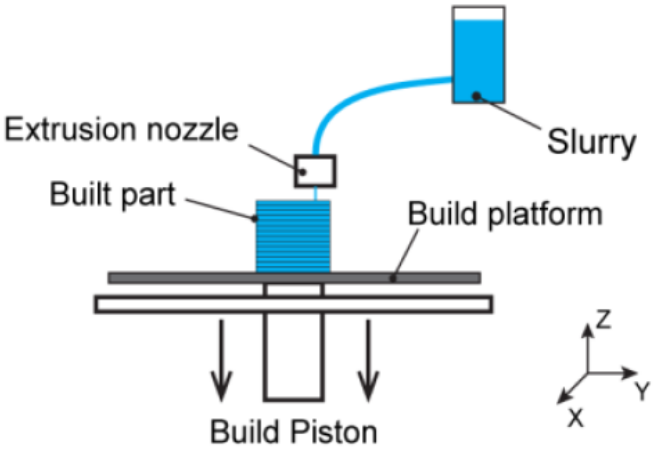

Figure 2.4: Conceptual model of the extrusion-based method, adapted from [27]

COUNTER CRAFTING (CC)

Khoshnevis's Contour Crafting (CC) is the most popular automated construction method for creating large-scale structures. The construction machine in the CC consists of a robotic arm attached to trowels that move along the x, y, and z axes, and it can create free-form components with smooth, exact surfaces. Modifying the side trowel's angle and orientation allows for the creation of a wide variety of geometric forms [10, 33] as shown in Figure 2.5a. The CC's benefits include its improved surface polish and faster production speed. The CC may be combined with other robotics systems to install pipelines, electrical conductors, and reinforcing modules to improve mechanical properties [27], Figure 2.5b shows the CC technique during building a structure. Y. Chen et al. [30] and Gosselin et al. [34] documented the following disadvantages of the CC method: This technology is limited to vertical extrusion, the initial formwork, and trowel system can be complex to implement for production, and weakened interfacial zones between layers because of one-hour backfilling segments [27].

3D CONCRETE PRINTING

Deposition setups, control units, and material transporting systems are the three key components of most 3DCP systems utilized in both education libraries and the construction sector. The gantry-based deposition systems have at least 3 directional degrees of freedom (DOF), in the x-, y-, and z-planes, among others. The rotation in the z-axis adds a fourth degree of freedom (DOF) to the 4-axis gantry robot. Industrial robotic arms can display up to 6 rotating degrees of freedom (DOF), allowing for the printing of more complicated shapes than is possible with 3- and 4-axis gantry-based deposition systems. Though 6-axis robot arms may be more flexible, 3- and 4-axis gantry-based deposition configurations may be more controllable [32]. Figure 2.6, Figure 2.7, and Figure 2.8 illus-

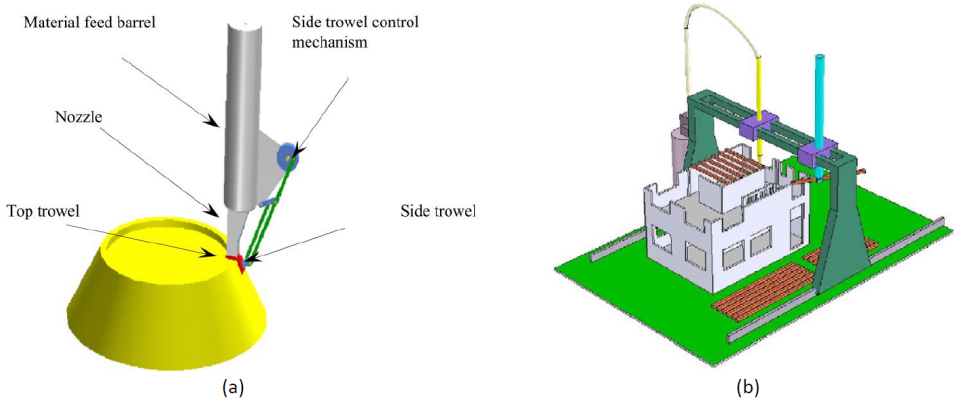

Figure 2.5: Contour Crafting method (a) Contour crafting building process (b) a schematic of a printed object by CC method, adapted from [33]

trate 3- 4 axis gantry-based and 6-axis robotic 3DCP systems.

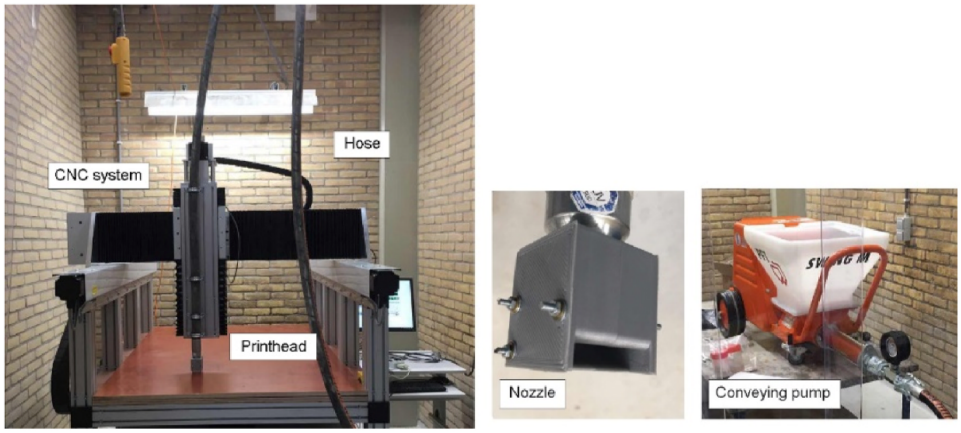

Figure 2.6: 3 DOF gantry-based system, CNC system (computer numerical control), adapted from [32]

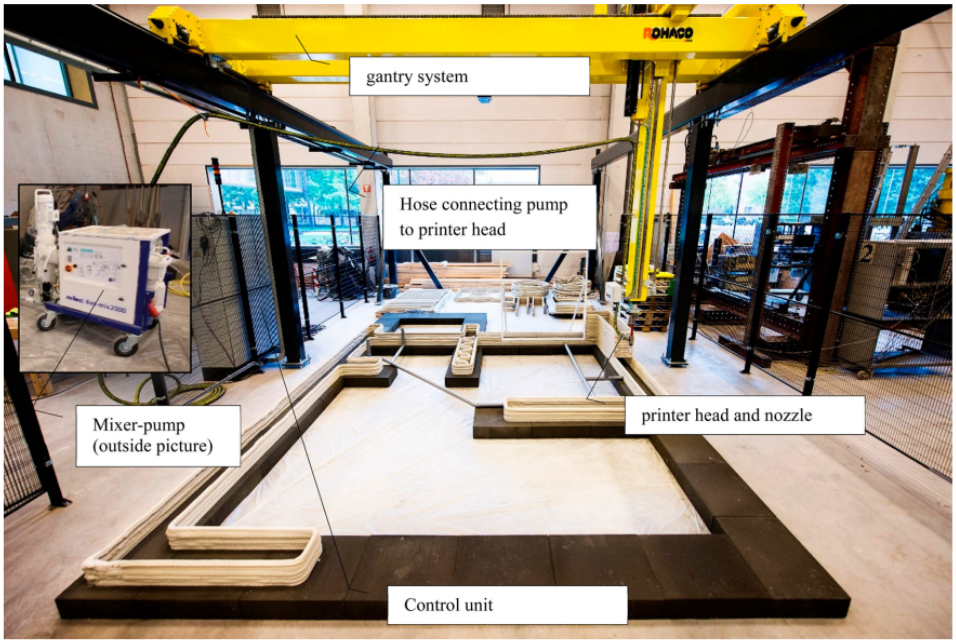

Figure 2.7: 4 DOF gantry-based system, adapted from [35]

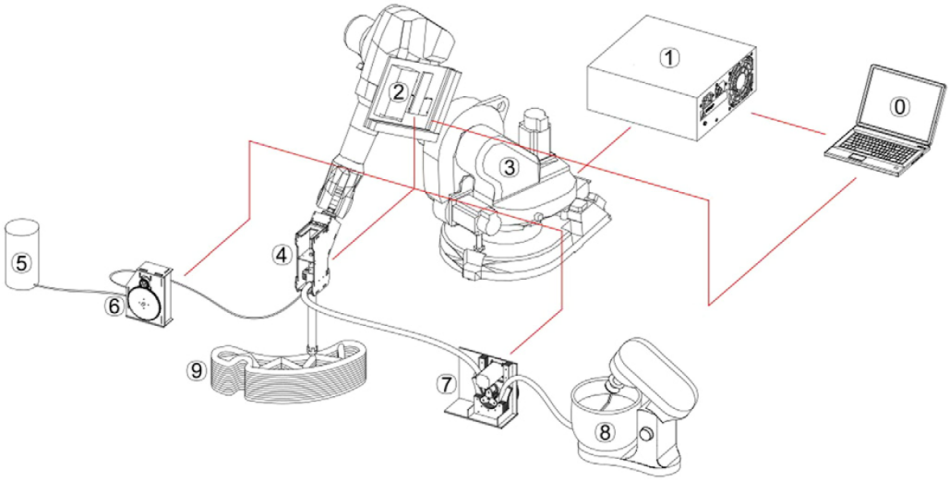

Figure 2.8: Diagram of the six DOF robotic arm: 0. Command system, 1. Controller of the robot, 2. Printing system controller, 3. Automated arm, 4. Printhead, 5. Accelerating agent, 6. Roller pump for accelerating agent 7. Roller pump for the mixture 8. Mixer, 9. Item printed in 3D, adapted from [34]

2.2. 3DCP EXTRUSION-BASED RHEOLOGICAL REQUIREMENTS

For optimal extrudability and buildability at each stage of 3D printing, certain rheological characteristics are needed. Cement mixtures must be easily pumped and have sufficient flowability to prevent extrusion pressure and separation of mixtures during the pumping operation. In other words, the yield stress of the mixture should be as low as feasible. While, immediately after deposition, fast development in the strength and stiffness of the extruded filaments becomes crucial. The mixture at this stage should be able to withstand stresses from the following layers and keep its shape properly. As in 1.2 noted, there is a conflict between the requirements for extrudability and buildability [20, 31, 36]. To achieve a high buildability rate, the freshly extruded materials must have a rapid stiffening rate or high hydration kinetics after leaving the nozzle. Accelerators can be utilized to accomplish this. The use of accelerators drastically reduces the open time, which in turn causes pumping issues including excessive pumping pressure and clogs [37, 38].

Several solutions were proposed to address these issues; one method included mixing the accelerator with water and dry ingredients beforehand, while others suggested injecting the accelerator into freshly pumped concrete during pumping or right after pumping. In the first scenario, the fresh concrete holding the accelerator would experience significant yield stress and a rapid stiffening rate, which would cause serious pumping issues and eventually destroy the entire pumping system, when unforeseen interruptions occur. As the accelerator is not combined in advance in the second scenario, the chance of pipe blockage is decreased. In such instances, however, effort must be taken to guarantee a proper homogeneity of mixing. So, it's important to know when and where to inject the accelerator, which is based on how the accelerator works and how it affects the rate of stiffening [37].

Tao et al [37]. recently introduced twin-pipe pumping (TPP), an extrusion-based inline mixing approach, to address the conflicts between the pumping and deposition processes in 3D concrete printing [39]. TPP is also known as an inline mixing system or print head mixing system [13, 40]. In this system, ordinary Portland cement, sand, water, and superplasticizer are mixed together and pumped from one pump during printing, while another pump pumps a combination of limestone powder (or other SCMs), sand, water, and the accelerator for instance at a volume ratio of 1:1, see Figure 2.9. The two mixes are subsequently combined in the immovable helical static mixer situated near the nozzle, see Figure 2.10a. Since the accelerator is not added to the concrete at the beginning of the mixing process, the mixture has excellent fluidity and a longer open time. However, the accelerator in the second combination has minimal impact without the presence of cement, therefore its open time is also rather large. The helical static mixer has internal mixing devices that continually mix the two mixes as they go through the mixer, see Figure 2.10b. The accelerator in the SCMs-based mixture reacts with cement in the cement-based mixture during mixing, causing rapid hydration kinetics and a rapid transformation from a fluid-like to a solid-like state [37].

As a result, adding the accelerator too early in the printing process is not desirable. Therefore, some academics have proposed various inline mixing solutions employing either a dynamic or a static mixer. A dynamic mixer is an electric-powered equipment having one or more shafts. A static mixer is a device that uses permanent baffles rather

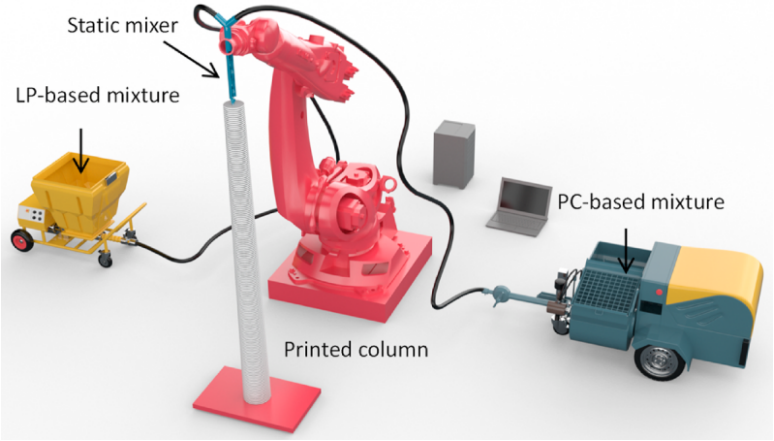

Figure 2.9: A schematic view of the twin-pipe pumping system, adapted from [39]

than moving components to continuously mix liquid material [37, 41]. The dead zone is a highly typical issue in dynamic mixers. As a result of the varying magnitude of fluid velocity inside the dynamic mixer, particularly in locations where the velocity is approximately nil, dead zones can form and blockages are more prone to occur. An alternative to a dynamic mixer is a stationary static mixer. Because there are no moving parts in a motionless mixer, they require less maintenance. They need less room to operate, cheaper machinery, and no additional energy sources beyond pumping [42]. On the other hand, static mixers require significant pumping pressure than dynamic mixers [37].

a)

b)

Figure 2.10: a) Overview image of the twin-pipe pumping system b) Helical static mixer, adapted from [37, 42]

2.3. AGGREGATE SIZE INFLUENCE ON 3DCP

According to european Standards (EN13139), in general there are two separate groups of aggregates: coarse aggregates, which range in size from 4 to 31.5 mm, and fine aggregates, which are typically less than 4 mm. 3D-printed concrete is now mostly on the mortar scale since the aggregates often used in 3DPC are fine sand. Though some academic institutions and private businesses are making progress in designing and employing printed concrete with coarse aggregates, for instance, Ji et al. [43], employed coarse aggregates in the 5-15 mm range in their 3DCP to construct a structure [20]. Specifying grading limits and nominal maximum aggregate size is important since it can have a significant impact on the concrete's workability, durability, mechanical performance, shrinkage, and pumpability [10].

From the perspective of the printhead, the aggregate content and maximum particle size have a direct relationship with the nozzle aperture, which is determined by the required filament width and thickness. Nozzles with bigger apertures are needed to prevent clogging when working with coarse aggregates; as a result, these nozzles produce broader filaments. However, nozzles with smaller apertures produce more precise results when building complicated shapes. The use of coarser particles frequently results in a rougher layer surface [10]. However, improving particle size distribution and increasing paste volume may help reduce surface roughness [20]. By using both experimental and computational methods, Cheikh et al. [44] were able to discover that the paste content and the ratio of the nozzle opening diameter to the diameter of aggregates are the two key criteria determining the blockage of the printing nozzle during mortar extrusion. The authors state that in order to prevent aggregates from clogging the nozzle, the aperture must be at least four times larger than the largest particle size [10]. From a rheological standpoint, the pumpability and extrudability of the 3DPC are greatly affected by the size of the aggregates. For example, at the same aggregate volume, finer aggregates enhance yield stress and buildability while lowering extrudability if a screw extruder is employed [20]. Moreover, extremely fine aggregates demand greater water and cement content, hence raising the cost of concrete [10]. Because the decrease in maximum aggregate size leads to an increase in the overall surface area of the aggregate, which in turn requires more mixing water to cover all the particles adequately[45].

2.4. FRESH-STATE CHARACTERIZATION APPROACHES FOR EXTRUSION-BASED METHOD

Flowability

Flowability is the characteristic of a fresh mixture that ensures the effortless passage of the fresh mixture from the storage system to the nozzle. It is an indicator of how well a substance will not lose its form in the absence of external pressure [40, 46].

Pumpability

The ability of a print mix to be "pumpable" means that it can be pumped under pressure from a storage tank to the printing head without losing any of its original qualities during the process [20].

Extrudability

The extrudability of a print mix is defined as its capacity to be extruded without clog-

ging the nozzle and as a continuous filament leaving the nozzle of the printhead with a continuous material flow [20].

Buildability

Buildability refers to the ability of deposited material to retain its form under the steadily increasing load imposed by subsequent layers [47]. In general, buildability is defined as the greatest number of layers that may be constructed using a fresh mixture. In other words, the yield stress of the initial layer of printed concrete must be high enough to support the weight of the concrete and any subsequent layers that are deposited on top of it for the structure to be buildable [12, 32].

Initial setting time

The time it takes for the cement paste in concrete to begin hardening and developing stiffness is known as the initial setting time. In other words, the period between when water is poured into the cement and when the cement paste loses its flexibility. When the cement paste has totally lost its fluidity, that is when the setting time is said to be complete (final setting time). The hydration kinetics of the cement is shown by the initial and final setting times [40, 48].

Green strength development

Green strength refers to the strength that fresh concrete possesses at an early stage in its development. Before the initial setting, shape stability and resistance to vertical stresses from following layers of extruded concrete filaments depend on the mixture's green strength. Green strength can be evaluated anywhere from immediately after mixing to 4 hours afterward [31, 32, 49].

2.5. INTERLAYER BEHAVIOR

An additional essential part of the 3D printing of concrete is concerned with the material's anisotropic characteristics, which might alter depending on the printing route [10]. To put it another way, the structures that are formed of 3DCP are likely to have poor layer-to-layer (or interlayer) strengths as a result of the essentially layered deposition of the material [20]. In this case, aside from the compressive strength of the 3DPC matrix, the bond strength between layers is an important component influencing the mechanical characteristics of the hardened 3DPC matrix [20].

Mechanical compressive and tensile strength, for instance, may differ according to the orientation of the load, see Figure 2.11. In this case, applying a force in the z-direction results in a greater compressive strength, whereas applying a load in the y- or x-directions results in a greater tensile strength [10, 50].

Overcoming a weak junction between layers requires that the duration between printed filaments corresponds to the length of the filaments and the printing speed [51]. The strength of the bonds between the layers is greatly affected by this correlation. If the time period is too brief, filaments may not be able to withstand the load and the structure may collapse. Cold joints may occur between layers if the time delay is too lengthy, creating a weak inter-layer connection [10].

Most significantly, durability issues arise from poor interlayer joints. Weak joints allow water and other damaging substances to flow into the concrete via capillary action, reducing the printed concrete's durability and, if existent, its protective role with relation

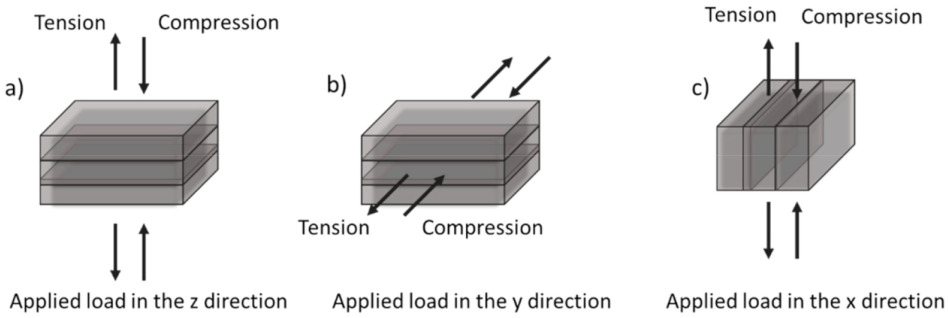

Figure 2.11: Modelling of tensile and compression loads applied to printed cementitious matrices in various directions, adapted from [10]

to the steel reinforcement [20, 52], see Figure 2.12.

Figure 2.12: Interfaces between printed concrete layers and cracks show evidence of local capillary suction, photo by V. Mechtcherine, adapted from [52]

This is why studying the impact of yield stress growth and the impact of various accelerator doses on the quality of the layer interconnecting is crucial. The insertion of the accelerator would result in a faster rate of structural development and the avoidance of collapse. On the other hand, it would result in restricted adhesion. In order to get an acceptable layer interlocking, we need to establish a maximum delay time t_{max} and maximum yield stress. The minimum duration between layers is denoted by the parameter t_{min} [4, 37], see Figure 2.13.

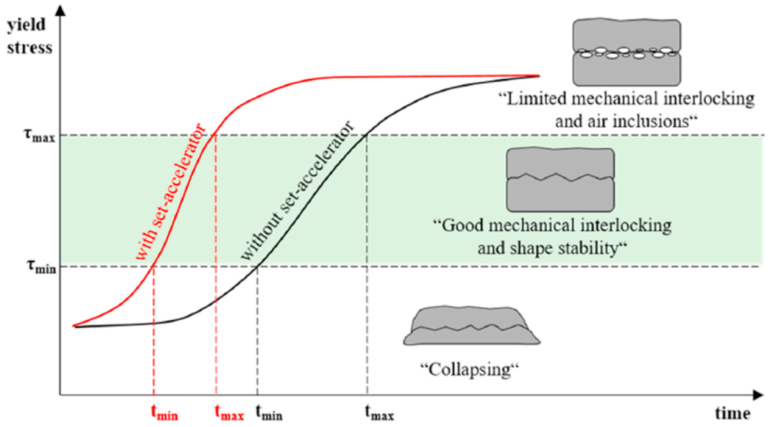

Figure 2.13: The evolution of yield stress over time with and without the accelerator, as well as the open window shown by t_{min} and t_{max}, adapted from [4]

The interface connection between two 3DCP layers is primarily influenced by two factors [4, 53]:

Mechanical effect: mechanical bonding relies exclusively on the physical properties of the layers, such as surface micro-roughness, coefficients of layer adhesion and friction [54], layer's age at the bottom, the time between layering [55], the printing speed, extrusion pressure [20], rate of surface water loss due to evaporation (ambient condition) [5, 20], nozzle geometry [20], the distance between the nozzle and depositing [5, 37, 56].

Chemical effect: There is chemical bonding if hydration and chemical bonding of particles occurs between two layers.

Consequently, efforts have been made to enhance the connection between consecutive layers by enhancing mechanical contact or spraying new cement paste in the interfacial zone before extruding the next layer [53], see Figure 2.14. However, more research into the causes of bond strength in 3D printed concrete is required [56].

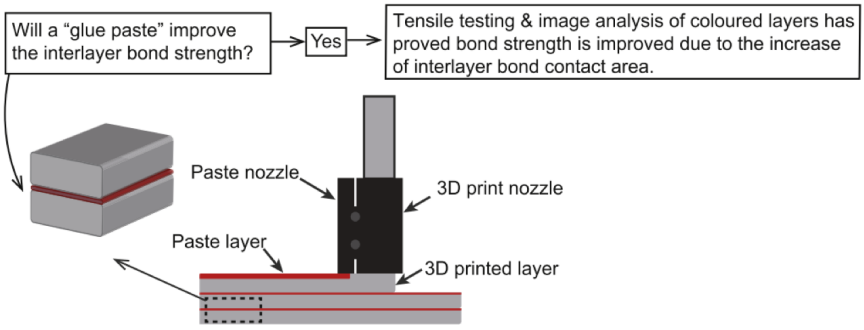

Figure 2.14: A diagram of the suggested twin-nozzle extruder that places the paste layer and 3D-printed layer, adapted from [53]

2.6. INFLUENCE OF NOZZLE GEOMETRY AND PRINTING NOZZLE SPEED ON LAYERS SHAPE

The ideal characteristics of an extrudable mixture are a low plastic viscosity and a high yield stress. The nozzle is crucial to the extrusion process because it controls how the concrete layer is created and how it looks while printed. To prevent the twisting of the newly deposited layer, the nozzle should be aligned perpendicular to the tool path. There are different nozzle orifice shapes utilized, including rectangular, square, round, and elliptical [20]. With a circular nozzle, one can easily print around any corners or changes in the angle of the structure you are making. A possible drawback of extruded layers is that they have a smaller contact area between each other, which might influence the stability of layers. Compared to circular or elliptical orifices, a square orifice offers better surface finishability and construction [20, 57].

In addition, the layer height and nozzle standoff distance are crucial characteristics. If the height of a nozzle (h) with a circular gap is more than or even equal to its diameter (d), the filament will have rounded sides and a rounded top. As a result, the link between the layers is weakened because of the reduced contact area, see Figure 2.15a. If h is less than d, the filament will be curved on the sides and flattened on the top because the nozzle flattens the surface, see Figure 2.15b. If h is significantly less than d, the concrete pushes the printed concrete back and to the sides, see Figure 2.15c. This design generates thicker layers and ripple-type defects at the filament's top. Rectangular nozzle openings make it feasible to get flat layers on top and sides even with a higher nozzle height than the nozzle edge (ne), as can be seen in Figure 2.15d. By setting the nozzle height less than the nozzle edge, thicker layers may be printed at the same speed to enhance strength, see Figure 2.15e. As with the circular opening nozzle, errors can also be observed if the nozzle height is significantly lower than the nozzle edge[10], see Figure 2.15f.

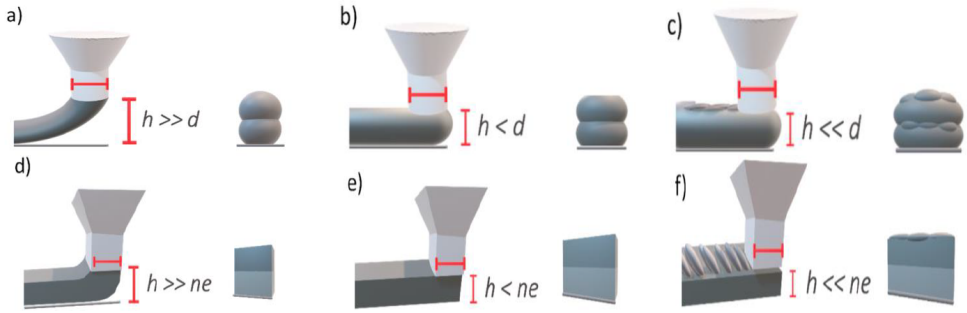

Figure 2.15: Filament shape governed by nozzle standoff distance and layer height, adapted from [10]

The speed of the printing nozzle and the rate at which material is flowing through it are other crucial parameters that may affect the final form of the layer. When the flow rate of the material is high or the speed of the printing nozzle is slow, the width of the layer is usually wider than the diameter of the nozzle, see Figure 2.16a. In such a case, the

printing process will be less capable of filling small spaces or steep curves. With middle flow and speed, the layer's thickness is like the nozzle's diameter, see Figure 2.16b. In this situation, the printing process can produce more accurate pieces. With low flow or high speed, the layer width is similar to or lower than the nozzle diameter, see Figure 2.16c. In this scenario, the stresses are partially balanced by the material's plastic viscosity, then the filament breaks [10].

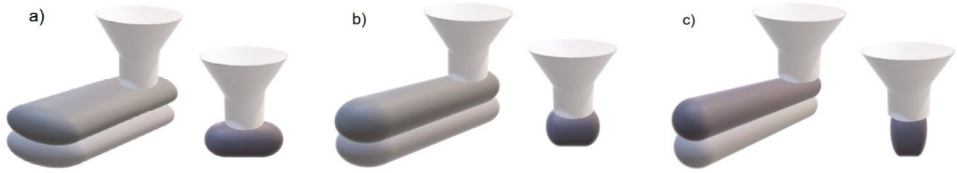

Figure 2.16: The effect of material flow rate and printing nozzle speed on layer thickness, (a) shape by high flow rate or slow speed of the printing nozzle (b) shape by middle flow and speed (c) shape by low flow or high speed, adapted from [10]

2.7. FAILURES THAT MAY OCCUR DURING AND AFTER 3DCP

During the manufacturing process of 3D printing, structures may collapse. As a result of an increasing dead weight loading, two mechanisms have been identified as the causes of collapse in the 3D printing of concrete: material failure and stability loss.

Loss of stability or elastic buckling (Figure 2.17) is described as a loss of balance of forces which causes uncontrolled displacements, whereas material failure or plastic collapse happens when the material strength is reached, leading in yielding, flow, or cracks [38, 58].

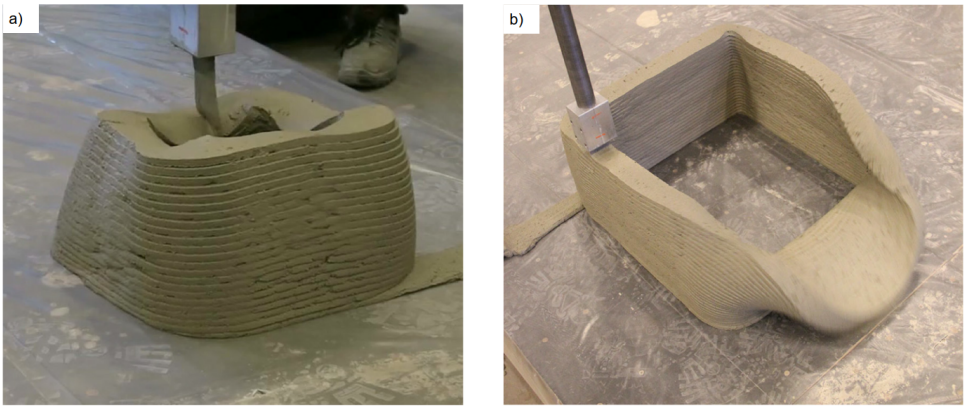

Figure 2.17: Collapse during manufacturing: a)plastic collapse (material failure), b)elastic buckling(stability failure) [58]

Other problems that may occur during and after printing include nozzle clogging, layers with varying widths and heights, cold joints, and cracking because of severe shrinking [10], see Figure 2.18.

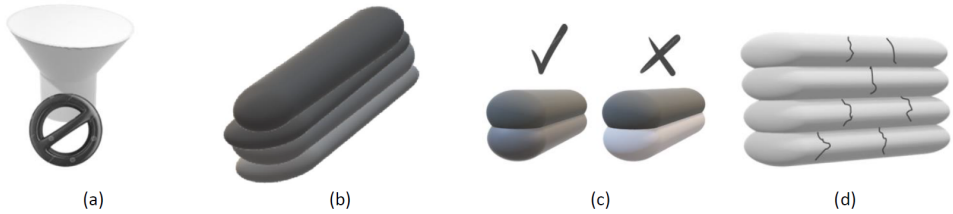

Figure 2.18: Possible printing and post-printing issues: a) nozzle clogging, b) variable-width and/or variable-height of layers, c) cold joints, d) cracking because of severe shrinking, [10]

Nozzle clogging

High aggregate content or particle sizes incompatible with the nozzle aperture, yield stress that is too high or plasticity that is insufficiently low, poor dispersion, or a high fiber content might cause nozzle clogging. By determining the appropriate size and aggregate content, using superplasticizers, or modifying the aspect ratio and fiber volume percentage by nozzle diameter, this issue might be resolved [10].

Layers with varying widths and heights

The reason for varying width and height of layers might be inadequate mixing, high concentration of superplasticizer, poor rheological characteristics, or low fiber distribution. Optimizing the admixture dose and using viscosity modifiers are the proposed solutions to the problems [10].

Cold joints

Possible causes of cold joints include large intervals of time between printed filaments (see 2.5), fast hydration, or water loss near the surface. The difficulties might be solved by optimizing the nozzle speed and mix design, or by reducing the accelerator content [10].

Cracking because of severe shrinking

Possible causes of shrinkage-related cracking include exposure to inappropriate conditions, such as hot weather or dry air, as well as a high cementitious binder content and low aggregate content [20]. Isolating the building site, redesigning the concrete mixture, or using shrinkage-reducing or compensating admixtures might fix the problems [10].

2.8. 3DCP SUPPLEMENTARY CEMENTITIOUS MATERIALS

The development of sustainable cementitious materials for use in 3DCP has been the subject of several recent research. Various strategies are utilized, such as substituting ordinary Portland cement (OPC) with supplementary cementitious materials (SCMs), partly replacing natural aggregate with recycled aggregate, or using other industrial byproducts. OPC production requires resources and energy and emits a considerable amount of greenhouse emissions, which harms the environment. 5–7% of worldwide anthro-

pogenic CO_2 emissions are attributable to the cement sector. Many of the cementitious materials used in 3D printing might need far more OPC than is typically used in conventional cast concrete. The percentage of OPC in most 3D printing cementitious materials is around 20 wt%, see Figure 2.19. Taking into account a typical unit weight of 2200 kg/m^3 for a concrete mixture, the majority of printed mixtures would need to contain a minimum of 330 kg/m^3 of OPC (Ordinary Portland Cement) [32].

The ratio of aggregate mass to binder mass, as seen in Figure 2.19, is less than 2 in the majority of printable mixes. While it is larger than 8 in low-strength mold-cast concrete (with a compressive strength of fewer than 20 MPa after 28 days), about 5 in moderate-strength mold-cast concrete (compressive strength of 20-40 MPa at 28 days), and about 3- 3.5 in high-strength mold-cast concrete (a compressive strength greater than 40 MPa after 28 days) [32, 59], see Figure 2.20.

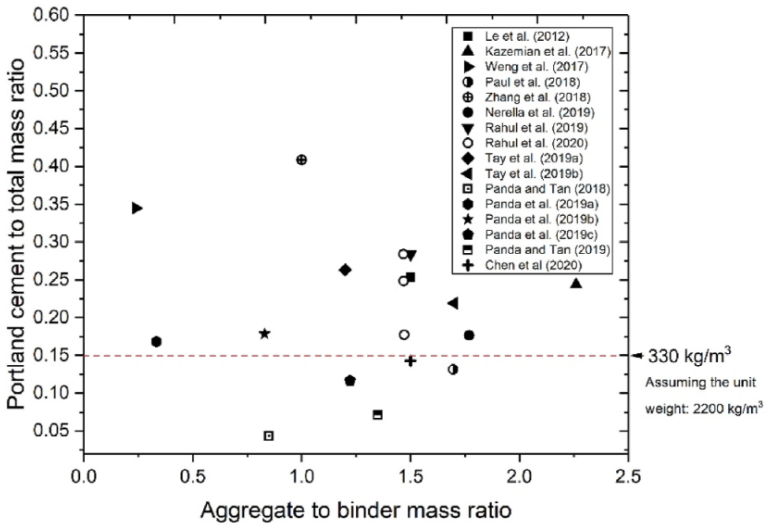

Figure 2.19: Literature analysis of several 3D printed mortars' OPC content and aggregate to binder weight ratio, adapted from [32]

For a number of reasons, 3DCP frequently calls for paste mixtures that are highly Portland cement enriched. Most digital concretes have a maximum aggregate size of 4 mm or smaller since pumping is involved in digital fabrication, which makes processing coarse aggregates more difficult. Moreover, the aggregate size must be reduced even further so that the concrete can be transported via an extruder. In addition, 3DCP demands a quick vertical building rate or a high "buildability," which correlates to a very rapid hydration. These factors cause the paste volume and cement content to rise. For all of these reasons, most digital concrete mix designs end up using a huge amount of Portland cement, which results in a big environmental impact [24].

In 3DCP, producing low OPC-content cementitious materials may be accomplished in two ways:

one option is to replace a large amount of OPC with supplemental cementitious ma-

	Low-strength (kg/m^3)	Moderate-strength (kg/m^3)	High-strength (kg/m^3)
Cement	255	356	510
Water	178	178	178
Fine aggregate	801	848	890
Coarse aggregate	1169	1032	872
Cement paste proportion			
percent by mass	18	22.1	28.1
percent by volume	26	29.3	34.3
Water/cement by mass	0.70	0.50	0.35
Strength, MPa	18	30	60

Figure 2.20: Material proportions often used in concrete of various strengths, adapted from [59]

terials (SCMs); another is to increase the aggregate proportion and decrease the binder quantity while keeping the binder composition the same. This study concentrated on the cement substitution approach. By several research teams, the binder of printing concrete was modified to partially replace OPC in 3D printing cementitious materials by fly ash, silica fume, blast furnace slag, and limestone see Figure 2.21. The total quantity of these alternatives to cement in binders ranges between 10 and 45 percent by weight. In the available printing concrete concepts, OPC still has the greatest binder mix concentration. The original motivation for adopting these SCMs was to increase packing density, cohesion, and flow consistency in printed mixes. The important point here is that the rheological properties of fresh mixes can be drastically changed by the incorporation of SCMs. However, various SCMs may have different effects on fresh characteristics [32], see Figure 2.22.

Cementitious binder content (by weight)
OPC (90%) and silica fume (10%)
OPC (70%), fly ash (20%) and silica fume (10%)
OPC (55%), fly ash (22%) and silica fume (23%)
OPC (60–67%), limestone filler (17–20%) and silica fume (17–20%)

Figure 2.21: The percentage of typical cementitious binders in 3D-printed concrete, adapted from [12]

Using a high volume of SCMs to replace more than 45% of OPC is not a revolutionary CO_2 reduction technique in the traditional cement technology, although it is not commonly used in 3DCP at the moment, see Figure 2.21. The restrictions for developing 3D-printed concrete based on SCMs are as follows [12]:

- Few investigations have explored low CO_2 3D printing concrete binder compositions. Therefore, there is insufficient data on how the substitution of different SCMs in 3D printing concrete influences its fresh and hardened qualities [12].
- 3DCP is a revolutionary technology. At the moment, there are no internationally

	Fly ash	Silica fume	GGBS	Limestone	Calcined clay
Material type	By-product	By-product	By-product	Natural material	Calcined natural SCMs
Morphology	smooth surface and rounded grains	Rounded particle	Smooth, fine granules	Rough, irregular form	Rough, layered structure
Fineness [μm]	10-150	0.01-0.5	3-100 (close to cement grains)	Similar to/finer than cement particles	Except SF, finer than other SCMs.
Chemistry	Si–Al–O	Si–O	Ca–Si–Al–Mg–O	CaCO3	Si–Al–O
Maximum proportion of binder mass in printable mixes	80%	20%	85%	55%	40%
Rheological effects	(1) Ball-bearing effect improves workability. (2) Dilution's influence on cement flocculation (by high-volume replacement).	(1) It might decrease workability. (2) It might increase the flocculation of cement particles.	(1) The workability can be improved by GGBS with a smooth particle surface and low reactivity. (2) GGBS with a high specific surface area and reactivity may have a negative impact on workability.	(1) Limestone with larger particle size might increase workability. (2) Ultrafine limestone particles might induce the opposite effect.	(1) It might diminish the workability. (2) It might increase the structural build-up.
Total estimated production [Mt/year]	700–1100	1–2.5	300–360	Abundant	Abundant

Figure 2.22: Various SCMs' material properties, adapted from [32]

accepted standards or guidelines for 3D printing concrete. Consequently, the development and evaluation of more specific and efficient test techniques for assessing the fresh and hardened characteristics of 3D-printable concrete are required [12].

- Particle size distribution, binder-to-aggregate proportion, admixture addition, water-to-binder proportion, and fiber-reinforcement dose are only a few of the numerous factors outside the binder mix that may influence the fresh qualities of 3D printing concrete. Consequently, using different types of SCMs to make a low-CO_2 printed cement becomes increasingly complex and challenging [12].
- The fundamental difficulty in using typical SCMs for long-term applications is that their production and availability definitely decrease. For instance, only 1-2.5 Mt of SF are produced annually as a whole, or the amount of slag is 5–10% of OPC. Reduced iron production as a result of higher steel recycling has a significant impact on the quantity of slag produced. On average, 700–1100 Mt of FA are produced per year, moreover not all FA is good for cement owing to quality. Coal-fired power plant retirement and closure in numerous nations also pose a danger to the FA supply chain. Finding alternative SCMs looks to be a vital issue if SCM-based cementitious materials are to be supplied on a consistent basis. Calcined clay and limestone are prominent as the most suitable substitutes due to their widespread availability [12, 32].

Over the past decade, calcined clay's potential as an SCM for concrete has garnered a lot

of interest. The advantages of substituting OPC with calcined clay are [32, 36]:

- The raw materials are abundant globally.
- Compared to the manufacturing of clinker, the calcination process uses less energy and produces less carbon dioxide. In other words, manufacturing calcined clay requires a substantially lower burning temperature (about 700-850 °C compared to 1450 °C for clinker), resulting in much lower CO_2 emissions (0.25 to 0.37 kg) per kilogram of calcined clay produced than for one kilogram of OPC (about 0.9 kg of CO_2) [32, 36].

Since limestone powder is used as a filler in binding material, the fineness and roughness of limestone particles might influence the rheology of the mixture. Moreover, the packing density and the amount of water and superplasticizer needed are both significantly influenced by limestone powder parameters. Limestone powder with equivalent or coarser fineness than cement may increase workability by lowering yield stress and plastic viscosity. Ultrafine limestone, on the other hand, can increase yield stress and plastic viscosity thanks to its high adsorption of water and superplasticizer. In other words, the decreased particle size of limestone or increased volume of limestone can both improve and speed up cement flocculation.

The filler effect is the principal effect of limestone addition on cement hydration by increasing nucleation sites offered by the limestone surface [32, 60]. The filler effect describes how the physical presence of supplementary cementitious materials affects the hydration of the clinker component. This effect is especially important at the early age of hydration when the microstructure is quickly growing and the supplementary cementitious materials are not yet reacting. Calcium silicate hydrate (C-S-H) is the most common type of hydrate and it is responsible for the link of cement grains, which causes the cement to set and get stronger [60].

In order to prove the filler effect, K. Scrivener et al. [60, 61] by examining the calorimetry curves at an early age of plain cement and its combination with quartz or slag, observed that the reaction of cement is accelerated in both situations when it is combined with quartz or slag. In this investigation, several combinations were utilized, including reference cement (black graph in Figure 2.23), then it was blended with 40% quartz (blue graph) and 40% slag (orange graph). The selection of slag and quartz was based on their similar particle size distribution. The enhancement of hydration will underline that it is a purely physical impact since quartz and slag are nonreactive at an early age. It was tested that even controlling the degree of reaction of quartz after 28 days, hardly any reaction was observable. As can be seen in Figure 2.23, after a period, the slag reactivity begins to increase, indicating that this is the slag itself reacting.

Limestone, as mentioned by K. Scrivener et al. [60, 61], affects the nucleation of C-S-H differently than the other SCM-cements, leading to a greater acceleration and also a shorter duration of induction. Within 4 hours of hydration, this reaction is also clearly visible in the micrographs as shown in Figure 2.24. For example, after 5 minutes of hydration, the surfaces of the limestone and cement are comparable (Figure 2.24a, d). while, the limestone surface is entirely covered with nuclei after 90 minutes (Figure 2.24e), which is not observed for other SCMs. Figure 2.24f depicts limestone grain after 4 h, with

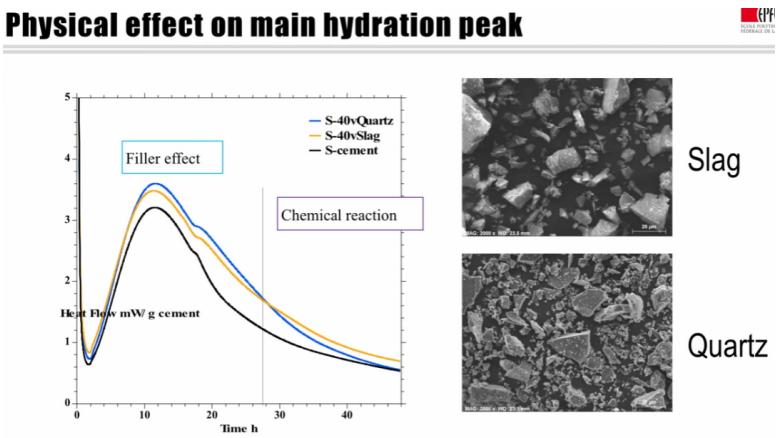

Figure 2.23: Physical effect of slag and quartz on main hydration peak, adapted from [61]

C-S-H needles growing thickly perpendicular to the surface, whereas C-S-H on cement grains exhibits diverging sea anemone shape. These results demonstrate the possible advantages of the limestone filler effect in cement hydration.

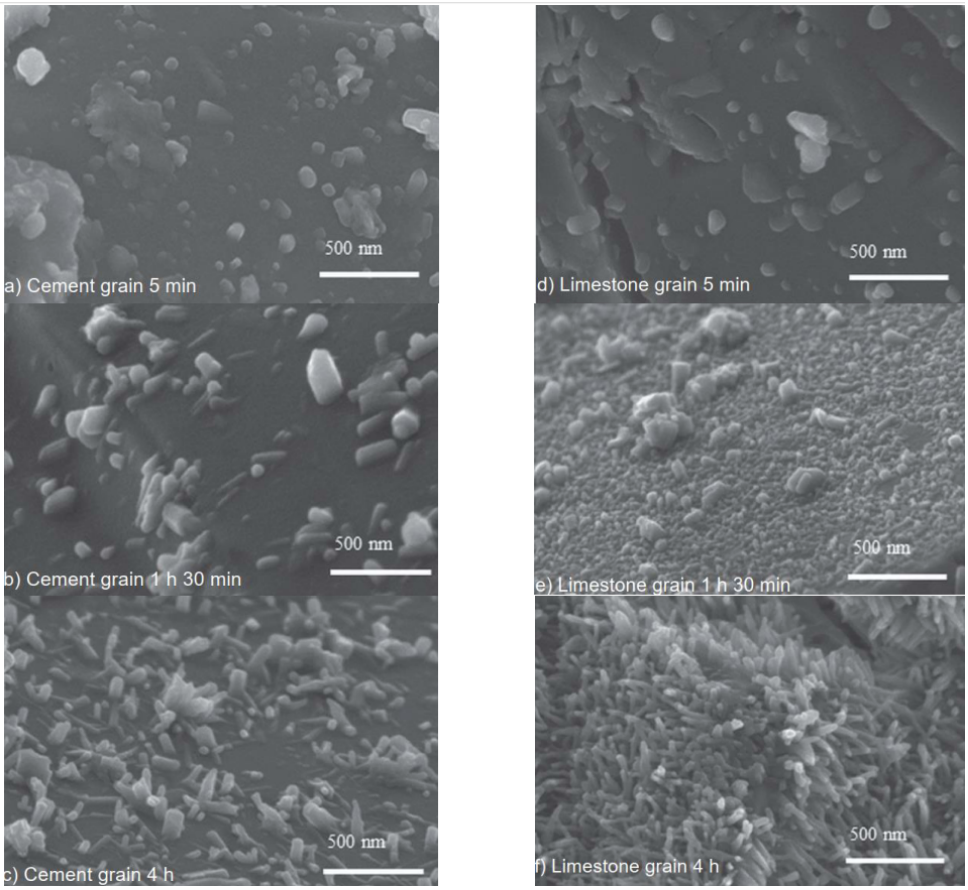

Figure 2.24: Micrographs in limestone and cement paste, adapted from [60]

2.9. CLASSIFICATION OF ACCELERATOR

Accelerating admixtures impact the reaction rates between cement and water, resulting in an increase in the total hydration rate. Therefore, accelerators in concrete reduce the amount of time needed for the material to set and/or enhance the rate at which strength is developed [62]. Accelerating the reaction of concretes might be useful in particular situations, such as urgent repair work, in cold climates, or the production speed in a precast concrete plant to remove the formworks as early as possible and so on [10]. For 3D printing, accelerators are particularly effective for small-scale projects with shorter print path lengths, resulting in a shorter time interval between printed layers. Their influence on strength and rheology is determined by their chemical composition, dose, the chemical composition of the binder, and ambient temperature [10].

To achieve the necessary early strength development, several accelerators have been designed, which may be roughly categorized as follows [37, 63]:

- categorization according to action: either physical or chemical action
- categorization based on the composition: inorganic or organic salts
- categorization according to the effect: improving setting or hardening
- categorization based on the presence of chloride: accelerators with chloride or without chloride.

Categorization based on the physical or chemical action

Cement hydration may be accelerated in a variety of methods, which can be categorized into physical and chemical processes. Chemical action is the term for admixtures that behave chemically; their effectiveness is directly correlated with the properties of cement and other additives used in the combination, for instance, inorganic or organic salts. The physical action relates to the substance in which their addition significantly enhances the surface accessible for subsequent hydrate precipitation, resulting in a quicker acceleration period, such as limestone filler and C–S–H seed [37, 49].

Categorization based on the inorganic or organic salts

It has been found that several inorganic and organic chemicals enhance the hydration of Portland cement [62]. Commonly, accelerators are classified as either inorganic or organic salts. Typical examples of inorganic salts are alkali and alkali earth salts of chlorides (Cl^-), nitrates($NO_3{}^-$), nitrites ($NO_2{}^-$), thiocyanates (SCN^-), and others [37]. See [37, 62] for a more in-depth introduction to the categorization of the accelerators based on the inorganic or organic salts.

Calcium chloride ($CaCl_2$) has shown to be one of the most cost-effective and efficient inorganic salt accelerators, and for many decades, it has been frequently utilized. Both the setting and hardening of Portland cement can be accelerated by $CaCl_2$. Calcium chloride's mechanism is mostly concerned with nucleation and dissolution rates. $CaCl_2$ can speed up the C_3A-gypsum reaction, which reduces the setting time. Also, $CaCl_2$ can promote C–S–H nucleation, resulting in accelerating the induction time. Nevertheless, it must be noted that the use of chloride-based admixtures is prohibited by a number of countries due to the possibility of reinforcement corrosion [63, 64]. Therefore, using it in steel-reinforced concrete is no longer advised. Currently, the majority of commercial accelerators for regular concrete comprise sodium and calcium salts of nitrate, nitrite, and/or thiocyanate.

Calcium nitrate has a less accelerating impact than calcium chloride ($CaCl_2$) because $NO_3{}^-$, has a smaller accelerating effect than Cl^-. Calcium nitrate has a similar mechanism as calcium chloride for accelerating [37]. Since the late 1960s, calcium nitrite ($Ca(NO_2)_2$) has likely been the most used non-chloride setting accelerator in the United States. In comparison to nitrates, nitrites have a significant commercial disadvantage. Nitrites are poisonous and ecologically unfriendly, despite the fact that calcium nitrite appears to be the most effective non-chloride additive to date [62].

Calcium nitrate and calcium nitrite are less efficient than $CaCl_2$ on setting and hardening, as evidenced by the isothermal conduction calorimeter curves given in Figure 2.25 that compare the effects of different calcium salts on the rate of hydration of C_3S. The values on the graph represent the slope of the temperature-time curves from the

end of the dormant period to the maximum temperature, compared to the untreated C_3S, which was assigned a value of 1.0.

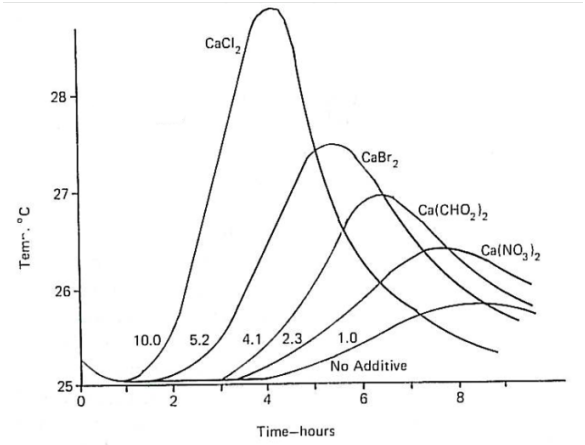

Figure 2.25: Isothermal conduction calorimeter curves for C_3S in the presence of different calcium salts, adapted from [62]

Categorization based on the improving setting or hardening

The standard BS EN 934-2 [65] makes a distinction between accelerators that speed up the setting time and those that speed up the hardening time. Setting accelerators accelerate the transition from a flexible to a rigid state, whereas hardening accelerators accelerate the development of early strength in concrete, with or without influencing setting time. Accelerators of the setting and hardening types can be identified by the mineral phase they influence. Accelerators for setting have a significant impact on the C_3A phase by encouraging the C_3A-gypsum reaction. Accelerators that cause hardness, work primarily on the C_3S phase, leading to the production of C-S-H gel [37]. For instance, both the setting and hardening of OPC are sped up by the addition of calcium chloride and calcium nitrate.

The rate of hydration, which is often monitored with a calorimeter, may also be used to examine the setting and hardening accelerator. A setting accelerator produces heat before the reference (cement paste without accelerator), but the slopes of the curves are the same or dQ/dt is the same for both. The heat generation rate of a hardening accelerator begins simultaneously with that of the reference but has a steeper slope or greater dQ/dt [62], see Figure 2.26.

Penetration tests (Vicat test) are commonly used to determine the influence on the setting, which is typically characterized by the setting times. The initial setting time is when the concrete begins to lose its flexibility and the final setting time is when the concrete completely loses its plasticity [37].

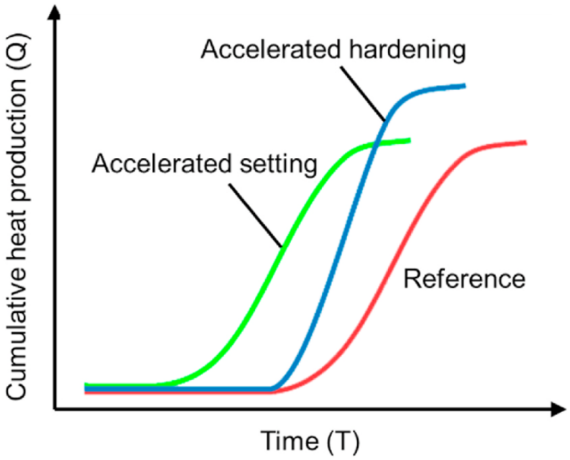

Figure 2.26: The impact of setting and hardening accelerators on the rate of heat, adapted from [37]

Categorization based on the presence of chloride

It should be noted that although the presence of chloride (Cl^-) ions might enhance concrete strength, they also substantially increase the potential of corrosion of steel reinforcement in concrete [63], see Figure 2.27. In other words, chloride-based accelerators have a low cost-to-performance ratio, but they induce severe corrosion. Consequently, as stated, several regulations prohibit the use of chloride-based accelerators. Accelerators that do not include chloride have no or little corrosion risks. However, they have a high cost-to-performance ratio. Factories of admixtures have struggled for years to create chloride-free accelerators with low cost and great performance [62]. Calcium chloride and calcium nitrate are, respectively, examples of chloride-based and chloride-free accelerators.

Figure 2.27: An example of calcium chloride effect on the reinforcement, adapted from https://fritzpak.com/

3

PUMPABLE MIXTURE DEVELOPING

3.1. INTRODUCTION

This chapter's purpose was to develop pumpable cementitious and accelerator slurry mixtures for use in the next chapter. The main idea of this study was to examine the impacts of the accelerator on two distinct ternary cementitious-based materials when combined with an SCMs-based accelerator slurry material, with a volume ratio of 1:1, for their buildability in 3DCP. Cement and SCMs-based mixtures were:

- Portland cement (PC), limestone, and calcined clay (LC^3-based cementitious material)
- Portland cement (PC), limestone, and slag (Slag-based cementitious material)
- Limestone (Limestone-based accelerator slurry)

This research investigates LC^3-based and Slag-based cementitious materials since the use of plain cement is not preferred for the long-term development of 3DCP technology. Since LC^3-based and slag-based cementitious material are ternary cement systems, then a portion of the Portland cement is replaced by the SCMs-based mixture, and therefore less Portland cement is required in the LC^3-based and slag-based cementitious material system [31]. In addition to being sustainable, adding limestone and calcined clay to the cementitious mixture may have a good impact on the cementitious materials' qualities due to their filler effect. The filler effect is a phenomenon caused by introducing a material that does not react at first but yet provides extra nucleation sites for hydrate phases. Furthermore, it increases w/c, which improves long-term hydration by providing more space for hydrates to precipitate [66], see 2.8.

At the end of this chapter, three pumpable mixes will be recommended, including two pumpable mixtures from LC^3-based and slag-based cementitious material, and one from limestone-based accelerator slurry, and only the proposed combinations will be employed further with calcium nitrate for the duration of the investigation.

3.2. MIXTURES

In this research, three different mixtures were tested. The binder for LC^3-based cementitious material consists of 55% PC, 15% limestone, and 30% calcined clay. The binder for slag-based cementitious material consists of 55% PC, 15% limestone, and 30% slag. As a binder for limestone-based accelerator slurry, just limestone was employed. For all three mixes, the mass ratio of binder to aggregate was 1 and the water-to-binder ratio was 0.3. Figure 3.1, Figure 3.2, and Figure 3.3 display the mixtures of LC^3-based cementitious material, slag-based cementitious material, and limestone-based accelerator slurry. For LC^3-based mixtures, the superplasticizer dose ranged between 0.5% and 1% of the binder's mass. The superplasticizer dose for slag-based mixtures varied from 0.2% to 0.6% of the binder's mass. Limestone-based accelerator slurry had a variable accelerator dose of 0%–14% of the cement weight.

Adjustments were made to the water content of all limestone-based accelerator slurry. For instance, by adding a 7% accelerator to the mixture, the amount of water decreased by 38.5 grams per liter, hence the total amount of liquid available in the mix was (300 - 38.5) + (550 x 0.07) = 300 grams per liter. If this step is omitted, the amount of available water in the mixture could increase, which might have a detrimental impact on the initial setting time, flowability of the mixture, and mechanical performance. Moreover, the purpose of this research was to examine the influence of varied dosages of the accelerator on the buildability of mixes containing fixed amounts of the key components (cement, SCMs, aggregate, and water) in the 3DCP mix.

To acquire the pumpable mixture from each of the above-mentioned mixes, first, the flowability of each mixture was evaluated, and then only one flowable mixture from each mix was chosen for further pumpability and flow curve testing. Obtaining pumpable mixtures is covered in further depth in the following sections.

The materials listed below were utilized during this whole investigation.

- CEM I 52.5R Portland cement
- Calcium nitrate ($Ca(NO_3)_2$) accelerator (Versneller HA-20 CON. 50% VS, CUGLA).
- Poly carboxylic Ether-Based superplasticizers (MasterGlenium51)

Mix	Binders			Aggregates				
LC3-based	PC	Limestone	Calcined clay	Sand (0.125-0.25mm)	Sand (0.25-0.5)	Sand (0.5-1)	Water	SP
LC3-0.5SP	550	150	300	250	550	200	300	0.5%
LC3-0.6SP	550	150	300	250	550	200	300	0.6%
LC3-0.8SP	550	150	300	250	550	200	300	0.8%
LC3-1SP	550	150	300	250	550	200	300	1%

Figure 3.1: LC^3-based cementitious material mix design for flowability test [kg/m^3]

Mix	Binders			Aggregates			Water	SP
Slag-based	PC	Limestone	slag	Sand (0.125-0.25mm)	Sand (0.25-0.5)	Sand (0.5-1)		
Slag-0.2SP	550	150	300	250	550	200	300	0.2%
Slag -0.3SP	550	150	300	250	550	200	300	0.3%
Slag -0.4SP	550	150	300	250	550	200	300	0.4%
Slag -0.6SP	550	150	300	250	550	200	300	0.6%

Figure 3.2: Slag-based cementitious material mix design for flowability test [kg/m^3]

Mix	Binder	Aggregates			Water	Acc
Limestone-based Acc slurry	Limestone	Sand (0.125-0.25mm)	Sand (0.25-0.5)	Sand (0.5-1)		
Limestone-0ACC	1000	250	550	200	300	0%
Limestone-7ACC	1000	250	550	200	262	7%
Limestone-14ACC	1000	250	550	200	223	14%

Figure 3.3: Limestone-based accelerator slurry mix design for flowability test [kg/m^3]

3.3. MATERIAL PREPARATION

During the investigation, a HOBART mortar mixer, which included three fixed speeds, was utilized to make mortar mixes. This mixer has a capacity of 4.7 to 7 liters and is perfect for preparing mortar mixture in low to moderate volumes. The following procedures were used to prepare the fresh mixtures for the flowability, pumpability, and flow curve tests:

0 min | 0 min - 2 min | 2 min – 4 min | 4 min – 5 min | 5 min – 7 min

0 min: The exact weighing of the necessary materials

0 min – 2 min: Mixing at a low speed (speed1) to create uniformity in dry ingredients

2 min – 4 min: Pour the liquid gently into, water and the superplasticizer for cement-based mixtures, water and the accelerator for SCMs-based mixture

4 min – 5 min: Stop and scrape the bowl's bottom and sides by hand

5 min – 7 min: Mix at fast speed (speed2) to ensure that all of the components are thoroughly combined, and then begin the test

3.4. METHODOLOGY

A flowability test was conducted on LC^3-based and slag-based cementitious materials with varying doses of superplasticizer, and then a flowability test was performed on a limestone-based accelerator slurry using varying doses of the accelerator in order to find the easily flowable mixtures.

According to Tay et al. [67], the flowability of fresh mixtures may be assessed using field-friendly techniques like the slump and slump-flow tests. The authors claim that a slump flow value between 150 and 190 mm produces a smooth surface with excellent buildability, moreover, the 3DCP mixes have acceptable flowability when the slump-flow value is between 130 mm and 210 mm. Because mixes with a slump-flow value under 130 mm are too rigid to be adequately pumped, while mixtures with a slump-flow value over 210 mm are too fluid to create a cohesive printed filament. As a result, the top and lower limits for the flowable mixture were selected at 130 and 210 mm, respectively. Only one of the tested combinations was chosen based on the type of cementitious material, and one for limestone-based accelerator slurry. Therefore, after finding the flowable mixture for each cement-based mixture and accelerator-based slurry, they were tested for pumpability and flow curve.

To ensure that the chosen flowable mixtures could be pumped without any hindrance and the flow rate of mixtures during pumping will stay unchanged, a pumpability test was conducted**.** Subsequently, the flow curve test was utilized to study the rheological behaviors of the mixtures. After confirming the mixtures with all three of the abovementioned tests, the pumpable mixtures with the optimal superplasticizer and accelerator dose were offered in 3.6.

3.4.1. FLOWABILITY TEST

In line with ASTM C1437–15, slump flow tests were carried out to investigate changes in the flowability of various mixtures after different resting intervals [36]. This test apparatus includes a mini Hagerman mold and a table. The mini Hagerman mold utilized in this test had an upper internal diameter of 7 cm, a below internal diameter of 10 cm, and a height of 6 cm; the diameter of the table was 30 cm. Before starting the test, the mold was oiled and put in the center of the flow table. It was lubricated to reduce friction between the specimen and the mold's surface. After half of the mold was filled with the fresh mixture, it was compacted roughly 20 times with a wooden stick. The second half of the mold went through the same process, a trowel was used to remove the extra material gradually, see Figure 3.4a. After removing the mold by carefully raising it vertically, see Figure 3.4b, the sample's height was recorded. Following this, the table was dropped 25 times in 25 seconds. The diameter of the spread was determined by measuring it in four perpendicular directions, and the average value was then determined, see Figure 3.4c. This test was conducted on each mixture, for each material age between 10 and 60 minutes, with 15- to 20-minute intervals. To avoid water evaporation, the fresh ingredients were packed in a plastic bag during the test [36].

(a) (b) (c)

Figure 3.4: Slump and slump flow test setup, (a) ready mold for the slump test, (b) before vibration (slump test), (c) after 25 droppings (slump flow test)

3.4.2. PUMPABILITY TEST

The pumpability test was carried out using a commercial PFT SWING-M conveying pump, as shown in Figure 3.5. This pump was equipped with a V-shaped material hopper and a screw extruder with a capacity of 38L and maximum aggregate size suitability of 3 mm and adjustable pumping speed ranging from 1 to 10 (20 RPM up to 200 RPM).

The freshly produced mixture was poured directly into the hopper and then pushed through a rubber hose, which had a conveying power of 9 L/min, via a screw extruder located at the bottom of the hopper, see Figure 3.6a, b. Throughout all of the pumping tests, the hose was held in an untwisted position then the pump test was carried out at five different pumping speeds ranging from 1 to 5. For each speed, the discharge material was collected in a plastic bag within ten seconds (Figure 3.7), and for each speed, two experiments were performed. On a scale, the mass of five gathered specimens was determined separately. In the end, the average mass was utilized to compute the material flow rate (L/s) at each pumping speed [31, 36].

Figure 3.5: A PFT SWING-M conveying pump and the hose

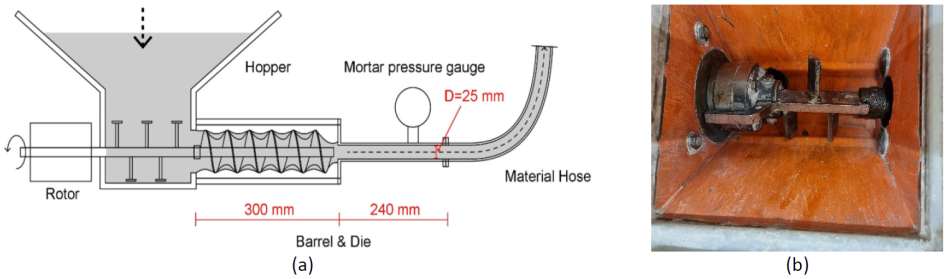

Figure 3.6: (a) concept representation of the PFT Swing-M conveying pump [36]- (b) screw extruder

Figure 3.7: Collecting of the material in a plastic bag

3.4.3. FLOW CURVE TEST

The rheological properties of the mixtures were investigated by calculating the flow curve at a constant temperature of 20 ± 0.5°C, using an Anton Paar MCR 102 rheometer, as shown in Figure 3.8. A four-blade vane and a cylindrical cup (with h= 25.8 mm, R1= 17.61 mm, and R2= 35 mm) was utilized to impart torque to fresh mixes. As part of the rheological evaluation process, a cage was inserted into the rheometer cup to reduce the impact of wall slippage, or the distancing of the concrete from the cup's walls [68]. After mixing the material in the Hobart mixer, it was poured into the rheometer cup, and the vane was then dipped in the fresh paste in order to run flow curve experiments. The top of the rheometer cup was covered with a plastic lid to prevent water evaporation [69].

A high-velocity pre-shear was used to break down the structural buildup prior to beginning the flow test. Accordingly, the shear rate was raised from 0 to 60 1/s in 90 s, followed by a resting interval to disperse the pre-shear residual stress [69]. After pre-shearing the mixture, a constant shear rate of 60 1/s for 60 s was applied. The shear rate was then lowered stepwise to zero. In order to determine the flow curves, the response

was collected every second, and the average value of the last 30 data points was recorded in each step as the equivalent shear stress. There were three separate runs of each experiment to assure consistency. For each mixture, a representative graph that provides the closest result to the average of the three experiments is provided.

Based on the findings of Le et al.[70] and several other researchers[71, 72], the investigation into achieving an ideal mixture for 3D concrete printing reveals that the dynamic yield stress of extrudable concrete typically falls within the range of 300 to 900 Pa, while the plastic viscosity ranges from 21.1 to 38.7 Pa.s. To ensure the stability of the printed layer's shape and prevent excessive spreading after extrusion, it was recommended to maintain a minimum value of 300 Pa.
As demonstrated in the equation below, the Bingham model was utilized to compute the dynamic yield stress and plastic viscosity of the mortars [69].

$$\tau = \tau_0 + \mu * \dot{\gamma}$$

Where:
τ : Shear stress [Pa]
τ_0 : Dynamic yield stress [Pa]
μ : Plastic viscosity [Pa * s]
$\dot{\gamma}$: shear rate [1/s]

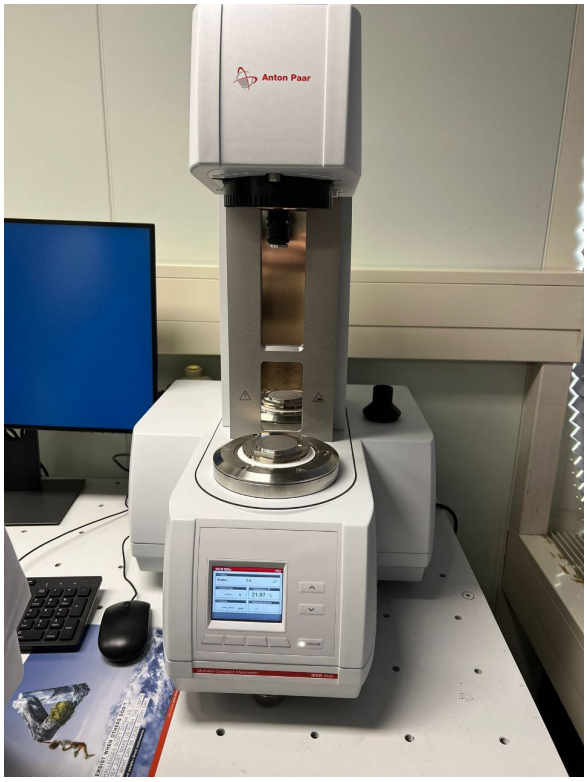

Figure 3.8: Anton Paar MCR 102 rheometer at TU-Delft

3.5. RESULTS AND DISCUSSION

3.5.1. FLOWABILITY

There were two mixtures of LC^3-based cementitious material with flow diameters within the desired limit (130 mm- 210 mm), according to Tay et al.[67] advice, including LC^3-0.5SP and LC^3-0.6SP, see Figure 3.9. Upon seeing that a concentration of 0.5% superplasticizer made the mixture too rigid to be pumped, the author settled on a 0.6% superplasticizer mixture for future study. The investigated LC^3-based cementitious material mixtures' slump flow outcomes are illustrated in Figure 3.9. The purpose for analyzing the mixture flowability behavior within 1h is because a hopper's capacity is 38L, then 1h is the maximum time required to pump all of the material within the hopper.

There was one combination (slag-0.2SP) for slag-based cementitious material whose flow diameter fell within the specified range. However, the flow curve test for this mixture yielded unfavorable results; hence, a mixture of slag-based cementitious material containing 0.3% superplasticizer was chosen for future exploration. The slump flow results of the examined slag-based cementitious material mixes are displayed in Figure 3.10.

For limestone-based accelerator slurry, there were two mixtures whose flow diameter fell within the predetermined range, including limestone-7ACC and limestone-14ACC. Whereas the flowability test is not the only test that can be utilized to identify the final optimal dosage of the accelerator. There are a number of other essential tests, such as the initial setting time, buildability, and compressive strength test. For all of the mentioned experiments, limestone-7ACC ultimately yielded the most encouraging results. The causes are addressed in subsequent chapters. Figure 3.11 depicts the studied slumps flow outcomes of limestone-based accelerator slurry mixtures.

Although there is no hydration-type chemical reaction between water and limestone filler, raising the dosage of the accelerator results in a smaller slump diameter. This can be explained by either the evaporation of water during the test or a portion of the water being sucked up by aggregate or limestone or even the viscosity of the mixture can be increased by increasing the concentration of ions in the pore solution. The quantity of water suction may be calculated by measuring the absorption capacity of dry ingredients, which was out of the scope of this study.

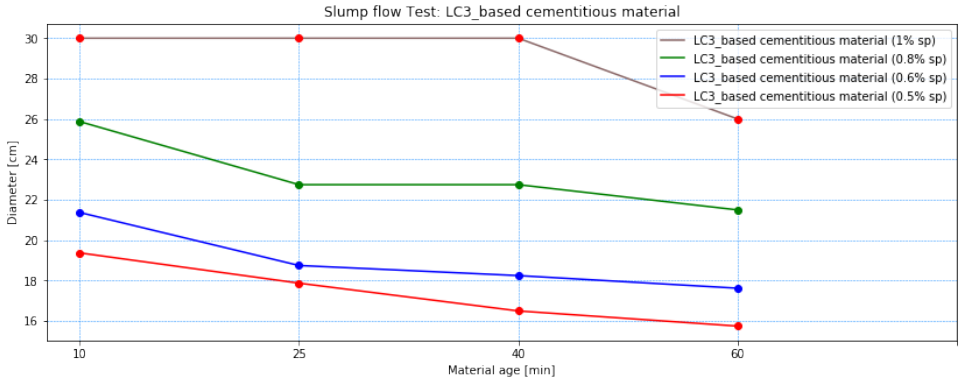

Figure 3.9: Slump flow diameter of LC^3-based cementitious material with various superplasticizer dosages

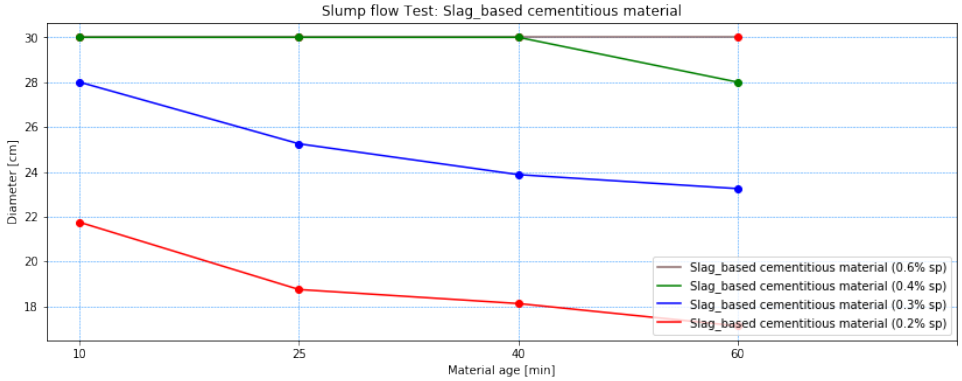

Figure 3.10: Slump flow diameter of slag-based cementitious material with various superplasticizer dosages

3.5.2. PUMPABILITY

Pumpability tests were performed on three different mixtures: LC^3-0.6SP, slag-0.3SP, and limestone-7ACC. The growth in the material flow rate that can be seen in Figure 3.12 was linear with the increase in the pumping speed. In other words, increased pump speed resulted in higher material flow rate. This linear correlation indicates that the selected material remained consistent in the hose under pump pressure and also indicates that there was no segregation [40]. Since they showed almost the same flow rate, it can be concluded that they can be mixed at a volume of 1:1 [73]. In conclusion, the chosen mixes could be pumped without issue based on the findings and inspections made during the pumping test.

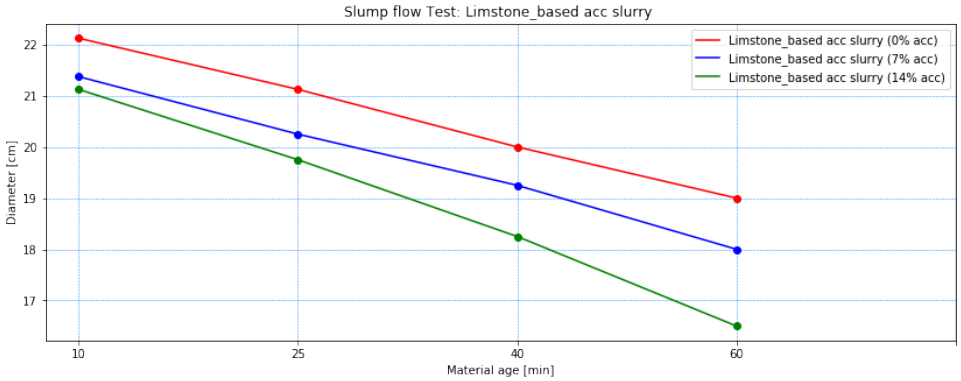

Figure 3.11: Slump flow diameter of limestone-based accelerator slurry with various dosages of accelerator

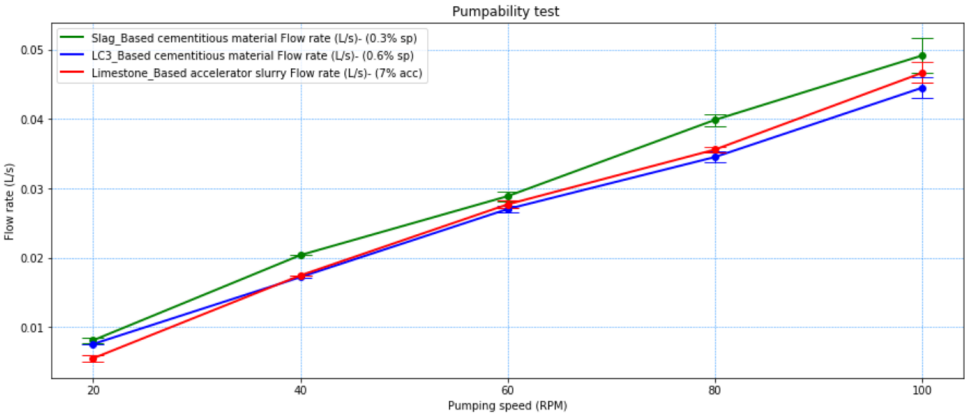

Figure 3.12: material flow rate vs. pumping speed correlation

3.5.3. FLOW CURVE

The graphs below depict the flow curves of the mixtures at the age of 10 minutes. Figure 3.13 shows LC^3-0.6SP and slag-0.3SP mixtures flow curves and Figure 3.14 illustrates limestone accelerator slurry with 0, 7 and 14% accelerator flow curves. Several models are available for fitting data to a curve; in this investigation, the linear Bingham model fit was utilized. The y-intercept and slope of the flow curve were used to calculate the yield stress and plastic viscosity, respectively. According to this model, the steeper the slope of the graph, the greater the plastic viscosity.

In cement-based mixtures, the dynamic yield stress and plastic viscosity of the Slag-0.3SP mix were considerably lower than those of the LC^3-0.6SP mixture. Lower dynamic yield stress of slag-0.3SP indicates that it flows through hoses more easily than LC^3-0.6SP mixture. In limestone-based accelerator slurry mixtures in general, increasing the accel-

erator dose enhanced the dynamic yield stress and plastic viscosity. Figure 3.15 summarizes the rheological properties of the all mixes, as can be seen the slump flow values for the first 10 minutes were consistent with the rheometer's readings of dynamic yield strength. A correlation was found between a larger flow diameter and a lower dynamic yield stress. In other words, more flowable materials need less stress to sustain the flow.

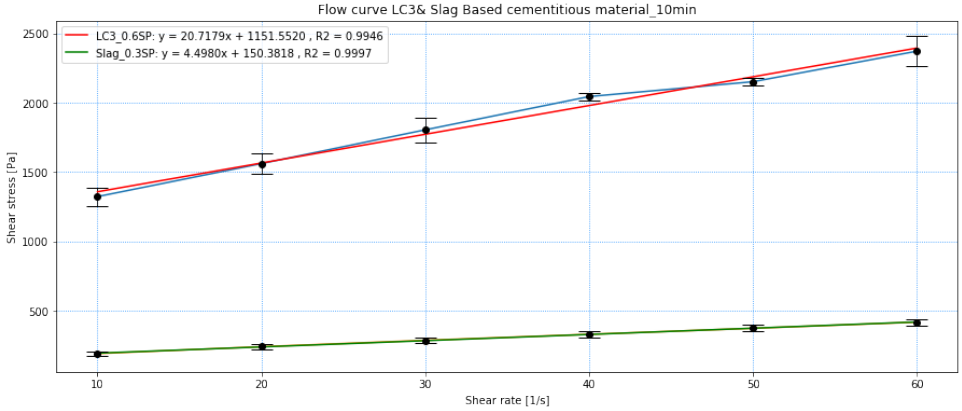

Figure 3.13: Cement-based mixes' flow curves, the straight lines denoting the Bingham model fit, and the dots representing different rheological observations at different shear rates

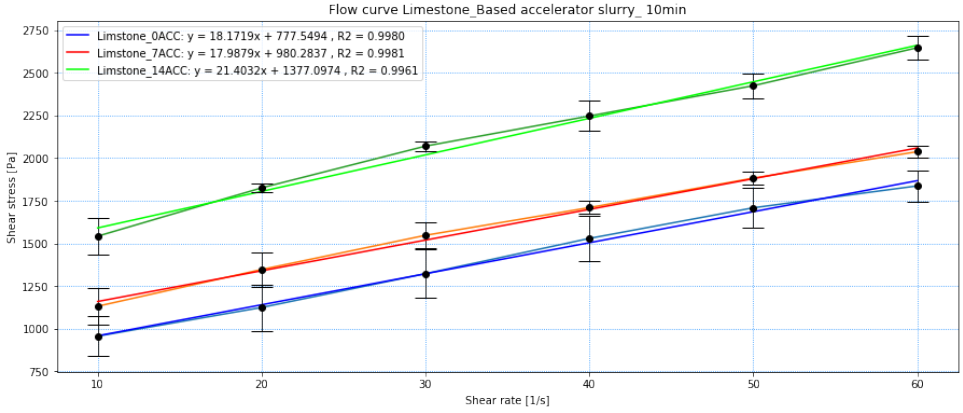

Figure 3.14: Limestone-based accelerator slurry mixes' flow curves, the straight lines denoting the Bingham model fit, and the dots representing different rheological observations at different shear rates

3.6. CHOSEN MIXTURES

After a comprehensive examination of all the mixtures through flowability, pumpability, and flow curve tests, the final pumpable mixtures were meticulously selected. The flowability test revealed that LC^3-0.6SP was the ideal candidate for LC^3-based cementitious material, slag-0.2SP was the suitable choice for slag-based cementitious material, and limestone-7ACC was the preferred option for limestone-based accelerator slurry. As a result of the fact that their flow diameters fell within the desired range of 130 mm to 210 mm. However, upon performing the flow curve test, except for LC^3-0.6SP, and limestone-7ACC, the results for slag-0.2SP were not promising. Consequently, it was decided to opt for slag-0.3SP as the final candidate within the slag-based cementitious material mixtures. Subsequently, pumpability tests were conducted on the three selected mixtures, namely LC^3-0.6SP, slag-0.3SP, and limestone-7ACC. All three mixtures demonstrated a strong linear correlation between the material flow rate and the pumping speed, which suggests that the selected materials remained consistent during the pumping process. Figure 3.15 provides a summary of the characterization of the chosen flowable mixtures.

	Flowability	Flow curve		
Mixture	Flow diameter in 10min [cm]	Dynamic yield stress [Pa]	Plastic viscosity [Pa*s]	R^2
LC3-0.6SP	21.3	1151.6	20.7	0.9946
Slag-0.3SP	28.0	150.4	1.5	0.9997
Limestone-0ACC	22.5	777.5	18.2	0.9980
Limestone-7ACC	21.4	980.2	18.0	0.9981
Limestone-14ACC	21.0	1377.1	21.4	0.9961

Figure 3.15: An overview of the characterization of the chosen flowable mixture

4

EFFECT OF THE ACCELERATOR ON FRESH PROPERTIES

4.1. INTRODUCTION

In this study, the extrusion-based inline mixing technique or twin-pipe pumping (TPP) was utilized to alleviate the incompatibilities between the pumpability and buildability in 3D printing, for the argumentations explained in section 2.2. Because of this contradiction, the concrete's yield strength growth was increased after printing and during mixing in the helical static mixer using the set-on-demand approach, without negatively impacting the concrete's rheology during pumping [13, 39]. The purpose of this section of the research was to evaluate the synergistic behavior of the selected cement-based and SCM-based mixes with different dosages of accelerators from the previous stage. Concrete fresh properties, such as green strength, initial setting time, and buildability, could be examined in order to identify the ideal combination in terms of buildability.

While it is possible to directly use 3D printing and inspect the buildability of any possible mixture of cement-based mixes and limestone-based accelerator slurry with varying dosages of the accelerator, this is a highly labor-intensive process. Therefore, it was necessary to conduct further testing beforehand in order to find the optimal mixture for 3D printing.

4.2. MIXTURES

This section's mixes comprise two fresh mixtures: one for cementitious materials, including LC^3- and slag-based cementitious material, and another for limestone-based accelerator slurry. These two mixes were combined with a volume ratio of 1:1 to create the final mixture. The preparation of both mixes was identical to that described in section 3.3.

For the initial setting time and the green strength tests, the limestone-based accelerator slurry mixture was prepared first, followed by the cementitious materials. After preparing both mixtures, they were combined in the Hobart machine's mixing bowl and mixed at low speed for 10 seconds. This time was a simulation of the 3D printer's helical

static mixer duration, where both materials were mixed before being extruded from the print head.

In order to conduct the buildability tests, two batches of 5- and 7-liter limestone-based accelerator slurry mixtures were initially prepared. Due to the limited capacities of the available Hobart mixers in the laboratory, they were prepared in two bowls. As soon as the accelerator slurry mixtures were ready, they were poured into one of the conveying pumps' hoppers. To avoid water evaporation while preparing the cementitious material, the top of the hopper was covered with a cloth. After this, identical quantities of cementitious materials (7 and 5 L) were prepared and placed into another conveying pump.

4.3. METHODOLOGY

The techniques utilized to evaluate the fresh characteristics were initial setting time, green strength, and buildability. To determine how changing the accelerator dose influenced the mixture's setting time, an initial setting time test was conducted. The initial setting time was predicted to reduce as the accelerator dose was increased. The green strength test was employed to determine how the different dosage accelerators affected the green strength development of the mixtures within 1 hour. Here also predicted that an increase in the accelerator dose would increase the green strength development. Ultimately, to determine the buildability of the developed mixtures, a buildability test was conducted by the 3DC printing machine.

4.3.1. INITIAL SETTING TIME

Setting time is a crucial certification criterion for 3D printing mixtures. In this study, a 90-minute initial setting time was desired for the mixes. Because a very short initial setting time could cause early stiffening and then extrusion problems due to high pressure in the hose and the printing head [74]. In addition, after the initial setting of the concrete has occurred, the printed layer loses its plasticity, resulting in poor interlayer bonding. A very prolonged initial setting time may result in a slow increase in stiffness, resulting in poor buildability and eventual collapse after a few layers of printing [4]. Therefore, it was vital to specify the setting time of 3D printing mixtures.

According to section 4.2, the fresh concrete mixture was made before the test. The mold was then loaded with the fresh mixture and it was put in a Vicat machine, then the test began. The Vicat automated device (Figure 4.1a) was used to test the fresh mixes' initial setting time following NEN-EN 196-part3. The setting was recorded by putting a needle of Ø = 1.13 ± 0.05 mm with a constant force (300 ± 1 g) into the cement mixture and then releasing it; the movement must be fully vertical and frictionless [75]. Thus, before starting the test, the needle is required to be lubricated to prevent material from adhering to it, see Figure 4.1b.

Every ten minutes, the needle was driven into the cement pastes while the container was automatically turned in such a way that the needle never returned to the same hole twice, as shown in Figure 4.1c. When the penetration depth was 36.5mm or less, the period between drops was reduced to 5 minutes.

Because the initial setting time was chosen based on the penetration depth being equal to or less than 36.5 [31, 40].

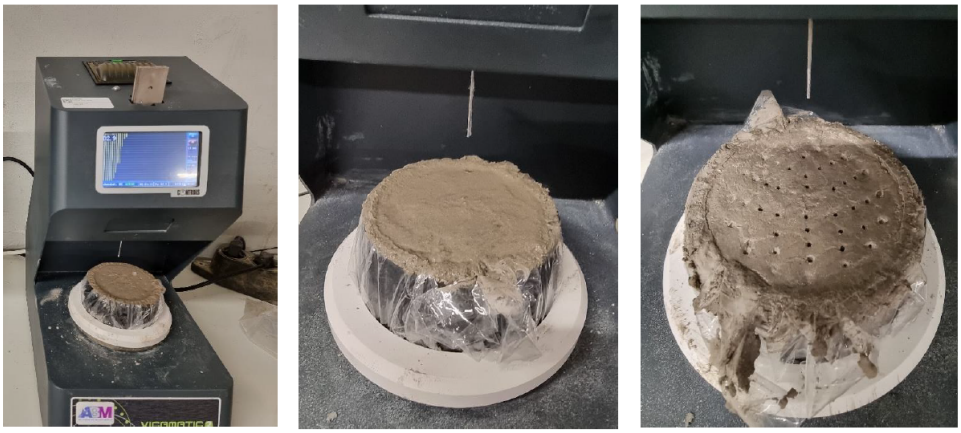

(a) (b) (c)

Figure 4.1: (a) a Vicat automated machine (b) a loaded mold and the lubricated needle (c) the sample after finishing the test

4.3.2. GREEN STRENGTH

Green strength is the term used to describe the strength of concrete in its earlier stages [20]. As mentioned in section 2.2, a 3D printing mixture must establish sufficient early strength in order to support the following layers. In this context, the green strength test offers very valuable data. Displacement control was used throughout the experiments, with a maximum displacement of 5 mm [31]. In this process, the fresh mixture is loaded vertically until the maximum displacement is attained.

The green strength of the fresh mixes was tested using samples cast in a mini Hagerman mold with a 70 mm upper internal diameter, a 100 mm lower internal diameter, and a 60 mm height. After the material was prepared as outlined in 4.2, the Hagerman mold was lubricated (Figure 4.2a) so that there would be less friction between the specimen and the inside surface of the mold during demolding. When the mold was halfway full, the fresh mixture was compacted with a wooden stick. The same method was followed on the other half of the mold; the excess was removed away by using a trowel.

After preparing the sample and waiting for the test time, the sample was sealed with a plastic sheet and then de-molded just before the test, see Figure 4.2b. After demolding, the sample's height was measured (Figure 4.2c), and then it was subjected to 5 mm of deformation by placing weighted plates on its top as shown in Figure 4.2d. Following this, the test was stopped, and the plates mass were noted. The green strength was taken at 15-minute intervals for one hour, then at 15, 30, 45, and 60 minutes after casting.

4.3.3. BUILDABILITY

Following the mixing of the fresh mixture by the Hobart mixer, as discussed in section 4.2, they were manually put into the hoppers, 12 L of the cement-based mixture in one and 12 L of limestone-based accelerator slurry in the other. Then, by adopting a TPP system, it was achievable to resolve the conflict between the mixes' flowability and buildability.

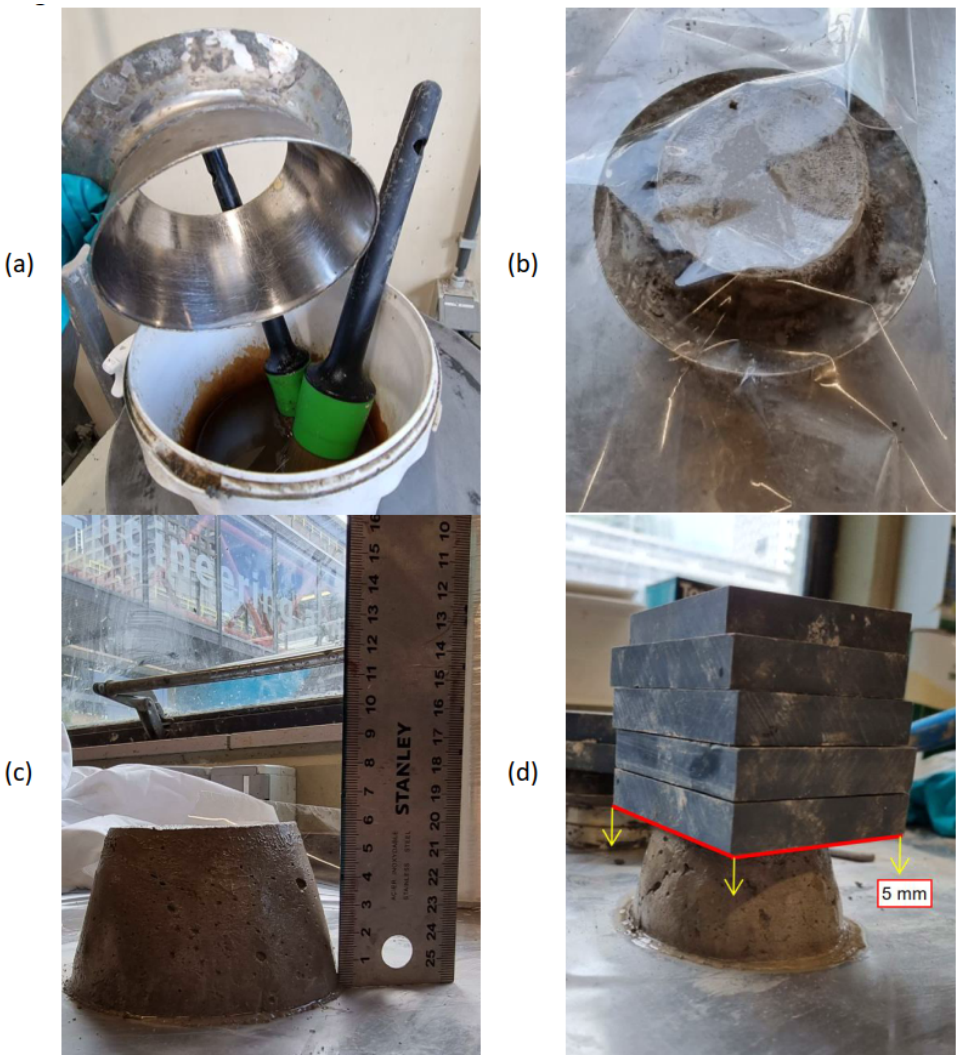

Figure 4.2: Methods for evaluating green strength (a) putting oil inside the mold (b) covering the sample while awaiting the desired age (c) determining the specimen's initial height (d) using weighted plates until a vertical deformation of 5 mm is achieved on the 4 edges of the plates equally

In this method, two distinct mixes were employed: cement-based mixtures with a given quantity of superplasticizer pumped by one of the pumps, and accelerator slurry with a particular amount of accelerator with another one, see Figure 4.3. Both mixtures benefit from the increased flowability and extended open time provided by these combinations [40].

The test was started by starting both conveying pumps simultaneously with identical

Figure 4.3: Two PFT Swing-M conveying pumps with separate mixtures and hoses [40]

speed and printing proceeded till failure. As soon as the mixes from both pumps arrived at the helical static mixer, just before extrusion, they were combined, and the accelerator in the slurry came into contact with the cement-based mixture (Figure 4.4a), at a room temperature of 20°C [76]. As a consequence of this new mixture, the hydration rate increased, and the buildability improved. Here, the accelerator dose had a key role in terms of buildability, the higher dosage of the accelerator resulted in a higher buildability rate. This project's objective was to create a cylindrical column with 16 layers, the maximum number of layers that the TU-Delft 3DCP system could support. The printed cylinder was 250 mm in diameter of the printing path and each printed layer was 15 mm thick.

The following elements made up the lab-sized 3DCP (3-axis gantry system) test equipment in TU-Delft [36, 40, 76]:

System for extrusion

Two commercial PFT Swing-M conveying pumps, like the one utilized in the pumpability experiment as described in section 3.4, and a nozzle constituted the core of the

extrusion system. Each pump consisted of a hopper that could hold up to 38 liters of material, a rotor, and a hose that was 5 meters long and had an internal diameter of 25 millimeters. To conduct the 3D printing test, a down-flow nozzle with a 15 mm circular hole was adopted. The printing nozzle's speed could be varied between 0 and 120 mm/s; for this investigation, it was 60 mm/s. In other words, 13.09 seconds were required to print a layer of the cylindrical column at the pumps' speed of 50 RPM.

Three-dimensional (DOF) Computer Numerical Control (CNC) system (see Figure 4.4a)
The printing material route was established by the controller-operated CNC machine which worked inside a boundary of 1100 mm x 720 mm x 290 mm (LxWxH).

4

Controller
A computer used to operate the CNC system.

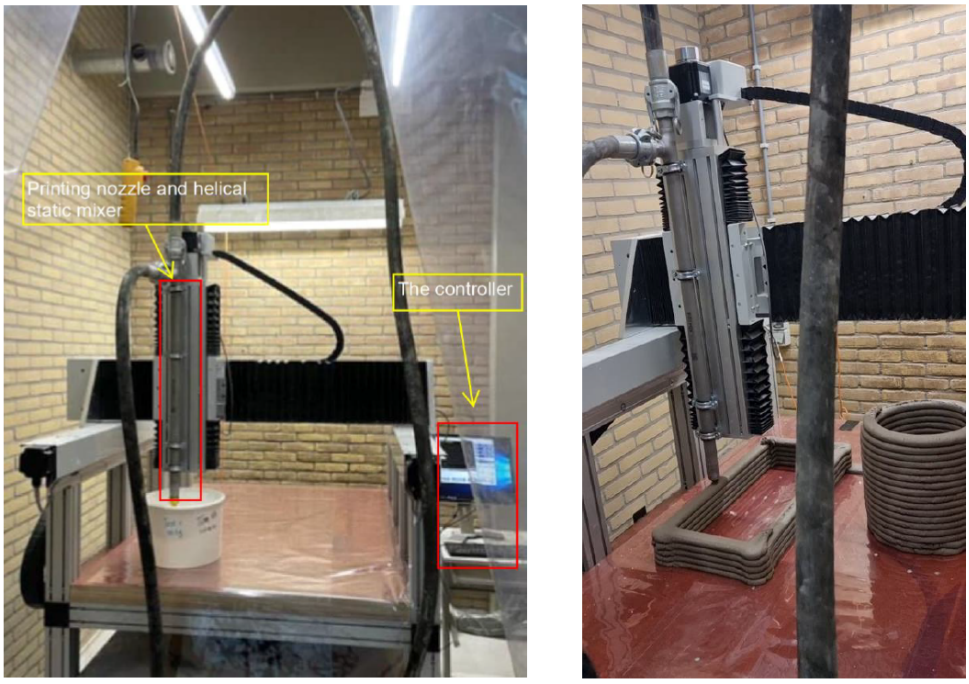

(a) (b)

Figure 4.4: 3DCP test setup (a) the CNC machine and the controller [40] (b) 3DCP operation during a printing session

4.4. RESULTS AND DISCUSSION

4.4.1. INITIAL SETTING TIME

The goal of this experiment was to determine how the reaction of fresh mixes would be affected in terms of setting time by varying dosages of the accelerator. Figure 4.5 and Figure 4.6 show the results of a time-dependent penetration resistance test performed on LC^3-based& limestone-based accelerator slurry and slag-based& limestone-based accelerator slurry, respectively. The findings indicated that both mixes exhibited a reduction in the time to reach the initial settings when the accelerator dose was increased.

The test was initiated using LC^3-based mixtures, and the initial setting time by adding 5.5% or 7% accelerator remained unchanged. For this reason, it was decided to employ a 7% accelerator for further investigation in both cementitious-based materials. The initial setting time for both combinations after adding 7% accelerator was roughly 90 min, which was a good outcome. On average, slag-based mixes with the same quantity of accelerator took somewhat longer to achieve their initial setting time than LC^3-based mixtures. Here, 0 and 14% accelerators were tried on both mixes to establish a lower and upper limit. Table 4.1 summarizes the penetration resistance results of all mixes.

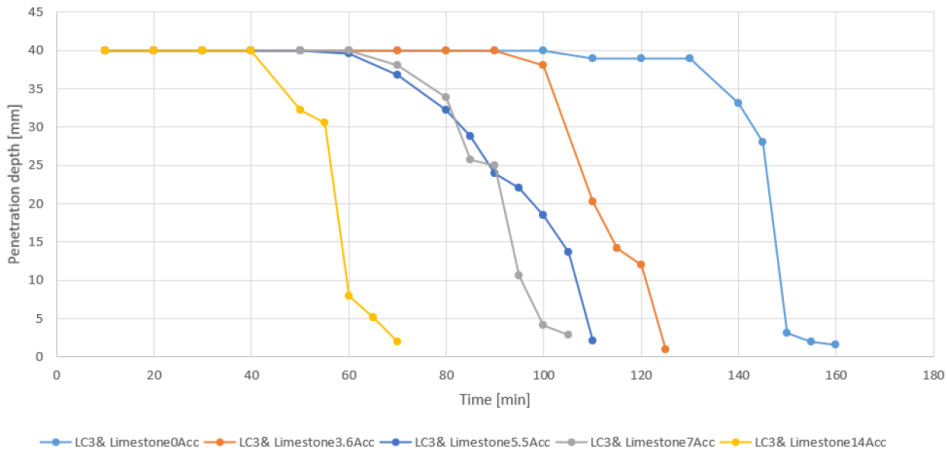

Figure 4.5: The penetration resistance test findings of LC^3-based& limestone-based accelerator slurry with varying accelerator doses

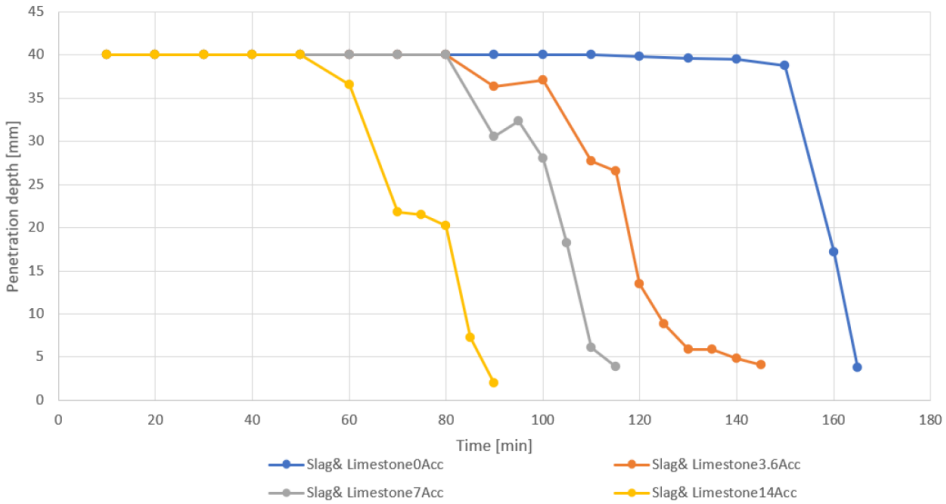

Figure 4.6: The penetration resistance test findings slag-based& limestone-based accelerator slurry with varying accelerator doses

Mixture	SP	ACC	Initial setting [min]
LC^3-based & Limestone-based acc slurry	0.6%	0%	140
LC^3-based & Limestone-based acc slurry	0.6%	3.6%	100
LC^3-based & Limestone-based acc slurry	0.6%	5.5%	80
LC^3-based & Limestone-based acc slurry	0.6%	7%	80
LC^3-based & Limestone-based acc slurry	0.6%	14%	50
Slag-based & Limestone-based acc slurry	0.3%	0%	160
Slag-based & Limestone-based acc slurry	0.3%	3.6%	110
Slag-based & Limestone-based acc slurry	0.3%	7%	90
Slag-based & Limestone-based acc slurry	0.3%	14%	70

Table 4.1: A summary of the initial setting time of the mixtures

4.4.2. GREEN STRENGTH

This field-friendly test provided a helpful indicator for the proper dosage of accelerator in each mixture in order to get satisfactory buildability. The development of the green strength of LC^3-based& limestone accelerator slurry and slag-based& limestone accelerator slurry over time are shown in Figure 4.7 and Figure 4.8, respectively. Results indicated that both combinations became more rigid as the accelerator dose was increased. As the findings reveal, the dose of the accelerator played a crucial role in the growth of green strength. The advancement in compressive strength could be linked to the encouragement of generating more hydration products like C-S-H gels, ettringite, and AFm. The quantity of green strength growth in all mixtures was linear with time, however, the slope was somewhat less steep in the first 15 minutes.

In addition, the green strength results coincided with the initial setting time. The mixtures with a quicker initial setting time exhibited a higher green strength development. For instance, slag-based mixes with 0% and 7% of accelerator exhibited longer initial setting time than LC^3-based mixtures with the same dosage of the accelerator, as shown in Table 4.1. Therefore, these mixtures had much lower green strength development than LC^3-based mixtures. The largest amount of the green strength growth was shown in LC^3- and slag-based mixes with 14% accelerator, and the lowest amount was seen in both cases with 0% accelerator. However, the green strength development of the LC^3-based mixture with 0% accelerator was by far higher than the slag-based mixture.

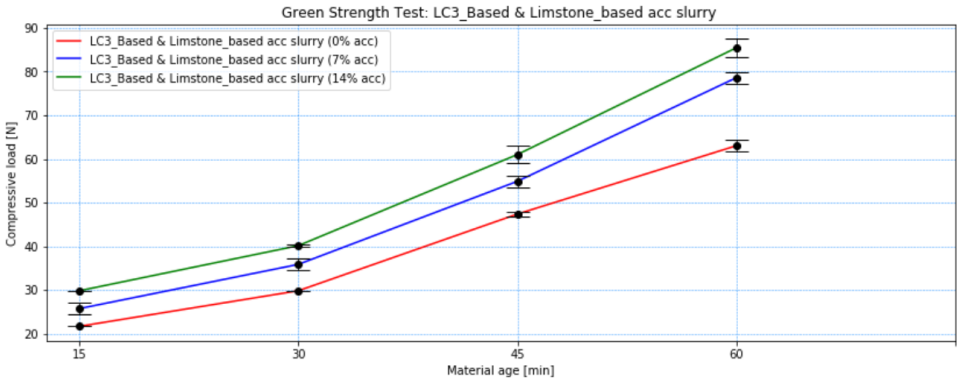

Figure 4.7: Green strength evolution of LC^3-based mixture with different dosages of accelerator

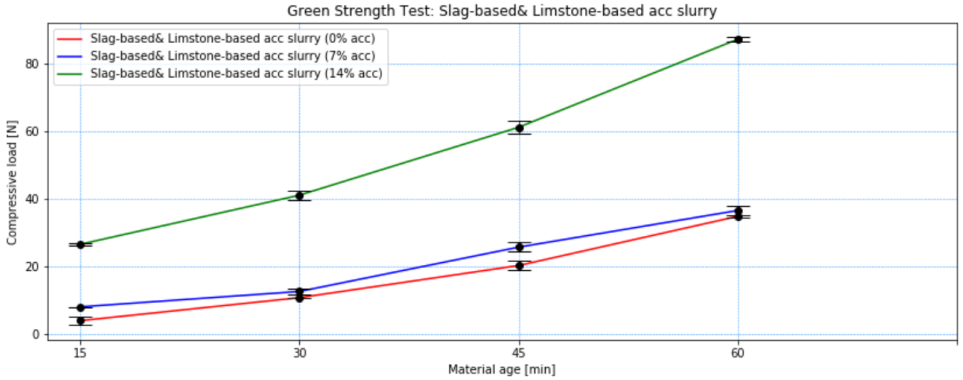

Figure 4.8: Green strength development of slag-based mixture with different dosages of accelerator

4.4.3. BUILDABILITY

The primary objective of this work was to examine the buildability of LC^3- and slag-based cementitious mixtures with the accelerator slurry mixture in a set-on-demand environment. Three printing sessions were utilized to print three different developed mixtures, including slag-based0.3SP& Limestone7ACC, LC^3-based0.6SP& Limestone0ACC, and LC^3-based0.6SP& Limestone7ACC. Neither the cement-based nor the accelerator slurry mixtures had any flowability issue during the printing session. Without creating excessive pressure in the pumps and hoses, the helical static mixer was able to successfully mix cement-based and accelerator slurry mixtures. The mixtures were extruded consistently and without nozzle blockage.

The buildability test of slag-based0.3SP& Limestone7ACC revealed a material failure (plastic collapse) of the bottom filament after printing 9 layers. It subsequently produced a stability failure and collapsed in layer 13; Figure 4.9a depicts the printing outcome shortly before collapsing. After printing 10 layers in the buildability test of LC^3-based0.6SP& Limestone0ACC, the bottom filament exhibited a material failure. This failure ultimately led to a stability failure, and in layer 15, the model completely collapsed. Figure 4.9b shows the printing result right before the collapse. The buildability test with LC^3-based0.6SP& Limestone7ACC yielded a very encouraging result, as this mixture was able to be printed and achieved the maximum number of layers that could be printed by the 3DCP machine at TU Delft, as shown in Figure 4.9c.

(a) (b) (c)

Figure 4.9: 3DCP results, (a) slag-based0.3SP& Limestone7ACC just before collapsing (b) LC^3-based0.6SP& Limestone0ACC just before collapsing (c) LC^3-based0.6SP& Limestone7ACC

The fresh mixture's buildability is influenced by two critical factors: its shape-keeping abilities and structural build-up behavior. The fresh mixture must meet both aspects' needs, in order for the printing process to be successful [31]. Shape keeping is critical immediately after material extrusion, whereas structural build-up rate is critical when the printed material is at rest. Therefore, a high structuration rate is required to support loads of succeeding layers.

Based on the results of the buildability test, between slag- and LC^3-based mixtures, it was found that the LC^3-based mixtures showed a greater ability to maintain their shape following extrusion and a greater structural build-up. Because LC^3-based cementitious

mixtures showed greater buildability by permitting more vertical layering of printed filaments than the slag-based mixtures.

The great fluidity of the slag-based cementitious mixture, on the other hand, made it difficult to preserve the printed filaments' original cross-sectional shape. This was consistent with the results of the slump flow tests performed in section 3.5.1. LC^3-based0.6SP& Limestone7ACC exhibited a greater degree of structural development compared to LC^3-based0.6SP& Limestone0ACC within the LC3-based mixtures. This was evident from the reduced initial setting time, as determined by the penetration resistance test, and a higher rate of development of green strength, as observed in the green strength test. Consequently, LC^3-based0.6SP& Limestone7ACC mixture showed the highest number of printed layers.

Based on the findings of the buildability test, it can be inferred that the accelerator exerted a significant influence on the buildability of the mixture. The accelerator's accelerating effects led to improved shape retention behavior. To put it another way, the accelerator improved the hydration process, which increased the buildability of the mixture by enhancing shape retention and structural build-up behavior.

5

MECHANICAL AND CHEMICAL PROPERTIES OF THE MIXTURES

5.1. INTRODUCTION

As discussed in the preceding chapter, the different dosage of calcium nitrate could affect the fresh characteristics of the mixtures. It had the potential to alter the initial set time, green strength development, and the buildability of the mixtures. The cause may be attributed to an acceleration of cementitious material's hydration products. Consequently, it was necessary to demonstrate this phenomenon by investigating the compressive strength, heat evolution, and hydration products of the mixtures. This chapter's observations could help us better understand how calcium nitrate influenced the hydration process.

5.2. MIXTURES

For compressive strength testing, LC^3-based and slag-based cementitious materials with various dosages of accelerator in limestone-based accelerator slurry were evaluated, including 0%- 3.6%- 7% and 14%. For isothermal calorimetry and thermogravimetric analysis (TGA) testing, both cementitious materials were blended with 0%-7% and 14% dosages of accelerator in the limestone-based accelerator slurry and examined.

5.3. METHODOLOGY

The compressive strength test was carried out to evaluate the influence of different accelerator dosages on compressive strength growth at various ages, including 7 and 28 days after casting. To examine the hydration process of the mixes over the first seven days, an isothermal calorimetry experiment was conducted. Using the results of the isothermal calorimetry test, it was feasible to determine the precise time to stop hydration prior to doing the thermogravimetric analysis (TGA) test. The TGA test made it possible to investigate and measure the amount of portlandite (CH) and hydrate water content in the specimens.

5.3.1. COMPRESSIVE STRENGTH

The aim of this experiment was to compare the compressive strength of the mixtures after 7 and 28 days of material age in response to varying accelerator dosages. A Servo Plus Evolution machine (Figure 5.1a) was used to conduct this test. The method for preparing the fresh mixture for this test was identical to that described in section 4.2 for the initial setting test. In accordance with NEN-EN 196-1, the examined material must measure 40 x 40 x 160 mm^3. Consequently, the samples were cast in polystyrene 3-gang prism molds measuring 40 x 40 x 160 mm^3, see Figure 5.1b. The samples were cast in molds and then covered with a plastic sheet to minimize moisture loss throughout the hydration process. All samples were de-molded and kept in a fug room 24 hours before testing. The compressive strength was examined using a loading rate of 2400 N/s with a starting load of 100 N. Three separate tests were conducted for each material to determine the average compressive strength.

(a)

(b)

Figure 5.1: Compressive strength test set-up (a) Servo Plus Evolution machine at TU-Delft (b) a loaded polystyrene 3-gang prism mold

5.3.2. ISOTHERMAL CALORIMETRY

The purpose of this experiment was to examine the effect of various accelerator dosages on heat evolution. An 8-channel TAM Air isothermal calorimeter from TA instruments (Figure 5.2) was used to perform an isothermal calorimetry test in order to monitor the rate of hydration in different mixtures over the first 7 days. There were eight independently operating channels in this device, each of which contained two parallel vessels. One of these vessels (a 20 mL tubular glass) was used for the reference, while the other was utilized for the sample.

Before beginning the test, the reference vessels were filled with a specified quantity of fine sand with a grain size of 0.125 to 0.25 mm. The weight of the fine sand was determined such that it had the same heat capacity as the tested sample nevertheless without heat production [66]. The following mixing protocol was followed after a 30-minute

baseline recording of the machine: The first 2 minutes were spent homogenizing the dry components (without aggregate) in a small mixer at low speed. Then, for a further 2 minutes, the liquid component was added, which consisted of water, superplasticizer, and accelerator, and mixed at a low speed. After scraping the cylindrical plastic mold and another 2 minutes of high-speed mixing, 6 grams of the freshly prepared material were poured into the 20 mL tubular glass vessel, and the sample and reference sealed vessels were immediately loaded into the calorimeter. The same protocol was repeated to make fresh material for each channel. The test was conducted at a constant temperature of 20 degrees Celsius, and the heat flow data were recorded every 51 seconds for seven days or 168 hours.

Figure 5.2: An 8-channel TAM Air calorimeter in TU-Delft

5.3.3. THERMOGRAVIMETRIC ANALYSIS (TGA)

TGA is a method that monitors the sample's weight while it undergoes controlled heating or cooling. The weight change of a specimen is affected by its composition, heating rate, temperature, and the kind of gas used in the furnace for instance nitrogen, argon, oxygen and etc. The existence of a certain chemical substance may be determined based on a change in mass that occurs within a certain temperature range. The amount of the weight variation reveals how much of that substance is present in the sample. Instead

of utilizing a TGA, the operation may be carried out in a number of furnaces at predetermined temperatures; however TGA can yield identical data as a single operation, moreover, the samples in the furnaces might react with the oxygen present in the air [40, 77].

The fresh mixes for the TGA test were prepared by homogenizing the dry components at a low speed in a small mixer for 2 minutes. The liquid component, which consisted of water, superplasticizer, and accelerator, was then added and mixed at a low speed for 2 minutes. Following that, the mixing was stopped, and the bottom and walls of the cylindrical plastic mold, which measured 33.5 mm in diameter and 67.5 mm in height, were scraped. The mixture was then blended for a further two minutes at a high speed. The cast cylindrical samples were kept in storage until the time came to stop hydration. After reaching the hydration stop time, the method described by Chen et al. [76] and Scrivener et al. [66] was used to prepare powder samples, which are based on using a solvent to dilute and remove the water in the pores. First, the sample was crushed and grinded in an isopropanol solvent-filled mortar and pestle. The pore solution was removed using isopropanol, which had a volume around ten times that of the sample. The suspension was then left for 20- 30 minutes to allow the free water in the fine particles to be replaced by isopropanol, as seen in Figure 5.3a,b. The suspension was filtrated by utilizing a Büchner funnel and an aspirator pump in combination with Whatman40 filter paper that had a size of 8 μm (Figure 5.3c). The wet solid was then washed with diethyl ether (by approximately 5 to 10 mL) to eliminate excess isopropanol and pumped until the sample became lighter in color, see Figure 5.3d. The powder was then transferred to a Watch Glass Dish (Figure 5.3e) before being placed in an aerated oven at a temperature of 40 ° C for a period of 15 minutes. The samples were then sealed in plastic bags and kept in a light vacuum desiccator until the testing time.

The TGA test was conducted following the technique of Chen et al. [76] to measure the amounts of hydrate water and calcium hydroxide in various mixes. This test was carried out using a Netzsch STA 449 F3 Jupiter thermal analyzer (Figure 5.3f) at the ages of 1 hour, 4 hours, and 7 days of the samples. To conduct the test, a powder sample of the mixture weighing around 50- 60 mg was put into an alumina crucible and then placed into the machine each time. After that, the machine heated the sample to temperatures ranging from 40 to 900°C in an argon atmosphere at a rate of 10 degrees Celsius per minute and a flow rate of 50 ml/minute.

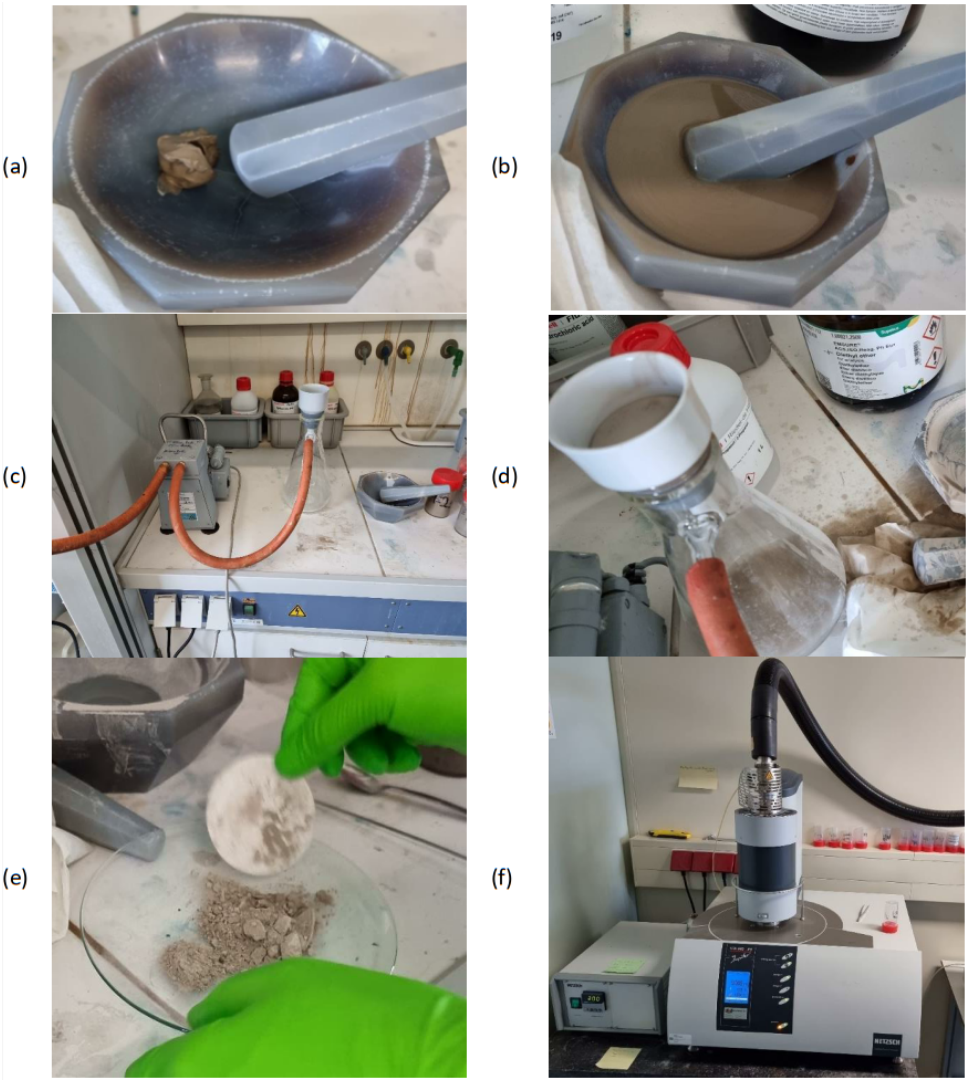

Figure 5.3: Stopping hydration process (a) pouring the sample in a mortar and pestle (b) grinding and crushing the paste into powder in isopropanol (c) Büchner funnel and an aspirator pump set-up (d) washing wet solid with diethyl ether (e) Watch Glass Dish before being placed in an aerated oven (f) Netzsch STA 499 F3 Jupiter thermal analyzer

5.4. RESULTS

5.4.1. COMPRESSIVE STRENGTH RESULTS

In order to determine how changing the accelerator dose affected the development of the compressive strength of LC^3-based and slag-based mixes, a compressive strength test was carried out.

LC^3-based mixtures

Graphic representations of the compressive strength of LC^3-based mixtures with various accelerator dosages (0%, 3.6%, 7%, and 14%) are shown in Figure 5.4. Without utilizing the accelerator in the mixture, the 7-day compressive strength rose from 20.5± 1.8 to 25.1 ± 1.9 MPa; the addition of 3.6% CN raised the 7-day compressive strength from 20.5 ± 2.8 to 25.7 ± 2.7 MPa; the addition of 7% CN increased the 7-day compressive strength from 24.9 ± 3.9 to 31.7 ± 1.6 MPa; and the addition of 14% CN increased the 7-day compressive strength from 28.5 ± 2.5 to 41.8 ± 2.7 MPa.

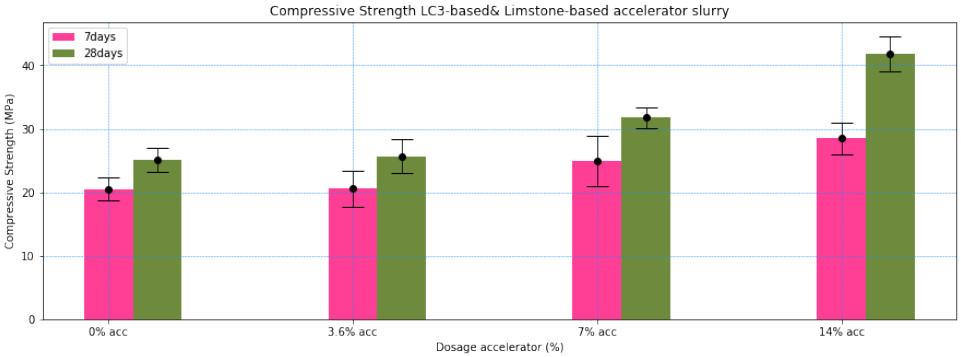

Figure 5.4: The development of compressive strength in LC^3-based mixes after 7 and 28 days of hydration

Slag-based mixtures

Figure 5.5 displays the compressive strength development of a slag-based mixture with varying amounts of accelerator (0%, 3.6%, 7%, and 14%).

In the absence of CN, the mixture's 7-day compressive strength improved from 17.8 ± 4.3 to 26.9 ± 2.1 MPa, 3.6% CN enhanced 7-day compressive strength from 20.6 ± 1.7 to 29.1 ± 3.0 MPa, 7% CN increased 7-day compressive strength from 28.3 ± 3.6 to 29.8 ± 2.2 MPa, and 14% CN grew 7-day compressive strength from 29.1 ± 5.5 to 36.4 ± 2.1 MPa.

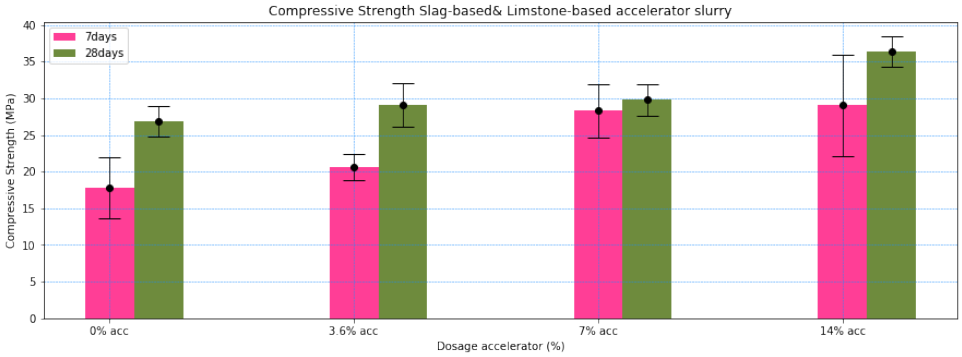

Figure 5.5: The development of compressive strength in slag-based mixes after 7 and 28 days of hydration

5.4.2. ISOTHERMAL CALORIMETRY (HEAT EVOLUTION) RESULTS

Figure 5.6 and Figure 5.7 demonstrate the normalized heat flow and cumulative heat results within 168 hours (7 days) of LC^3- and slag-based mixtures with 0%, 7%, and 14% accelerators. The heat released by the wetted cement surface was responsible for the initial peak of all curves. The quick dissolution of the dry component led to the formation of the ettringite at an early stage. Immediately after this sharp peak, there was an induction phase and a short period of dormancy [76]. Following the induction period, an acceleration stage was detected, which corresponded to the enormous precipitation of calcium silicate hydrate (C-S-H) and portlandite (CH).

When comparing LC^3-based and slag-based mixes with varying dosages of the accelerator, the main hydration peak of the LC^3-based mixtures was seen to occur at an earlier age of hydration with greater cumulative heat released, except for the LC^3-based mixture with 0% accelerator, which had the lowest cumulative heat released. Slag-based mixes, on the other hand, had a greater heat flow intensity than LC^3-based mixtures with the same quantity of accelerator, except the slag-based mixture with 0% accelerator, which had a lower heat flow intensity than the LC^3-based mixture with 0% accelerator. At an early age of hydration, the slag-based mixture with a 14% accelerator produced more cumulative heat than the LC^3-based mixture with a 7% accelerator. After 70 hours till the end, however, the accumulated heat was highest in the LC^3-based mixture with the 7% accelerator.

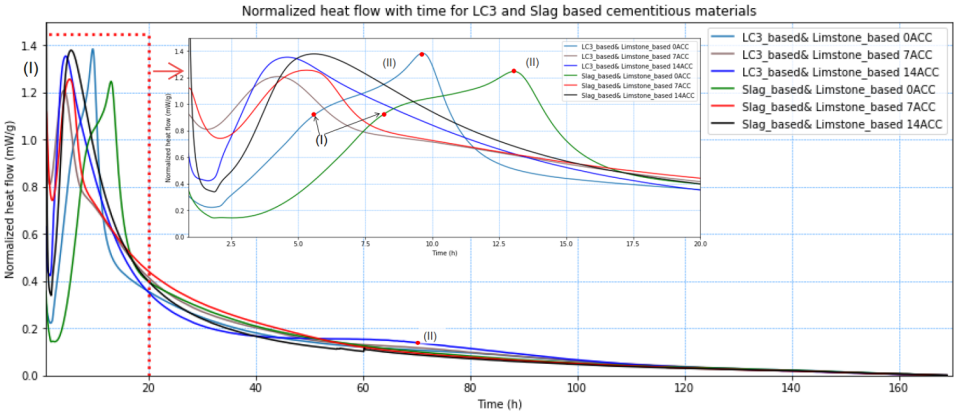

Figure 5.6: Normalized heat flow during 168 hours of hydration of LC^3- and slag-based mixtures

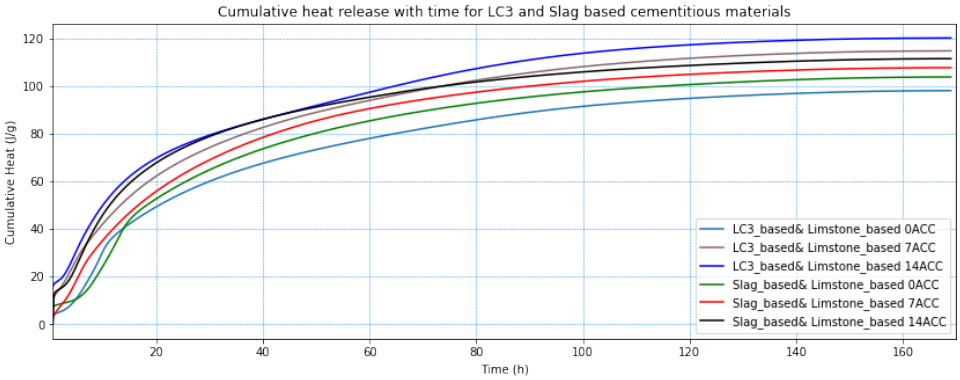

Figure 5.7: Normalized cumulative heat during 168 hours of hydration of LC^3- and slag-based mixes

5.4.3. THERMOGRAVIMETRIC ANALYSIS (TGA) RESULTS

In hydrated PC, there are a significant number of overlaps between weight loss zones; nevertheless, by thermogravimetric analysis (TGA) test, three borders of mass losses, including water loss of C-S-H, portlandite, and calcium carbonates (calcite), are readily identifiable [66]. Consequently, thermogravimetric (TG) and derivative thermogravimetric (DTG) curves of different mixtures were plotted at 1, 4, and 168 h to see how they developed throughout curing.

According to Chen et al. [76], and Scrivener et al. [66], the temperature range for which it may consider as hydrated water loss is between 40 degrees Celsius and 600 degrees Celsius. The mass loss between 360°C and 500°C was regarded as the mass of portlandite based on the DTG data, over this temperature range portlandite ($Ca(OH)_2$) degrades to

calcium oxide (CaO) and water. The mass loss over 600°C resulted from two phenomena: first, the decarbonization of calcite ($CaCO_3$), which originated from the limestone filler in the mixtures, and second, the carbonation of portlandite (CH) during the curing period, since CO_2 can react with CH nearly anywhere in the environment.

The following calculation was employed to obtain the normalized quantity of chemically bonded water and portlandite as a proportion of the dry sample weight at 600 °C:

$$W_{[H_2O]} = \frac{M_{40°C} - M_{600°C}}{M_{600°C}} * 100\%$$

$$W_{[Ca(OH)_2]} = \frac{M_{360°C} - M_{500°C}}{M_{600°C}} * \frac{m_{[Ca(OH)_2]}}{m_{[H_2O]}} * 100\%$$

Where:
$W_{[H_2O]}$: Mass percentage of H (chemically bound water) in the mixture
$W_{[Ca(OH)_2]}$: Mass percentage of CH (calcium hydroxide) in the mixture
$M_{x°C}$: The mass at x°C
$m_{[Ca(OH)_2]}$: Molar mass of calcium hydroxide (74 g/mol)
$m_{[H_2O]}$: Molar mass of water (18 g/mol)

The TG and DTG results of LC^3-based and slag-based mixtures were plotted individually, and the results of H and CH mass loss are shown in Table 5.1.

LC^3-based mixtures

The TG and DTG curves of LC^3-based mixtures with varying accelerator dosages (0%, 7%, and 14%) are plotted in Figure 5.8 and Figure 5.9, respectively. Table 5.1 demonstrates the calculated amounts of H and CH based on the supplied formula and they are also represented on the graphs in Figure 5.10 and Figure 5.11.

As the data indicate, the quantity of H and CH in each combination grew as time passed. Furthermore, by increasing the accelerator dose, a greater quantity of H and CH was achieved in all three different tested times within 7 days. As an instance, among all the mixes, the one with the 14% accelerator dose had the greatest levels of H and CH after 1, 4, and 168 hours of curing. The change in hydrate water content between 1 and 4 hours after hydration was negligible, however, it grew dramatically between 4 and 168 hours; a similar trend was also observed for CH content.

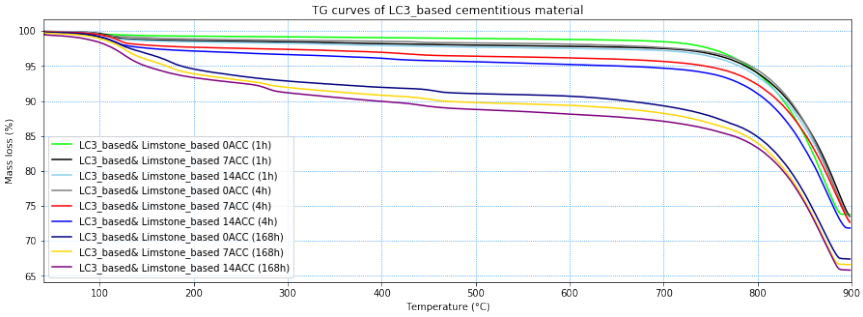

Figure 5.8: TG curves of LC^3-based mixtures at 1, 4, and 168h

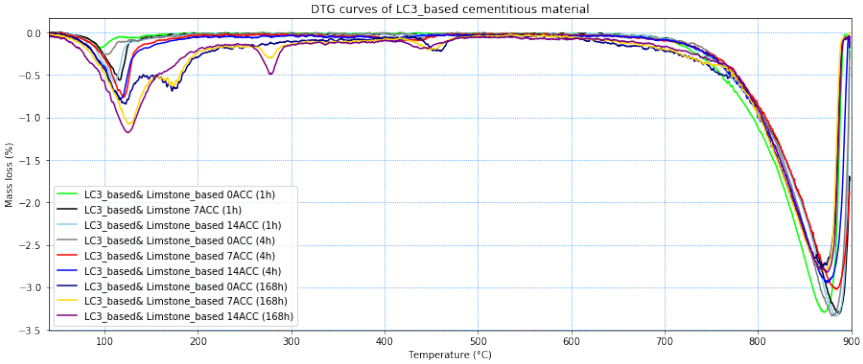

Figure 5.9: DTG curves of LC^3-based mixtures at 1, 4, and 168h

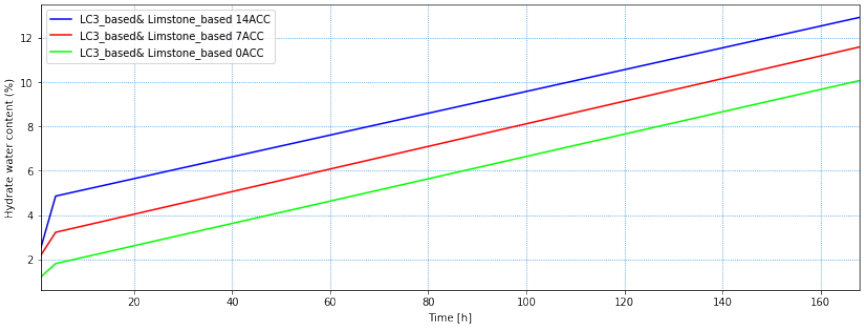

Figure 5.10: Hydrate water content (H) normalized to the weight of the dry sample at 600°C of LC^3-based mixtures

Slag-based mixture

In Figure 5.12 and Figure 5.13, the TG and DTG curves of slag-based mixtures with vary-

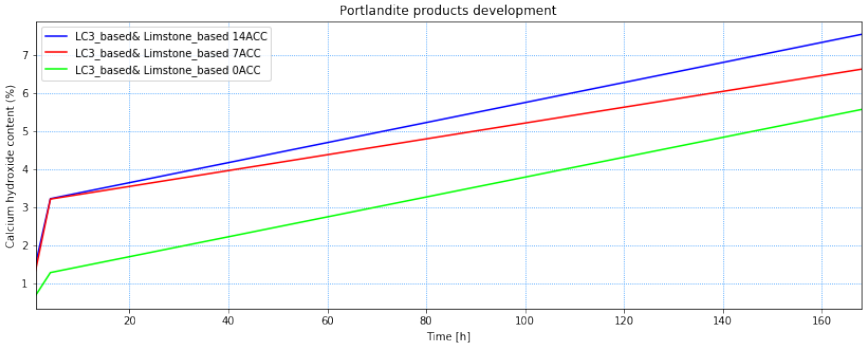

Figure 5.11: Calcium hydroxide content (CH) normalized to the weight of the dry sample at 600°C of LC^3-based mixtures

ing doses of accelerator (0%, 7%, and 14%) are illustrated. Following the stated formula, Table 5.1 displays the obtained amounts of H and CH and graphically shown in Figure 5.14 and Figure 5.15. As can be seen, the quantity of H and CH grew as hydration time passed, furthermore, by increasing the accelerator dose, a greater quantity of H and CH was achieved in all three different curing times within 7 days.

In contrast to the other mixtures, slag-based& limestone-based 0ACC exhibited a greater amount of CH in 168 h of curing. In Slag-based mixtures as well as LC^3-based mixtures, the difference in the quantity of H and CH in mixtures in 1 and 4 hours of hydration was negligible, however, the difference rose significantly between 4 and 168 hours.

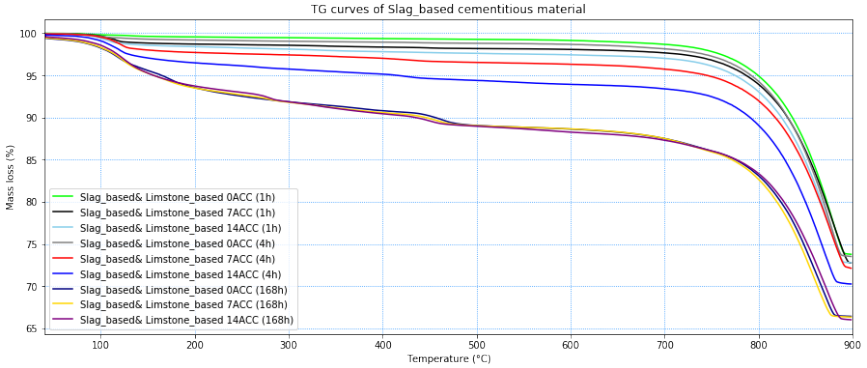

Figure 5.12: TG curves of slag-based mixtures at 1, 4, and 168h

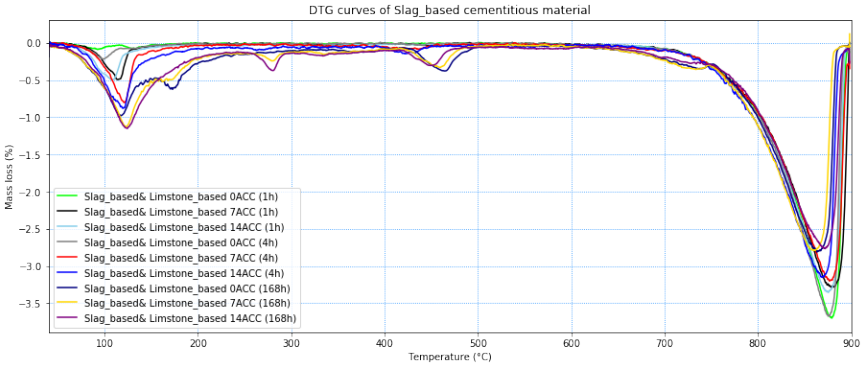

Figure 5.13: DTG curves of slag-based mixtures at 1, 4, and 168h

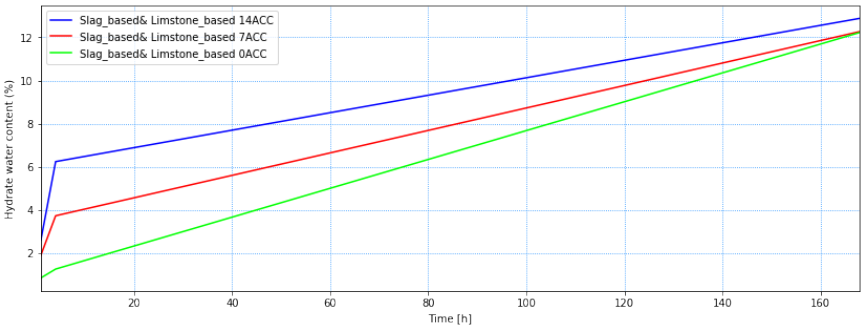

Figure 5.14: Hydrate water content (H) normalized to the weight of the dry sample at 600°C of slag-based mixtures

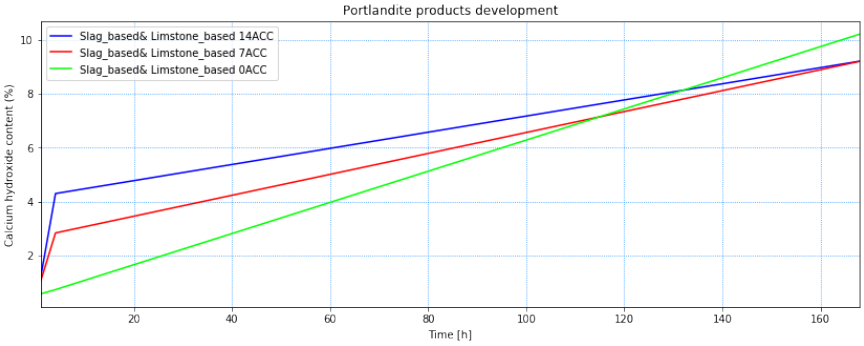

Figure 5.15: Calcium hydroxide content (CH) normalized to the weight of the dry sample at 600°C of slag-based mixtures

5.5. DISCUSSION

Compressive strength

According to the results from the studied mixtures' compressive strength development at 7 and 28 days, the addition of $Ca(NO_3)_2$ resulted in a minor improvement in compressive strength at 7 days. Nevertheless, the development of compressive strength was significantly improved by the increase in CN dosage at 28 days. According to the norms provided by standard EN-934-2, CN accelerator cannot be classified as a hardening accelerator because, based on its performance, it is more effective as a setting accelerator than a hardening accelerator [64]. Studies by Aggoun et al. [78], and Dorn et al. [79] also reported a slight improvement at an early age and a significant improvement at 28 days.

Compressive strength increased more over the course of the 28-day curing period for the same amount of superplasticizer (0.6% in LC^3-based and 0.3% in slag-based mixtures), due to the mixtures' higher $Ca(NO_3)_2$ dosage. According to earlier research by Dorn et al. [78], the increased strength caused by the addition of CN can be attributed to improvements in cement hydration and microstructure flocculation. This may be related to the increased formation of AFm phases, ettringite, and C-S-H gels, according to his findings.

Overall, the results from section 5.4.1 showed that LC^3-based mixtures containing 7% or more CN may be suitable for use as construction materials due to their high compressive strength (more than 30 MPa) at 28 days.

The relationship between heat production and concrete strength is not straightforward, as aggregate, water content, and porosity all have a significant impact on strength. However, a correlation between strength and heat can be established by comparing the measured heat of hydration with the measured strength at a specific hydration time [66]. As shown in Figure 5.16 and 5.17, it is possible to derive a linear correlation between compressive strength of LC^3- and slag-based mixtures and normalized cumulative heat at 7 days of curing by combining the results of isothermal calorimetry and compressive strength development.

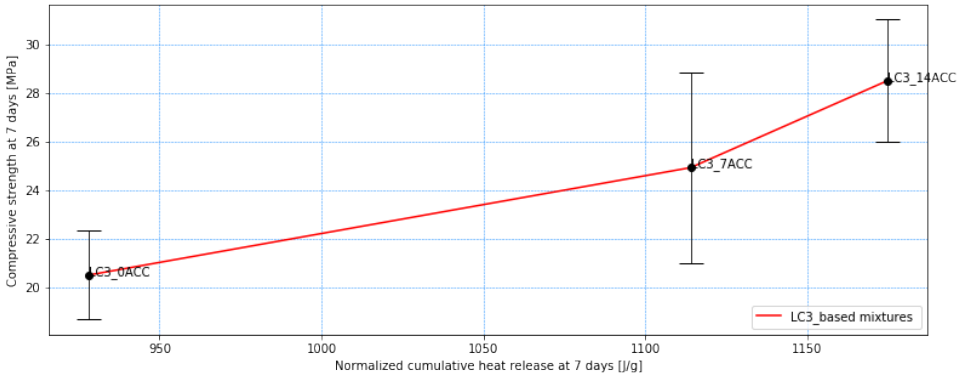

Figure 5.16: LC^3-based mixtures linear correlation between compressive strength and normalized cumulative heat at 7 days of hydration

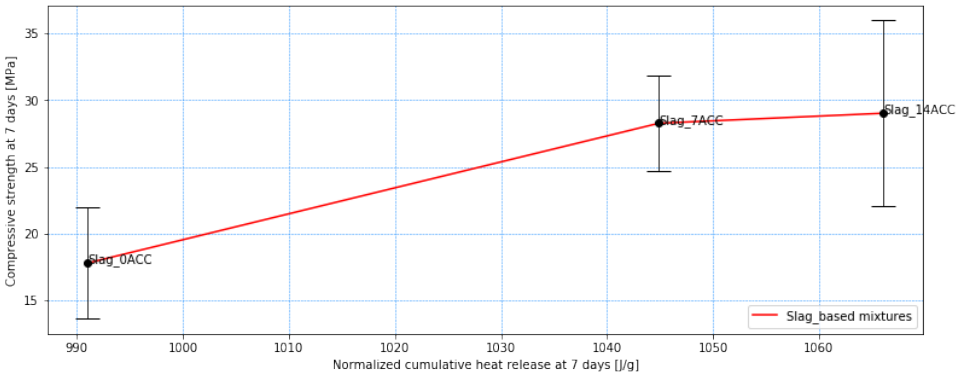

Figure 5.17: Slag-based mixtures linear correlation between compressive strength and normalized cumulative heat at 7 days of hydration

5

Heat evolution

In the absence of the accelerator (0% accelerator), slag- and LC^3-based mixes had the longest dormant period, at 4h and 2.5h, respectively. Furthermore, the main hydration peak was reached in 8 hours for the slag-based mixture and 6 hours for the LC^3-based mixture (peak (I)), see Figure 5.6. In these two mixtures, a second shoulder peak that was higher than the main hydration peak was found (peak (II)). Scrivener et al. [66] and Quennoz [80] hypothesize that as gypsum is depleted, a portion of the sulfate ions adsorbed on the C-S-H surface at an early age may be freed. Ettringite is produced once again as a result of the interaction between these sulfate ions and C_3A (Tricalcium aluminate). It is hence known as the second formation of ettringite.

As a rule of thumb, the second shoulder peak should occur several hours after the main hydration peak [66]; for slag- and LC^3-based mixes, this occurred 5.5h and 3.5h after the main peak, respectively. Despite this, after 18 hours of curing, the slag-based mixture's cumulative heat began to exceed the LC^3-based mixture. As a result, it was discovered that the slag-based mixture's total heat at 168 hours was slightly greater than that of the LC^3-based mixture. This is consistent with Laurent Steger et al. [81] findings regarding GGBS's contribution to heat development during the hydration reaction. According to their research, slag hydration significantly contributes to heat in blended cement between 15 and 24 hours. It should be noted that this time period corresponds to the onset of AFm formation.

A second peak with a lower intensity than the main hydration peak was observed for the LC^3-based mixture with a 14% accelerator between the ages of 50 and 80 hours (peak (II)) of hydration (Figure 5.6), which may be attributable to the second formation of ettringite. In mixes, increasing the accelerator dosage shortened the induction time, pushed the main hydration peak to an earlier age of hydration, and made it more intense. According to Dorn et al. [82] experimental data, the mechanism behind $Ca(NO_3)_2$ accelerating effect on cement hydration is that CN increases the formation of ettringite and an AFm phase. In addition, CN increases alite (C_3S) hydration because the addition

of CN reduces the aluminum content in the pore solution, which may accelerate the formation of calcium silicate hydrate (C–S–H) and portlandite (CH).

TGA

At 1 and 4h of curing, the quantity of hydrate water and CH in LC^3-based mixes with 0 and 7% accelerator was greater than in slag-based mixtures with the same accelerator concentration. While this tendency almost flipped for LC^3-based mixtures including 14% accelerator throughout the same curing period. The slag-based mixes with 0 and 7% accelerator dosage at 168h material age had a higher hydrate water content than LC^3-based mixtures with the same accelerator dosage while slag-based mixture with 14% accelerator showed a smaller number (see Table 5.1). This result was consistent with the compressive strength findings in section 5.4.1 of the mixtures at 7 days of curing. The results demonstrated that slag-based mixtures had a somewhat quicker rate of compressive strength growth than LC^3-based mixtures.

By comparing the quantity of H in slag-based and LC^3-based mixes, it was discovered that mixtures with a greater amount of H were connected to mixtures with a greater amount of cumulative heat generation as measured by isothermal calorimetry in section 5.4.2. This correlation between hydrate water content and cumulative heat production is consistent with Toosumran's observation [31]. Figures 5.18 and 5.19 depict the relationship between chemically bound water content and normalized cumulative heat (derived from isothermal calorimetry) of LC^3- and slag-based mixtures, respectively.

Although the LC^3-based mixture with 7% accelerator produced more cumulative heat than the slag-based mixtures with 7% and 14% accelerator, it contained less H; the reasons for this were not fully understood.

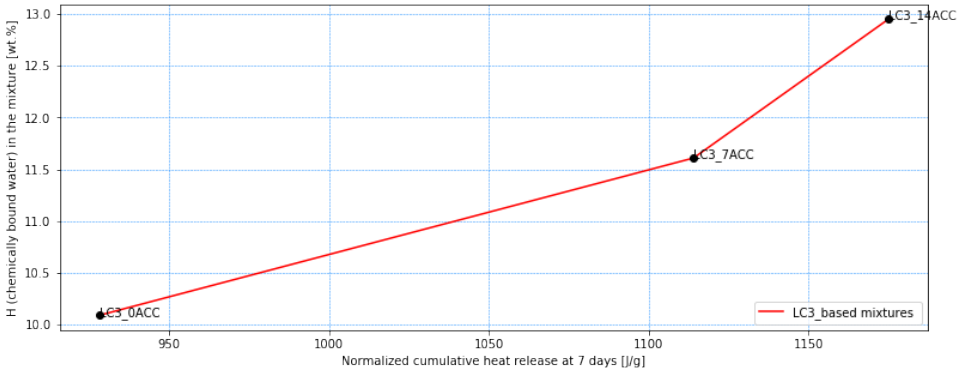

Figure 5.18: LC^3-based mixtures correlation between hydrate water [H] and normalized cumulative heat at 7 days of hydration

Mixture	Time [h]	H [wt.%]	CH [wt.%]
LC^3-based0.6SP& Limestone0ACC	1	1.20	0.69
	4	1.80	1.29
	168	10.09	5.57
LC^3-based0.6SP& Limestone7ACC	1	2.18	1.34
	4	3.89	3.22
	168	11.61	6.62
LC^3-based0.6SP& Limestone14ACC	1	2.53	1.51
	4	4.86	3.23
	168	12.95	7.53
Slag-based0.3SP& Limestone0ACC	1	0.87	0.56
	4	1.28	0.72
	168	12.22	10.22
Slag-based0.3SP& Limestone7ACC	1	1.92	1.05
	4	3.74	2.83
	168	12.27	9.21
Slag-based0.3SP& Limestone14ACC	1	2.62	1.20
	4	6.25	4.30
	168	12.88	9.22

Table 5.1: The amount of hydrate water [H] and calcium hydroxide [CH] at 1, 4 and 168 h

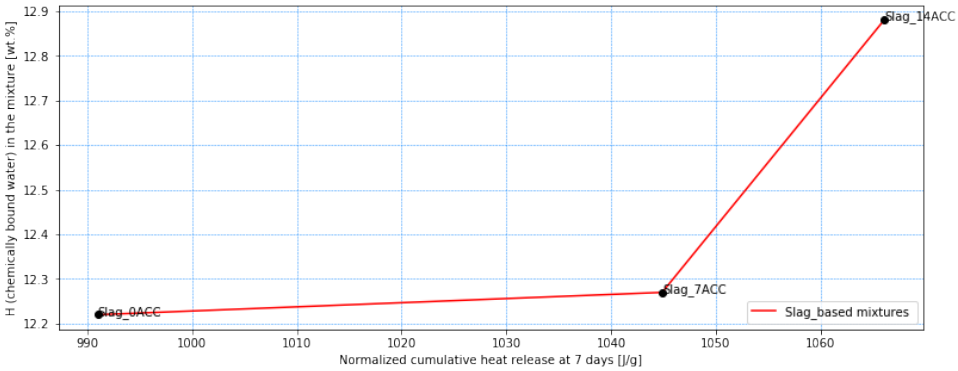

Figure 5.19: Slag-based mixtures correlation between hydrate water [H] and normalized cumulative heat at 7 days of hydration

6

THE DEVELOPED MIXTURE'S PRACTICAL APPLICABILITY

6.1. INTRODUCTION

This study examined the buildability of two different cementitious-based materials (LC^3 and slag-based) in combination with a limestone-based accelerator slurry in a set-on-demand configuration. The buildability test described in section 4.4.3 established that LC^3-0.6SP& limestone-7ACC produced the best structural build-up compared to the other mixtures. In addition, this mixture demonstrated relatively high compressive strength development, hydration product, and hydration heat; for instance, after 28 days of curing, it attained a compressive strength of 31.7 MPa. Consequently, the LC^3-0.6SP& limestone-7ACC mixture has the most potential for usage in both on-site and off-site printing applications. Therefore, this chapter intended to give some insight into the prospective future of a structural application including LC^3-0.6SP& limestone-7ACC mixture. The developed mixture's possible structural applications was examined from the perspective of a case study of a 3D-printed concrete cycling track. The load-bearing capacities of the 3D-printed bridge were evaluated in accordance with European norms.

6.2. BACKGROUND INFORMATION

There is an outdated footbridge in Burgemeester In 't Veldpark in Zaandam which is used by cyclists and pedestrians. This bridge can be replaced by a 3D-printed cycle bridge which its mixture was developed in this study. Two sections of the park will be connected by this bridge, and small boats will be able to leave their dock and navigate the Zuidervaart canal from beneath the bridge, as can be seen in Figure 6.1.

Due to the impossibility of providing reinforcement during the 3D printing process and the low tensile strength of concrete, the structural choices are quite restricted. In Gemert, a 3D-printed cycle bridge was designed using the same concept. The bridge was constructed with no reinforcement, and all tensile forces are absorbed by the prestressing load, see Figure 6.2 and Figure 6.3. To eliminate the need for prestressing and reinforcing, a logical construction would consist of an arch bridge in which the whole arch is under pressure. Arch bridges have traditionally been constructed using masonry,

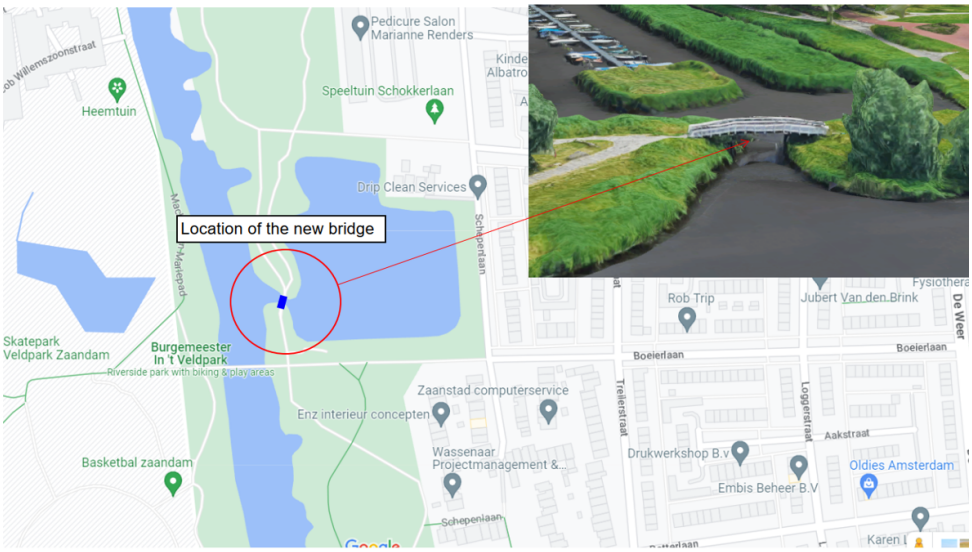

Figure 6.1: Location of the new cycle bridge, adapted from www.google.com/maps

6

in order to reduce tensile stress, compared to reinforced concrete or steel bridges, these constructions are much larger [83].

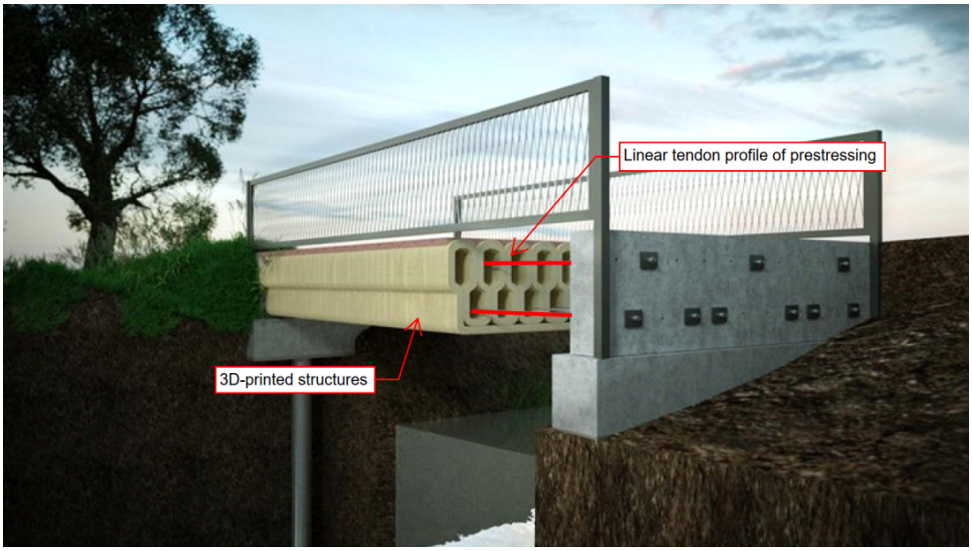

Figure 6.2: The world's first 3D-printed concrete bridge in Gemert, adapted from www.nu.nl

Figure 6.3: 3D-printed structure of Gemert bridge in Tu-Eindhoven, adapted from https://nos.nl/

In terms of statics, the force in a compressive arch is quite comparable to the tensile force in a cable. This concept originates from the reversibility of tensile and compressive systems, see Figure 6.4. A chain or cable's self-weight causes it to curve when suspended between two points, creating what is known as a chain line. The cable or chain can only withstand tensile forces and cannot withstand compression, shear, or bending moments. By inverting the cable and then replacing it with a material that can withstand compression, then the arch will only be subject to compressive stresses. In this case, the reversibility between a tensile and compressive system holds true. The arch is stable in this approach if the line of thrust stays within the cross-section [84], see Figure 6.5a.

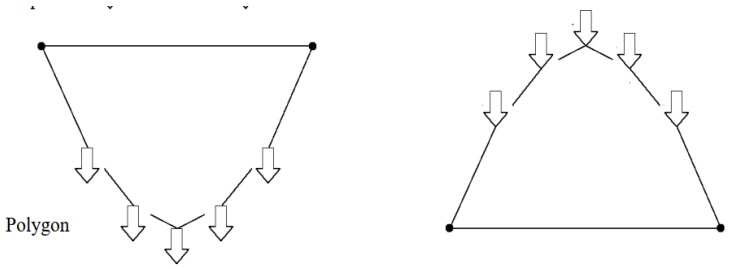

Figure 6.4: Tensile and compressive systems' reversibility, adapted from [84]

As soon as the thrust goes beyond the arch, the structure can no longer withstand the force and collapses, see Figure 6.5b. To avoid this issue, the arch should have enough

thickness (height) to readily transfer the compressive load to the supports, in other words, the thrust line will remain inside the cross-section.

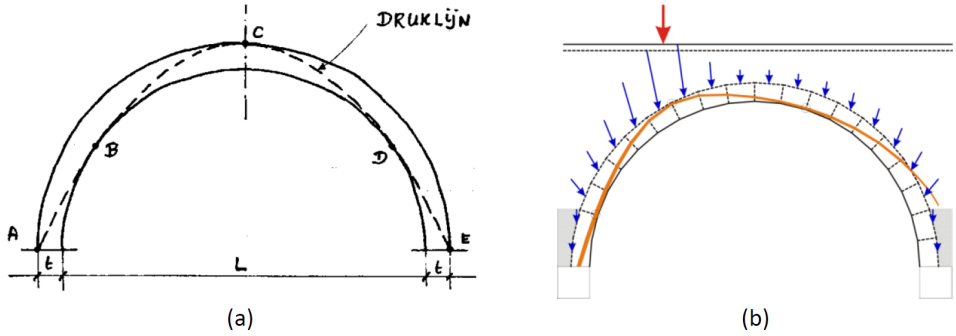

Figure 6.5: The flow path of compressive load in an arch, (a) a stable arch with the line of thrust inside the cross-section [84] (b) an unstable arch structure with the thrust line outside the cross-section, adapted from billharvey.typepad.com

According to a general rule of thumb, an arch needs to have the following minimum global dimensions in order to withstand certain loads is as follows [84]:

$$d = \frac{L}{28} \dots \frac{L}{40}$$

Where: d: the thickness of the arch ℓ : the span h: the height of the arch

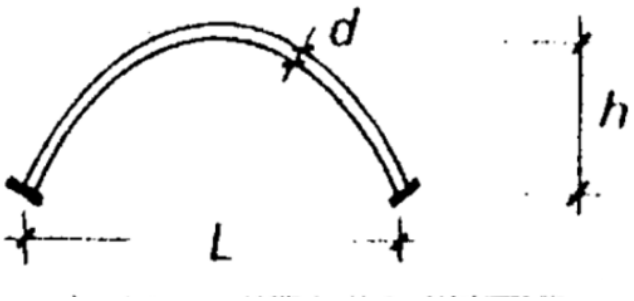

Figure 6.6: A schematic illustration of an arch [84]

6.3. DESIGN OF 3D-PRINTED CONCRETE BRIDGE

6.3.1. GENERAL

The structure of the 3D-printed bridge consists of three main components: a 3D-printed deck, a 3D-printed arch, and 3D-printed columns. According to the rule of thumb thickness of the arch might be $158.1 < d < 226\ mm$, which a height of 300 mm was chosen in this study.

6.3.2. BRIDGE DIMENSION

The span [m]	Width [m]	Height [m]
6	2	2.4

6.3.3. OVERVIEW OF THE BRIDGE

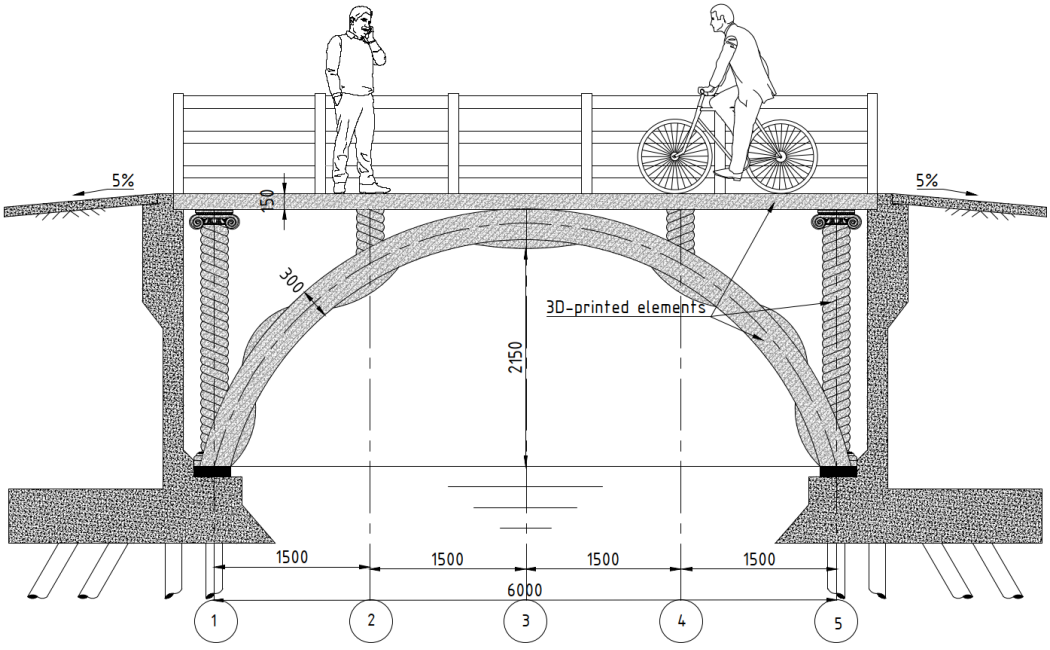

Figure 6.7: Cross section of the 3D-printed Bridge, column shape adopted from www.royalcorinthian.com

6.3.4. PRINCIPLES

Standards and guidelines

The Dutch Building Decree must be met by every bridge in the Netherlands. Therefore, the design of the 3D-printed bridge was verified by taking into account the following principles and criteria.

- NEN-EN 1990:2002/NB:2019: Basis of structural design
- NEN-EN 1991-2: Traffic loads on bridges

- NEN-EN 1991-1-4:2005: Wind actions
- NEN-EN 1992-1-1+C2: Design of concrete structures

Software
The following software packages were utilized for the calculations and drawing:

- DIANA FEM software (version 10.5)
- AutoCAD (version 2023)
- Revit (version 2023)

6.3.5. LOADS

General
Unit weight: $\gamma_{concrete} = 25.0\ kN/m^3$

Permanent loads
Bridge deck

$$Qc{=}hc{*}\text{characteristic weight} = 0.15[\text{m}] * 25[kN/m^3] = 3.75\ kN/m^2$$

$$Q_{wearing\ course\ layer} = 0.2\ kN/m^2$$

$$Q_{bridge\ railing} = negligible$$

The arch and the columns

$$Q_{c,\ columns} = 0.15[\text{m}] * 25[kN/m^3] = 3.75\ kN/m^2$$

$$Q_{c,arch} = 0.3[\text{m}] * 25[kN/m^3] = 7.5\ kN/m^2$$

Variable loads (NEN-EN 1991-2:2003- 5.3.2.1-2)
A uniformly distributed load of $Qq = 5.0\ kN/m^2$
A characteristic value of the concentrated load $Q_{fvd} = 7.0\ kN$ acting on a surface of 0.10 m × 0.10 m.
Service vehicle: The bridge will be closed for service and unintentional traffic.

Wind load(NEN-EN 1991-1-4) Wind force: $F_w = \frac{1}{2} * \rho * v_b^2 * C * A_{ref}$
where:
ρ : the density of air
V_b : fundamental value of the basic wind speed
C : the wind load factor
$A_{ref} = d$: the reference area of the structure in m, see Figure 6.8
$\rho = 1.25\ kg/m3$, according 4.5 NEN-EN1991-1-4
$V_b = 27\ m/s$, in terrain category II, according to Figure NB.2 in NEN-EN1991-1-4
$A_{ref} = 0.5\ m$ height of the deck and the arch

$C = 3$, $\frac{b}{d_{tot}=A_{ref}} = \frac{2m\ (width\ of\ the\ bridge)}{0.5\ m} = 4$, according to the table NB.18, NEN-EN1991-1-4, by $z_e \leq 20m$, and unbuilt area. (z_e = the reference height)

$$F_w = \frac{1}{2} * 1.25 * 27^2 * 3 * 0.5 = 0.7 \sim 1\ kN/m$$

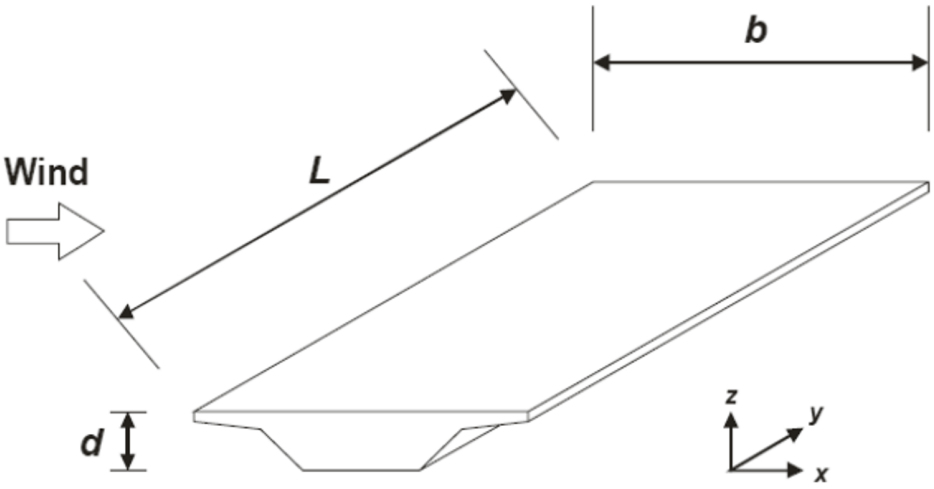

Figure 6.8: Wind force direction on the bridge, adapted from www.briswarenhuis.nl

6.3.6. DESIGN VERIFICATION OF THE 3D-PRINTED BRIDGE

Once the primary loads were identified, the bridge was simulated using DIANA software, which utilizes the Finite Element Method (FEM) to determine the stress levels in the structural components. The objective of this examination was to evaluate the bridge's highest stress levels as a result of the applied loads. In order to determine whether the developed mixture was appropriate for use in the construction of the 3D-concrete bridge, the maximum stress levels could be compared to the mixture's strength.
In addition to self-weight, three separate loads were added to the structure, including a variable load of 5 kN/m^2, a wind load of 1 kN/m, and a variable line load of 3.5 kN/m. In order to determine the critical stress levels in different parts of the structure, two different load cases with variable loads were generated, as depicted in Figure 6.9a and b. The 3D model was created utilizing quadratic quadrilateral finite elements with a mesh size of 50x50 mm^2 (see 6.9c).

(a) DIANA model, the bridge fully loaded

(b) DIANA model, the bridge half loaded

(c) DIANA mesh model

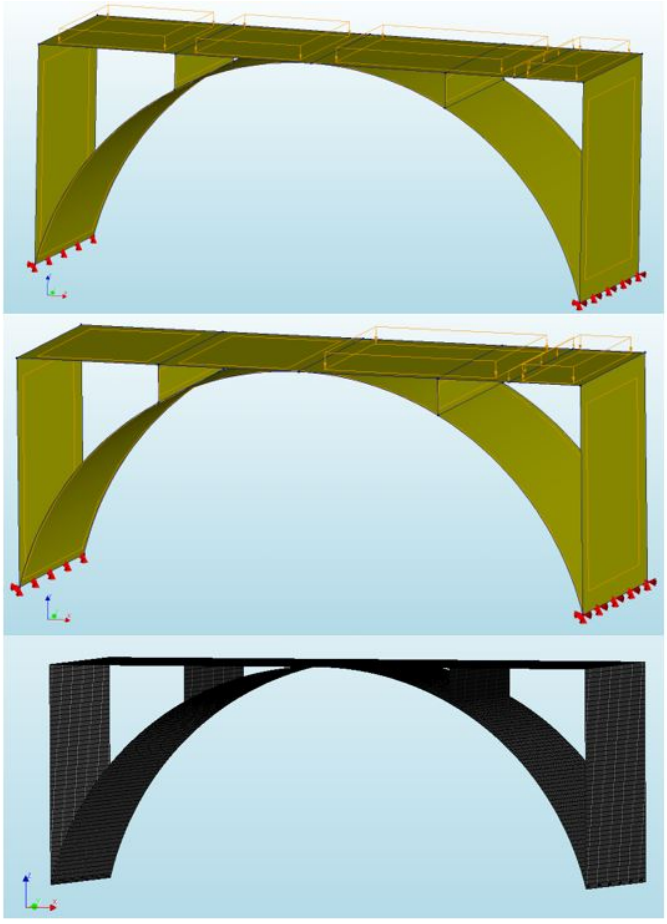

Figure 6.9: Diana models for the 3D-printed bridge

The results obtained from a linear static analysis are as follows:

- The bridge deck experienced maximum horizontal stress of 0.35 MPa in the longitudinal direction (SXX), as observed in Figure 6.10.
- The side columns at the top of the support had a maximum horizontal stress of 0.14 MPa in the transverse direction (SYY), see Figure 6.11.
- The top of the support on the side columns experienced maximum vertical stress of 0.78 MPa in the Z-direction (SZZ), as indicated in Figure 6.12.
- Additionally, a maximum shear stress of 1.04 MPa occurred in the YZ-direction (SYZ) between the middle columns and the arch, as depicted in Figure 6.13.

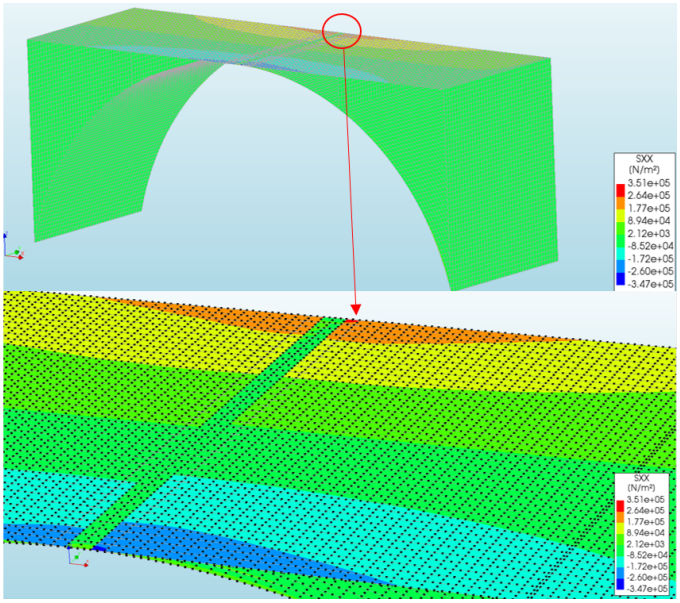

Figure 6.10: Stresses in the 3D-printed bridge in the longitudinal direction

According to the findings presented in section 5.4.1, the LC^3-0.6SP&limestone-7ACC mixture achieved a compressive strength perpendicular to the printing path of 24.9 MPa at 7 days of curing. However, the FEM analysis showed that the maximum compressive strength in the SZZ direction was only 0.78 MPa, which was lower than the strength of the printed sample. It should be noted that this study did not evaluate the strength of the printed samples in the longitudinal or transverse directions. After verifying the strength of printed samples in different directions at 7 days, it can be concluded that the chosen mixture achieved adequate strength to endure the given loads based on this simplified analysis.

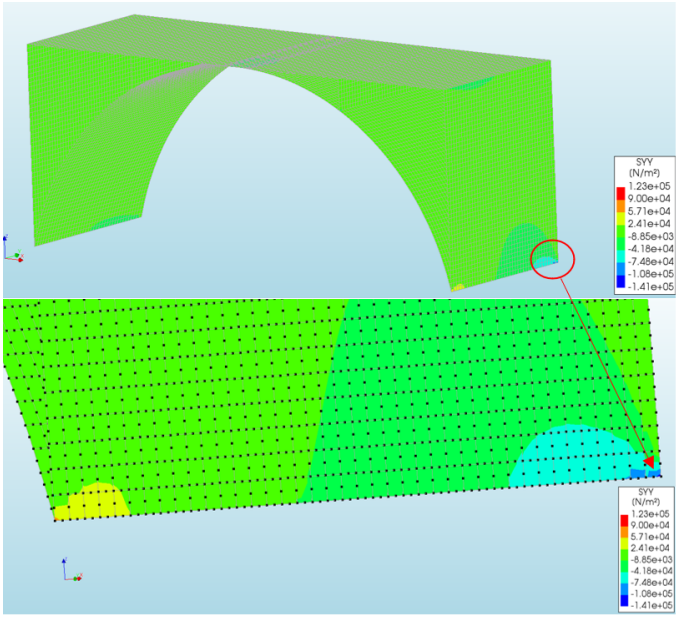

Figure 6.11: Stresses in the 3D-printed bridge in the transverse direction

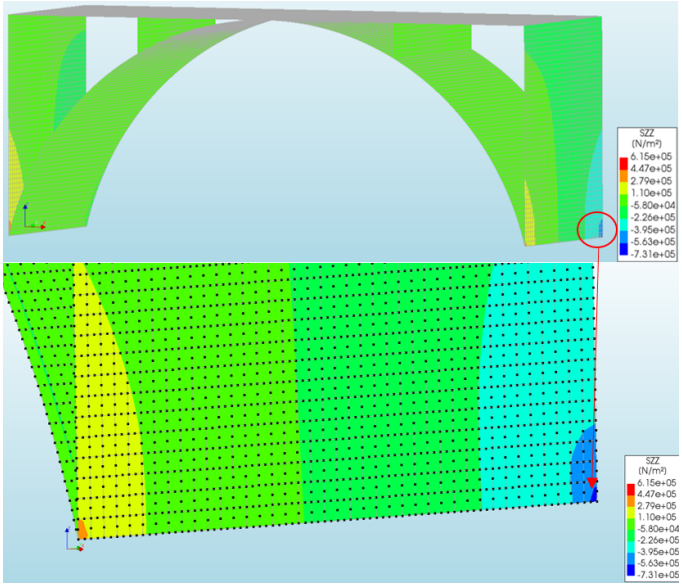

Figure 6.12: Stresses in the 3D-printed bridge in the Z-direction

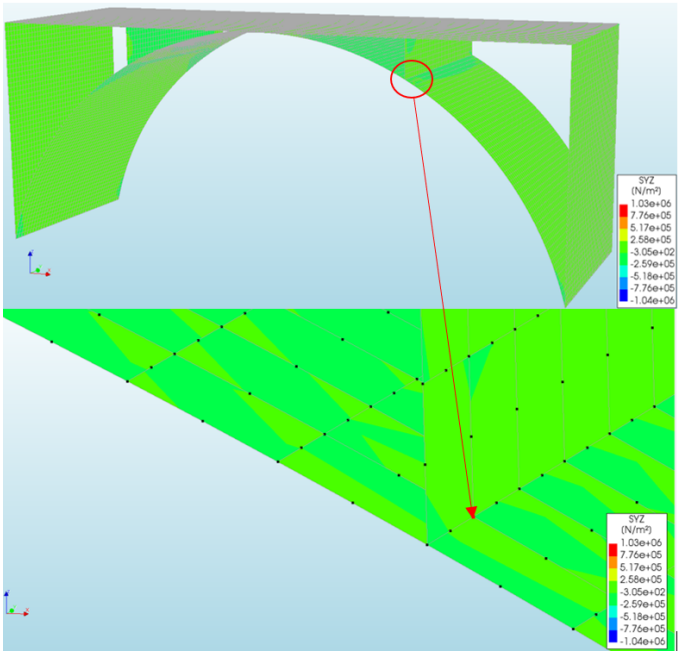

Figure 6.13: Shear stresses in the 3D-printed bridge in the YZ-direction

6.4. APPLICATION OF THE DEVELOPED MIXTURE TO THE 3D-PRINTED BRIDGE

The use of 3D concrete printing provides the advantage of being able to print any desired shape, which is why an arch bridge with twisted columns and a sinusoidal wave arch was chosen for this case study. The sinusoidal wave arch was implemented for two primary reasons. Firstly, it enhances the aesthetic appeal of the bridge. Secondly, incorporating the waveform into the cross-section increases the structural strength of the bridge in areas where higher stresses are anticipated. However, for the conservation calculation of stresses in the bridge, the sinusoidal wave was not taken into account. It is important to highlight that the twisted shape of the columns is exclusively incorporated at the initial sections on both sides for aesthetic considerations. These sections will be printed separately and subsequently anchored to the columns.
Without additional support, the entire structure might be printed once, if done transversely (along the width of the bridge), and filaments can be stacked on top of one another. According to Mechtcherine et al. [85], a nozzle with a rectangular opening of 150 mm by 50 mm can be used without difficulty for printing large-size filaments. Therefore, columns and the bridge deck can be printed with one line, and the arch can be printed with two lines on top of each other, each line being 150 mm wide. In Figure 6.14, the printing path is demonstrated.

Printing the entire structure in one session results in a monolithic structure with strong,

stress-resistant connections. Because there is not enough room between the filaments to apply reinforcement bars, the durability of the bridge is affected when reinforcement is not present [40]. However, it could be solved by employing a post-tensioned pre-stressing technique. For instance, during the printing process, a number of ducts could be embedded in the deck, after which steel strands could be threaded through the ducts. Following the curing of the concrete, the steel strands are tensioned with the aid of a hydraulic jack before being anchored at either end of the bridge abutment.

The printing session could occur on-site or off-site. In the on-site method, there is sufficient space near the bridge location, therefore the massive printed bridge does not need to be transported to the location. However, unforeseen circumstances such as equipment failures or bad weather might have a big impact on the entire operation. The primary advantage of off-site applications is that climatic conditions can be easily controlled, allowing printing to take place throughout the year regardless of weather conditions. However, moving a large structure requires the use of heavy equipment, such as trucks and cranes, which might have a negative impact on the cost and CO_2 footprint.

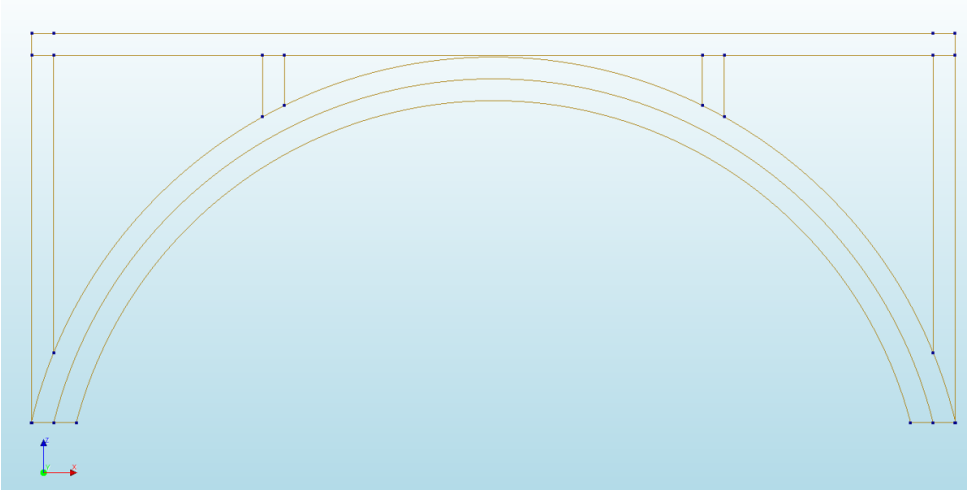

Figure 6.14: Printing path of the 3D-printed bridge (top view)

After the 3D printing process finishes in the transverse direction, the bridge must be turned 90 degrees and raised to be positioned on the bridge abutment. In off-site applications, the bridge needs to be transported to a different location. Since the printed bridge's tensile strength in the absence of the reinforcement is dominant and it weighs approximately 20 tons, rotating and lifting it could create considerable tensile stress in its cross-section. To address this transportation challenge, a feasible solution is to print the bridge on a steel frame structure, see Figure 6.15. A high-strength steel frame could be tailored in a such way that distributes the weight of the bridge and provide sufficient support to prevent any unexpected stresses in the bridge's cross-section as depicted in Figure 6.16.

Three connection points can be designed to securely attach the steel frame to the

bridge: two at the bridge feet and one in the middle, facilitating easier and more stable lifting and transportation, see Figures 6.17 and 6.18. Once the printing is complete, a mobile crane can be utilized to hoist the bridge onto a flatbed truck. The steel frame can be easily pulled at designated lifting points (steel square hollow sections) and lifted alongside the bridge, effectively minimizing stress on the bridge's cross-section. During transportation, appropriate cushioning materials such as airbags or foam pads, as well as vibration isolation techniques, can be employed to absorb shocks and vibrations that may occur during the transportation. These precautions help safeguard the bridge from sudden impacts or jolts that could potentially induce unforeseen stresses.

Figure 6.15: Top view of the 3D printed bridge on the steel frame structure

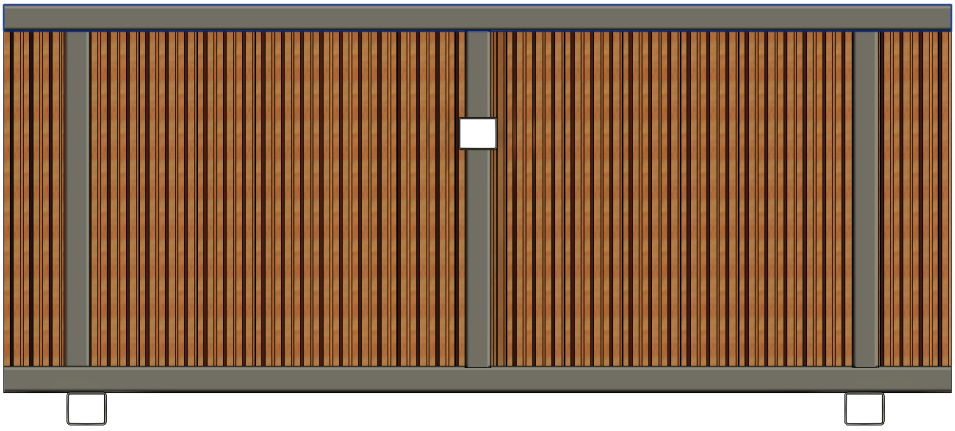

Figure 6.16: Bottom view of the steel frame structure

Figure 6.17: A 3D view of three locations where the steel frame connects to the 3D printed bridge

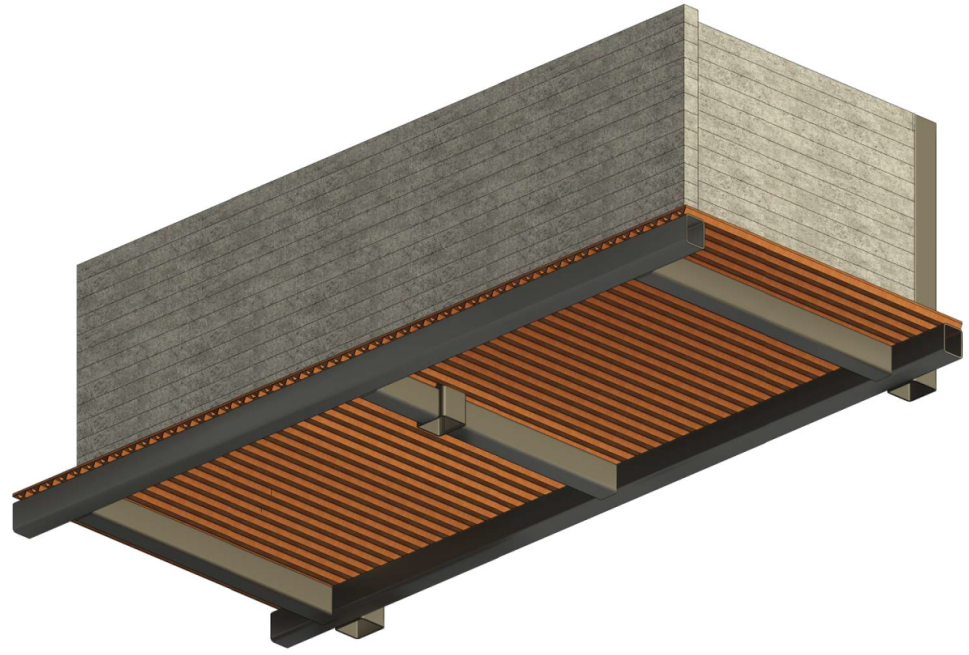

Figure 6.18: A 3D view of three locations where the steel frame connects to the 3D printed bridge

7

CONCLUSIONS AND RECOMMENDATIONS

7.1. GENERAL CONCLUSIONS

In this part, the findings from previous chapters are summarized in order to address all of the study questions posed in section 1.3.

- In the slump test, the diameter of all examined accelerator slurry mixes ranged between 130 mm and 210 mm, while LC^3-0.6SP and slag-0.2SP exhibited a similar range in cementitious materials. By increasing the amount of resting time, the spread diameter of the accelerator slurry mixes and cementitious material reduced. This decrease in accelerator slurry might be the result of water evaporation or a fraction of water absorption by aggregates. The flocculation of cementitious particles may account for the reduction in cementitious material's spread diameter.

- The pumpability test was conducted on three separate mixtures, including limestone-based 7ACC, LC^3-0.6SP and slag-0.3SP. All mixes demonstrated a linear relationship between flow rate (L/s) and pumping speed, with almost identical flow rates. Therefore, at a volume ratio of 1:1, both the cementitious material-based mixtures and the limestone-based accelerator slurry mixture may be pumped and combined at the same speed.

- The flow curve test was carried out on limestone-based accelerator slurry (containing 0%- 7% and 14% $Ca(NO_3)_2$, as well as slag-0.3SP and LC^3-0.6SP. In accordance with the findings of the slump test, the dynamic yield stress and plastic viscosity of the limestone-based accelerator slurry mixtures increased when the $Ca(NO_3)_2$ concentration was increased. The LC^3-0.6SP mixture had larger dynamic yield stress and plastic viscosity than the slag-0.3SP mixture, which was consistent with the slump test findings.

- The initial setting time of the LC^3-based mixture without $Ca(NO_3)_2$ was 140 minutes; by increasing the amount of the accelerator, this period was lowered further.

Adding 7% $Ca(NO_3)_2$ lowered its initial setting time to 80 minutes, and adding 14% $Ca(NO_3)_2$ reduced it to 50 minutes. The initial setting time of the slag-based mixture reference mixture was 160 minutes. Likewise, by raising the dose of the accelerator, the initial setting time was reduced. By adding 7% $Ca(NO_3)_2$, the initial setting time decreased to 90 minutes, and by adding 14% accelerator, it decreased further to 70 minutes. The faster initial setting time development in both mixtures may be ascribed to the generation of ettringite and facilitated C-S-H nucleation.

- The buildability of three distinct mixtures was evaluated: slag-based0.3SP& limestone7ACC, LC^3-based0.6SP& limestone0ACC, and LC^3-based0.6SP& limestone7ACC. The slag-based mixture's buildability test indicated a plastic collapse of the bottom filament after printing 9 layers, then it collapsed in the 13th layer. The LC^3-based mixture with 0% $Ca(NO_3)_2$ experienced material failure at the 10th layer and collapsed at the 15th layer. Finally, the LC^3-based mixture with 7% $Ca(NO_3)_2$ accomplished encouraging results by stacking 16 layers.

- All mixes' compressive strength development was evaluated at 7 and 28 days of curing. Both LC^3- and slag-based mixes had a faster rise in compressive strength at 28 days as a result of the accelerator's increased content. At 28 days, the LC^3-based mixture with 0% $Ca(NO_3)_2$ had a compressive strength of 25 MPa, while the compressive strength of mixtures with 7% and 14% accelerator exceeded 30 MPa. The growth of compressive strength in slag-based mixes at 28 days was less than 30 MPa when 0% to 7% accelerator was added. However, the compressive strength development of the slag-based mixture with a 14% accelerator was more than 30 MPa. The increase in hydration products might be the cause of this improvement.

- Increasing the accelerator dose in both LC^3- and slag-based mixes reduced the induction time, shifted the primary hydration peak to an earlier age of hydration, and increase its intensity. Furthermore, increasing the $Ca(NO_3)_2$ dose in all mixes resulted in an increase in the amount of cumulative heat, portlandite, and chemically bound water. Among the investigated mixes, the LC^3-based mixture with 14% accelerator produced the most cumulative heat after 7 days of curing. Taking into account the standard deviation, this mixture exhibited the greatest degree of compressive strength development and chemically bound water among all the mixtures.

- The 3D-printed concrete bridge could be constructed using the developed 3DCP mixture (LC3-based0.6SP & limestone7ACC). The use of this mixture in the 3D concrete printing approach offers several advantages in addition to creating an aesthetically pleasing structure. Firstly, since Portland cement is partially replaced in the mixture, it helps ensure the sustainability of the concrete industry by significantly lowering CO_2 emissions. Secondly, since less manpower is needed in the 3D printing method, it has the potential to reduce construction costs.

7.2. RECOMMENDATIONS

This experiment was completed within specified limitations, and several features of the developed mixtures need further investigation. As a result, the recommendations and areas for additional investigation are provided below.

- Three distinct accelerator slurry mixtures, including those based on limestone, fly ash, and slag were tested for their initial setting times when combined with LC^3-based cementitious material. The intended result was demonstrated by the LC^3-based and limestone-based accelerator slurry mixture. The initial setting time for the LC^3-based and slag-based accelerator slurry mixture (with 7% CN) exceeded 150 minutes. The initial setting time for the LC^3-base and fly ash-based accelerator slurry mixture (with 7% CN) exceeded 300 minutes.
- It is recommended to investigate the interlayer properties. The strength and bonding between the different filaments are referred to as interlayer properties. Because they have an impact on the general strength and durability of the printed structure, these characteristics necessitate further study. Several variables may influence the interlayer properties of filaments, including mixture composition, surface preparation (e.g., roughening the surface), printing parameters (such as printing speed, ambient temperature, and layer thickness), and post-processing (e.g., applying a coating).
- To ensure a high-quality and durable printed structure in 3D concrete printing with the use of a static mixer, it is recommended to verify that the material is well-mixed before extrusion. Investigating this factor is crucial since well-mixed material is essential in producing an excellent final product.
- It is recommended to investigate how to enhance the durability of the hardened material in order to produce high-quality and long-lasting printed structures in 3D concrete printing. For instance, proper curing, such as keeping the printed structure moist. This can help to increase the material's durability and prevent the printed structure from deteriorating prematurely.
- More research on drying shrinkage is recommended. Because cracks caused by shrinkage can drastically reduce the strength of the cementitious material, especially if reinforcing is not present.
- In actual applications of the developed mixture, the nozzle type should be configured such that the printed filaments have the most possible contact with one another in order to increase the contact area between the layers.
- Due to the use of a chloride-free accelerator ($Ca(NO_3)_2$) in this work, the mixes are not restricted to using steel reinforcement due to corrosion. Regarding the usefulness of reinforcement in 3DCP technologies, more study is still required for its applicability.
- For evaluating the buildability of a newly developed mixture, the green strength test may be a quick approach to acquire a first impression of the material's behavior.

BIBLIOGRAPHY

[1] D. Fiľarská, S. Unčík, and T. Cabanová. "Specification of the Properties and Effects of Additives and Admixtures on a Mixture Suitable for 3D Printing of Buildings". In: *Slovak Journal of Civil Engineering* 28.4 (Dec. 2020), pp. 38–44. DOI: 10.2478/sjce-2020-0029. URL: https://www.sciendo.com/pdf/10.2478/sjce-2020-0029.

[2] T. Economist. *The third industrial revolution*. 2012. URL: https://www.economist.com/leaders/2012/04/21/the-third-industrial-revolution.

[3] T. Wangler, E. Lloret, L. Reiter, N. Hack, F. Gramazio, M. Kohler, M. Bernhard, B. Dillenburger, J. Buchli, N. Roussel, and R. Flatt. "Digital Concrete: Opportunities and Challenges". In: *RILEM Technical Letters* 1 (Oct. 2016), pp. 67–75. DOI: 10.21809/rilemtechlett.2016.16. URL: http://dx.doi.org/10.21809/rilemtechlett.2016.16.

[4] I. Dressler, N. Freund, and D. Lowke. "The Effect of Accelerator Dosage on Fresh Concrete Properties and on Interlayer Strength in Shotcrete 3D Printing". In: *Materials* 13.2 (Jan. 2020), p. 374. DOI: 10.3390/ma13020374. URL: http://dx.doi.org/10.3390/ma13020374.

[5] N. Roussel. "Rheological requirements for printable concretes". In: *Cement and Concrete Research* 112 (Oct. 2018), pp. 76–85. DOI: 10.1016/j.cemconres.2018.04.005. URL: http://dx.doi.org/10.1016/j.cemconres.2018.04.005.

[6] A. Gyekenyesi and M. Halbig. *Advanced Processing and Manufacturing Technologies for Nanostructured and Multifunctional Materials, Volume 35, Issue 6*. 6. John Wiley & Sons, 2015.

[7] S. M. Allen and E. M. Sachs. "Three-dimensional printing of metal parts for tooling and other applications". In: *Metals and Materials* 6 (2000), pp. 589–594.

[8] J. Schwaiger, T. C. Lueth, and F. Irlinger. "G-Code generation for a new printing process based on 3D plastic polymer droplet generation". In: *ASME International Mechanical Engineering Congress and Exposition*. Vol. 56185. American Society of Mechanical Engineers. 2013, V02AT02A006.

[9] G. H. Vardhan, G. H. Charan, P. S. Reddy, and K. S. Kumar. "3D printing: The dawn of a new era in manufacturing". In: *International Journal on Recent and Innovation Trends in Computing and Communication* 2.8 (2014), pp. 2373–2376.

[10] M. T. Souza, I. M. Ferreira, E. G. de Moraes, L. Senff, and A. P. N. de Oliveira. "3D printed concrete for large-scale buildings: An overview of rheology, printing parameters, chemical admixtures, reinforcements, and economic and environmental prospects". In: *Journal of Building Engineering* 32 (2020), p. 101833.

[11] M. Xia, B. Nematollahi, and J. Sanjayan. “Compressive strength and dimensional accuracy of portland cement mortar made using powder-based 3D printing for construction applications”. In: *First RILEM International Conference on Concrete and Digital Fabrication–Digital Concrete 2018*. Springer. 2019, pp. 245–254.

[12] Y. Chen, F. Veer, O. Copuroglu, and E. Schlangen. “Feasibility of using low CO 2 concrete alternatives in extrusion-based 3D concrete printing”. In: *First RILEM International Conference on Concrete and Digital Fabrication–Digital Concrete 2018*. Springer. 2019, pp. 269–276.

[13] S. Muthukrishnan, S. Ramakrishnan, and J. Sanjayan. “Set on demand geopolymer using print head mixing for 3D concrete printing”. In: *Cement and Concrete Composites* 128 (2022), p. 104451.

[14] B. Heater. *MIT’s giant mobile 3D printer can build a building in 14 hours, and some day it may be headed to Mars*. 2017. URL: https://techcrunch.com/2017/04/27/mits-giant-mobile-3d-printer-can-build-a-building-in-14-hours-and-some-day-it-may-be-headed-to-mars/?guccounter=2.

[15] L. Reiter, T. Wangler, N. Roussel, and R. J. Flatt. “The role of early age structural build-up in digital fabrication with concrete”. In: *Cement and Concrete Research* 112 (2018), pp. 86–95.

[16] P. Wu, J. Wang, and X. Wang. “A critical review of the use of 3-D printing in the construction industry”. In: *Automation in Construction* 68 (2016), pp. 21–31.

[17] L. Reiter, T. Wangler, A. Anton, and R. J. Flatt. “Setting on demand for digital concrete–principles, measurements, chemistry, validation”. In: *Cement and Concrete Research* 132 (2020), p. 106047.

[18] M. Chen, L. Li, Y. Zheng, P. Zhao, L. Lu, and X. Cheng. “Rheological and mechanical properties of admixtures modified 3D printing sulphoaluminate cementitious materials”. In: *Construction and Building Materials* 189 (2018), pp. 601–611.

[19] M. T. Souza, I. M. Ferreira, E. G. de Moraes, L. Senff, S. Arcaro, J. R. C. Pessôa, M. J. Ribeiro, and A. P. N. de Oliveira. “Role of chemical admixtures on 3D printed Portland cement: Assessing rheology and buildability”. In: *Construction and Building Materials* 314 (2022), p. 125666.

[20] C. Zhang, V. N. Nerella, A. Krishna, S. Wang, Y. Zhang, V. Mechtcherine, and N. Banthia. “Mix design concepts for 3D printable concrete: A review”. In: *Cement and Concrete Composites* 122 (2021), p. 104155.

[21] L. Reiter. “Structural build-up for digital fabrication with concrete-materials, methods and processes”. PhD thesis. ETH Zurich, 2019.

[22] B. Panda, C. Unluer, and M. J. Tan. “Investigation of the rheology and strength of geopolymer mixtures for extrusion-based 3D printing”. In: *Cement and Concrete Composites* 94 (2018), pp. 307–314.

[23] M. K. Mohan, A. Rahul, K. Van Tittelboom, and G. De Schutter. “Rheological and pumping behaviour of 3D printable cementitious materials with varying aggregate content”. In: *Cement and Concrete Research* 139 (2021), p. 106258.

[24] F. Boscaro, E. Quadranti, T. Wangler, S. Mantellato, L. Reiter, and R. J. Flatt. “Eco-friendly, set-on-demand digital concrete”. In: *3D Printing and Additive Manufacturing* 9.1 (2022), pp. 3–11.

[25] V. Mechtcherine, V. N. Nerella, F. Will, M. Näther, J. Otto, and M. Krause. “Large-scale digital concrete construction–CONPrint3D concept for on-site, monolithic 3D-printing”. In: *Automation in construction* 107 (2019), p. 102933.

[26] B. Panda, N. A. Noor Mohamed, S. C. Paul, G. Bhagath Singh, M. J. Tan, and B. Šavija. “The effect of material fresh properties and process parameters on buildability and interlayer adhesion of 3D printed concrete”. In: *Materials* 12.13 (2019), p. 2149.

[27] B. Nematollahi, M. Xia, and J. Sanjayan. “Current progress of 3D concrete printing technologies”. In: *ISARC. Proceedings of the international symposium on automation and robotics in construction*. Vol. 34. IAARC Publications. 2017.

[28] T. Wangler and R. J. Flatt. *First RILEM International Conference on Concrete and Digital Fabrication–Digital Concrete 2018*. Vol. 19. Springer, 2018.

[29] C. Barnatt. *3D Printing: Third Edition*. ExplainingTheFuture.com, 2016.

[30] Y. Chen, F. Veer, and O. Copuroglu. “A critical review of 3D concrete printing as a low CO2 concrete approach”. In: *Heron* 62.3 (2017), pp. 167–194.

[31] N. Toosumran. “Feasibility study for the use of desalineation brine to improve the structural build-up behavoir of the 3D concrete printing mixture”. In: (2022).

[32] Y. Chen, S. He, Y. Gan, O. Çopuroğlu, F. Veer, and E. Schlangen. “A review of printing strategies, sustainable cementitious materials and characterization methods in the context of extrusion-based 3D concrete printing”. In: *Journal of Building Engineering* 45 (2022), p. 103599.

[33] B. Khoshnevis. “Automated construction by contour crafting—related robotics and information technologies”. In: *Automation in construction* 13.1 (2004), pp. 5–19.

[34] C. Gosselin, R. Duballet, P. Roux, N. Gaudillière, J. Dirrenberger, and P. Morel. “Large-scale 3D printing of ultra-high performance concrete–a new processing route for architects and builders”. In: *Materials & Design* 100 (2016), pp. 102–109.

[35] F. Bos, R. Wolfs, Z. Ahmed, and T. Salet. “Additive manufacturing of concrete in construction: potentials and challenges of 3D concrete printing”. In: *Virtual and physical prototyping* 11.3 (2016), pp. 209–225.

[36] Y. Chen, S. C. Figueiredo, Z. Li, Z. Chang, K. Jansen, O. Çopuroğlu, and E. Schlangen. “Improving printability of limestone-calcined clay-based cementitious materials by using viscosity-modifying admixture”. In: *Cement and Concrete Research* 132 (2020), p. 106040.

[37] Y. Tao, A. Rahul, K. Lesage, Y. Yuan, K. Van Tittelboom, and G. De Schutter. “Stiffening control of cement-based materials using accelerators in inline mixing processes: possibilities and challenges”. In: *Cement and Concrete Composites* 119 (2021), p. 103972.

[38] V. Mechtcherine, F. P. Bos, A. Perrot, W. L. da Silva, V. Nerella, S. Fataei, R. J. Wolfs, M. Sonebi, and N. Roussel. “Extrusion-based additive manufacturing with cement-based materials–production steps, processes, and their underlying physics: a review”. In: *Cement and Concrete Research* 132 (2020), p. 106037.

[39] Y. Tao, A. Rahul, K. Lesage, K. Van Tittelboom, Y. Yuan, and G. De Schutter. “Mechanical and microstructural properties of 3D printable concrete in the context of the twin-pipe pumping strategy”. In: *Cement and Concrete Composites* 125 (2022), p. 104324.

[40] M. Spek. “Pre-treatment and utilization of recycled fine glass dust for 3D Concrete Printing”. In: (2022).

[41] R. Thakur, C. Vial, K. Nigam, E. Nauman, and G. Djelveh. “Static mixers in the process industries—a review”. In: *Chemical engineering research and design* 81.7 (2003), pp. 787–826.

[42] A. Ghanem, T. Lemenand, D. Della Valle, and H. Peerhossaini. “Static mixers: Mechanisms, applications, and characterization methods–A review”. In: *Chemical engineering research and design* 92.2 (2014), pp. 205–228.

[43] G. Ji, T. Ding, J. Xiao, S. Du, J. Li, and Z. Duan. “A 3D printed ready-mixed concrete power distribution substation: Materials and construction technology”. In: *Materials* 12.9 (2019), p. 1540.

[44] K. El Cheikh, S. Rémond, N. Khalil, and G. Aouad. “Numerical and experimental studies of aggregate blocking in mortar extrusion”. In: *Construction and Building Materials* 145 (2017), pp. 452–463.

[45] R. Kozul and D. Darwin. “Effects of aggregate type, size, and content on concrete strength and fracture energy. University of Kansas Center for Research”. In: *Inc.: Lawrence, KS, USA* (1997), pp. 47–63.

[46] G. Ma, Z. Li, and L. Wang. “Printable properties of cementitious material containing copper tailings for extrusion based 3D printing”. In: *Construction and building materials* 162 (2018), pp. 613–627.

[47] S. Lim, R. A. Buswell, T. T. Le, S. A. Austin, A. G. Gibb, and T. Thorpe. “Developments in construction-scale additive manufacturing processes”. In: *Automation in construction* 21 (2012), pp. 262–268.

[48] F. U. Rahman. *Initial Setting Time and Final Setting Time of Concrete*. 2019. URL: https://theconstructor.org/concrete/initial-final-setting-time-concrete/25819/.

[49] D. Marchon, S. Kawashima, H. Bessaies-Bey, S. Mantellato, and S. Ng. “Hydration and rheology control of concrete for digital fabrication: Potential admixtures and cement chemistry”. In: *Cement and Concrete Research* 112 (2018), pp. 96–110.

[50] S. C. Paul, Y. W. D. Tay, B. Panda, and M. J. Tan. “Fresh and hardened properties of 3D printable cementitious materials for building and construction”. In: *Archives of civil and mechanical engineering* 18 (2018), pp. 311–319.

[51] R. A. Buswell, W. L. De Silva, S. Z. Jones, and J. Dirrenberger. "3D printing using concrete extrusion: A roadmap for research". In: *Cement and Concrete Research* 112 (2018), pp. 37–49.

[52] C. Schröfl, V. N. Nerella, and V. Mechtcherine. "Capillary water intake by 3D-printed concrete visualised and quantified by neutron radiography". In: *First RILEM International Conference on Concrete and Digital Fabrication–Digital Concrete 2018*. Springer. 2019, pp. 217–224.

[53] T. Marchment, J. Sanjayan, and M. Xia. "Method of enhancing interlayer bond strength in construction scale 3D printing with mortar by effective bond area amplification". In: *Materials & Design* 169 (2019), p. 107684.

[54] V. N. Nerella, S. Hempel, and V. Mechtcherine. "Effects of layer-interface properties on mechanical performance of concrete elements produced by extrusion-based 3D-printing". In: *Construction and Building Materials* 205 (2019), pp. 586–601.

[55] T. T. Le, S. A. Austin, S. Lim, R. A. Buswell, R. Law, A. G. Gibb, and T. Thorpe. "Hardened properties of high-performance printing concrete". In: *Cement and Concrete Research* 42.3 (2012), pp. 558–566.

[56] B. Panda, N. A. Noor Mohamed, S. C. Paul, G. Bhagath Singh, M. J. Tan, and B. Šavija. "The effect of material fresh properties and process parameters on buildability and interlayer adhesion of 3D printed concrete". In: *Materials* 12.13 (2019), p. 2149.

[57] L. H. Anell. "Concrete 3d printer". In: (2015).

[58] A. S. Suiker, R. J. Wolfs, S. M. Lucas, and T. A. Salet. "Elastic buckling and plastic collapse during 3D concrete printing". In: *Cement and Concrete Research* 135 (2020), p. 106016.

[59] P. K. Mehta and P. J. Monteiro. *Concrete: microstructure, properties, and materials*. McGraw-Hill Education, 2014.

[60] E. Berodier and K. Scrivener. "Understanding the Filler Effect on the Nucleation and Growth of C-S-H". In: *Journal of the American Ceramic Society* 97.12 (2014), pp. 3764–3773.

[61] K. Scrivener. *Cement Chemistry and Sustainable Cementitious Materials, Kinetics, the Filler*. 2018. URL: https://www.youtube.com/watch?v=2d8nEk72c78&t=8s&ab_channel=CementChemistryandSustainableCementitiousMaterials.

[62] R. Myrdal. "Accelerating admixtures for concrete. State of the art". In: (2007).

[63] Q. Yuan, D. Zhou, H. Huang, J. Peng, and H. Yao. "Structural build-up, hydration and strength development of cement-based materials with accelerators". In: *Construction and Building Materials* 259 (2020), p. 119775.

[64] T. Oey, J. Stoian, J. Li, C. Vong, M. Balonis, A. Kumar, W. Franke, and G. Sant. "Comparison of Ca (NO 3) 2 and CaCl 2 admixtures on reaction, setting, and strength evolutions in plain and blended cementing formulations". In: *Journal of Materials in Civil Engineering* 27.10 (2015), p. 04014267.

[65] T. E.-9.-2. A1. *Admixtures for concrete, mortar and grout–Part 2: Concrete admixtures–Definitions, requirements, conformity, marking and labelling*. 2013.

[66] K. Scrivener, R. Snellings, B. Lothenbach, *et al. A practical guide to microstructural analysis of cementitious materials*. Vol. 540. Crc Press Boca Raton, FL, USA: 2016.

[67] Y. W. D. Tay, Y. Qian, and M. J. Tan. "Printability region for 3D concrete printing using slump and slump flow test". In: *Composites Part B: Engineering* 174 (2019), p. 106968.

[68] S. Muthukrishnan, S. Ramakrishnan, and J. Sanjayan. "Effect of alkali reactions on the rheology of one-part 3D printable geopolymer concrete". In: *Cement and Concrete Composites* 116 (2021), p. 103899.

[69] Y. Sun, S. Ghorbani, X. Dai, G. Ye, and G. De Schutter. "Evaluation of rheology and strength development of alkali-activated slag with different silicates sources". In: *Cement and Concrete Composites* 128 (2022), p. 104415.

[70] T. T. Le, S. A. Austin, S. Lim, R. A. Buswell, A. G. Gibb, and T. Thorpe. "Mix design and fresh properties for high-performance printing concrete". In: *Materials and structures* 45 (2012), pp. 1221–1232.

[71] A. U. Rehman, S.-M. Lee, and J.-H. Kim. "Use of municipal solid waste incineration ash in 3D printable concrete". In: *Process Safety and Environmental Protection* 142 (2020), pp. 219–228. ISSN: 0957-5820. DOI: https://doi.org/10.1016/j.psep.2020.06.018. URL: https://www.sciencedirect.com/science/article/pii/S0957582020315627.

[72] S. Cho, J. Kruger, A. van Rooyen, and G. van Zijl. "Rheology and application of buoyant foam concrete for digital fabrication". In: *Composites Part B: Engineering* 215 (2021), p. 108800. ISSN: 1359-8368. DOI: https://doi.org/10.1016/j.compositesb.2021.108800. URL: https://www.sciencedirect.com/science/article/pii/S1359836821001918.

[73] "An approach to develop set-on-demand 3D printable limestone- calcined clay-based cementitious materials using calcium nitrate". In: (2023).

[74] "Insights into material design, extrusion rheology, and properties of 3D-printable alkali-activated fly ash-based binders". In: *Materials & Design* 167 (2019), p. 107634.

[75] *Methods of Testing Cement — Part 3: Determination of Setting Times and Soundness*. 2003.

[76] "Effect of different grade levels of calcined clays on fresh and hardened properties of ternary-blended cementitious materials for 3D printing". In: *Cement Concrete Composites* 114 (Nov. 2020), p. 103708. DOI: 10.1016/j.cemconcomp.2020.103708. URL: https://doi.org/10.1016/j.cemconcomp.2020.103708.

[77] *Design and Control of Concrete Mixtures ,The Guide to Applications*. Portland Cement Association, 2011.

[78] S. Aggoun, M. Cheikh-Zouaoui, N. Chikh, and R. Duval. "Effect of some admixtures on the setting time and strength evolution of cement pastes at early ages". In: *Construction and Building Materials* 22.2 (Feb. 2008), pp. 106–110. DOI: 10.1016/j.conbuildmat.2006.05.043.

7

[79] T. Dorn, T. Hirsch, and D. Stephan. “Working mechanism of calcium nitrate as an accelerator for Portland cement hydration”. In: *Journal of the American Ceramic Society* 106.1 (Sept. 2022), pp. 752–766. DOI: 10.1111/jace.18782.

[80] *Hydration of C3A with calcium sulfate alone and in the presence of calcium silicate*. Tech. rep. EPFL, 2011.

[81] L. Steger, S. Blotevogel, L. Frouin, C. Patapy, and M. Cyr. “Experimental evidence for the acceleration of slag hydration in blended cements by the addition of CaCl2”. In: *Cement and Concrete Research* 149 (Nov. 2021), p. 106558. DOI: 10.1016/j.cemconres.2021.106558.

[82] “Working mechanism of calcium nitrate as an accelerator for Portland cement hydration”. In: *Journal of the American Ceramic Society* 106.1 (2023), pp. 752–766.

[83] K. Choy. “Haalbaarheidsonderzoek 3D betonnen geprinte verkeersbrug”. In: (2018).

[84] *Structural Design*. Eindhoven University of Technology Faculty: Build Environment, 2015.

[85] V. Mechtcherine, F. Will, M. Näther, J. Otto, and M. Krause. “Large-scale digital concrete construction – CONPrint3D concept for on-site, monolithic 3D-printing”. In: *Automation in Construction* 107 (Nov. 2019), p. 102933. DOI: 10.1016/j.autcon.2019.102933.